

## Radiative and chiral corrections to elastic lepton-proton scattering in chiral perturbation theory

Pulak Talukdar<sup>1,2,\*</sup>, Vanamali C. Shastry<sup>3,4,†</sup>, Udit Raha<sup>1,‡</sup> and Fred Myhrer<sup>5,§</sup>


<sup>1</sup>*Department of Physics, Indian Institute of Technology Guwahati, Guwahati—781039, Assam, India*

<sup>2</sup>*Department of Physics, S. B. Deorah College, Guwahati, Assam 781007, India*

<sup>3</sup>*Department of Education in Science and Mathematics, Regional Institute of Education Mysuru, Mysore—570006, India*

<sup>4</sup>*Institute of Physics, Jan Kochanowski University, ul. Uniwersytecka 7, P-25-406 Kielce, Poland*

<sup>5</sup>*Department of Physics and Astronomy, University of South Carolina, Columbia, South Carolina 29208, USA*

 (Received 2 November 2020; revised 14 June 2021; accepted 12 July 2021; published 8 September 2021)

A unified treatment of both chiral and radiative corrections to the low-energy elastic lepton-proton scattering processes is presented in Heavy Baryon Chiral Perturbations Theory. The proton hadronic chiral corrections include the next-to-next-to-leading-order corrections, whereas the radiative corrections include the next-to-leading-order terms in our novel power counting scheme. We find that the net fractional well-defined chiral corrections with respect to the leading-order Born cross section can be as large as 10% (20%) for electron (muon) scattering process for MUon Proton Scattering Experiment (MUSE) kinematics. We show *via* our model-independent treatment of the low-energy lepton-proton kinematics that the largest theoretical uncertainty is due to the recent different published values of the proton's rms radius, while, e.g., the next-higher-order hadronic chiral terms are expected to give rather nominal errors. For the radiative corrections, we demonstrate a systematic order by order cancellation of all infrared singularities and present our finite ultraviolet regularization results. We find that the radiative corrections for muon-proton scattering is of the order of 2%, whereas for electron scattering, the radiative corrections could be as large as 25%. We attribute such a contrasting result partially to the fact that in muon scattering the leading radiative-order correction goes through zero in some intermediate low-momentum transfer region, leaving the subleading radiative chiral-order effects to play a dominant role in this particular kinematic region. For the low-energy MUSE experiment, the often-neglected lepton mass as well as the Pauli form factor contributions of the relativistic leptons are incorporated in all our computations.

DOI: [10.1103/PhysRevD.104.053001](https://doi.org/10.1103/PhysRevD.104.053001)

### I. INTRODUCTION

Scattering processes involving charged particles, like the lepton-proton ( $\ell$ -p) elastic scattering, involve an arbitrary number of real and virtual photons. The inelastic bremsstrahlung process,  $\ell + p \rightarrow \ell + p + \gamma^*$ , where  $\ell \equiv e^\pm, \mu^\pm$ , constitutes the most significant undetected background radiative process.<sup>1</sup> Many prominent works have estimated radiative corrections nearly as large as 30%, for electron scattering, based on analyses over a wide range of momentum transfers and a variety of experimental conditions, *viz.* detector designs and resolutions [1]. Especially for soft (low-energy) photons, these corrections must be

theoretically evaluated as they are inaccessible to direct experimental probes.

The  $\ell$ -p elastic scattering process has particularly engendered extensive interests in the scientific community over the past two decades because of its significant role in bringing forth various discrepancies in our basic understanding of the electromagnetic properties of the proton. An accurate experimental determination of the proton's electromagnetic form factors can shed much-needed light on the proton's basic hadronic structure and internal dynamics. The original discrepancies in the measurements of the electric ( $G_E^p$ ) and magnetic ( $G_M^p$ ) proton form factors (called the “proton form factor ratio puzzle”) that emerged about two decades ago stemmed from the utilization of the novel experimental recoil polarization transfer technique [2–5]. Such measurements led us not only to question the validity of the conventional Rosenbluth separation technique but also raised serious concerns regarding our basic understanding of the proton structure itself. In order to

\*t.pulak@iitg.ac.in

†vanamalishastry@gmail.com

‡udit.raha@iitg.ac.in

§myhrer@mailbox.sc.edu

<sup>1</sup>The  $\gamma^*$  symbol denotes an emitted real bremsstrahlung photon to distinguish it from the virtual loop-photon  $\gamma$ .

resolve these problems, a flurry of ingenious ideas and methodologies ensued, which were extensively discussed in numerous published works as well as reviews; see, e.g., Refs. [6–9]. Furthermore, the 2013 revelation of the so-called proton radius puzzle [10–14] concerns the irreconcilable inconsistency among the different measurement techniques in determining the proton’s *root-mean-squared* (*rms*) charge radius. Subsequently, unremitting efforts geared toward the development of high-precision experimental [15–22] and novel theoretical [23–46] techniques have been pursued over the last nine years, seeking a definitive answer to the conundrum. However, despite the efforts, such discrepancies are yet to be conclusively resolved, requiring further improved approaches on either front.

In contrast to the previously designed experiments, the Muon Proton Scattering Experiment (MUSE), currently underway at the Paul Scherrer Institute (PSI), aims at a resolution of the proton radius puzzle. The MUSE Collaboration plans to carry out simultaneous high-precision measurements of low-energy electron-proton ( $e^\pm p$ ) and muon-proton ( $\mu^\pm p$ ) scattering cross sections [47,48]. MUSE’s goal is to measure the proton’s *rms* radius at sub-percentage precision [49]. On the theoretical side, an improved assessment of the systematic uncertainties is needed in order to meet the expected level of accuracy of future MUSE data analysis. In this work, we utilize a systematic *model-independent perturbative* procedure to determine higher-order corrections of the *leading-order* (LO) Born contribution (i.e., with pointlike lepton and proton) for the unpolarized elastic  $\ell$ -p scattering cross section. In particular, our analysis demonstrates how we handle both the strong interaction as well as the standard QED radiative corrections in our formalism. We work in the framework of a low-energy effective field theory (EFT), namely, *Chiral Perturbation Theory* ( $\chi$ PT) [50], which reflects the inherent low-energy nonperturbative features of QCD manifested in hadrons, where chiral symmetry and its violations play decisive roles in determining the observables. The rationale for using  $\chi$ PT to evaluate the sub-leading corrections in an essential perturbative framework is that the methodology allows us to systematically extend the theoretical predictions to higher levels of accuracy through a well-defined power counting scheme. This is a distinctive feature of our approach, which sets our analysis in contrast to the existing conventional approaches where hadron structure effects are empirically modeled through the use of phenomenological proton form factors.

Our evaluations are based on the well-established non-relativistic version of  $\chi$ PT, namely, heavy baryon  $\chi$ PT (HB $\chi$ PT), e.g., Refs. [51,52]. HB $\chi$ PT provides a convenient tool to study processes like the low-energy  $\ell$ -p scattering, where nonrelativistic baryons and relativistic mesons and leptons are the fundamental degrees of freedom. Furthermore, all these particles naturally couple to the photon in a gauge invariant manner. Here, we adopt the

so-called SU(2) isospin scheme, which is tailor made to deal with the low-energy hadron dynamics of the nucleon. The HB $\chi$ PT power counting incorporates a chiral expansion in terms of powers of the ratio of a generic small momentum  $Q$  over the large chiral scale  $\Lambda_\chi \simeq 4\pi f_\pi \simeq 1$  GeV ( $f_\pi \approx 92.4$  MeV is the pion decay constant), plus a *recoil expansion* in powers of the typical momentum scale of the process,  $Q \simeq 0.2$  GeV/c (in regard to MUSE kinematics), over the “heavy” proton mass  $M \simeq 1$  GeV,

$$\frac{Q}{\Lambda_\chi} \sim \frac{Q}{M} \ll 1.$$

Apart from the above-mentioned chiral momentum expansion, the counting scheme also includes the standard QED perturbative expansion where the effective Born amplitude (see the next section), including all its non-radiative chiral effects, counts as order  $\alpha = \frac{e^2}{4\pi} \simeq 1/137 \simeq 0.007$ . In fact, for the evaluation of our “effective Born” contribution, we make a chiral expansion to include corrections up to and including  $Q^2/M^2 \simeq 0.04$  in this work. For the sake of transparency, we assign distinct nomenclatures to the various chiral corrections. For example, we denote the leading-order Born amplitude  $\mathcal{M}_\gamma^{(0)} \sim \mathcal{O}(e^2)$  as “LO $_\chi$ ” or simply “LO Born,” the *next-to-leading-order* chiral Born amplitude  $\mathcal{M}_\gamma^{(1)} \sim \mathcal{O}(e^2 Q/M) \simeq \mathcal{O}(e^2 \cdot 0.2)$  as “NLO $_\chi$ ”, and the *next-to-next-to-leading-order* chiral Born amplitude  $\mathcal{M}_\gamma^{(2)} \sim \mathcal{O}(e^2 Q^2/M^2) \simeq \mathcal{O}(e^2 \cdot 0.04)$  as “NNLO $_\chi$ ” (cf. Fig. 1). We note that at the order  $Q^2/M^2$  and higher, the  $Q^2$  dependence of the proton form factors enters naturally in the chiral expansion. At NNLO $_\chi$  the *low-energy constants* (LECs) of HB $\chi$ PT parametrize the short-distance physics and, in addition, regulate the *ultraviolet* (UV) divergences in diagrams with pion loops [51–53]. The  $\chi$ PT evaluation of these NNLO $_\chi$  contributions are well known and yield analytical expressions for the proton’s charge and magnetic radii [51,52,54]. In this work, however, we do not repeat such evaluations. Instead, we use the analytical expression of the  $\chi$ PT renormalized effective Born amplitude  $\mathcal{M}_\gamma^{(2),\text{rms}} \sim \mathcal{O}(e^2 Q^2/M^2)$ . In this work, we shall denote the chirally corrected NNLO $_\chi$  fractional contributions as  $\delta_\chi^{(2)} \sim \mathcal{O}(Q^2/M^2)$ , with respect to the LO Born cross section of  $\mathcal{O}(\alpha^2)$  (cf. Sec. II for details). Furthermore, it should be noted that the *next-to-next-to-next-to-leading-order* (N<sup>3</sup>LO $_\chi$ ) contributions from terms of  $\mathcal{O}(e^2 Q^3/M^3) \simeq \mathcal{O}(e^2 \cdot 0.008)$ , which are not included in this work, constitute an important theoretical uncertainty. We remark that including possible contributions arising from spin-3/2  $\Delta(1232)$  and other excited nucleon resonances would be a significant extension of our present analysis, and they are therefore not included in this work. In particular, the inclusion of  $\Delta(1232)$  in  $\chi$ PT requires the chiral counting to be supplemented by the

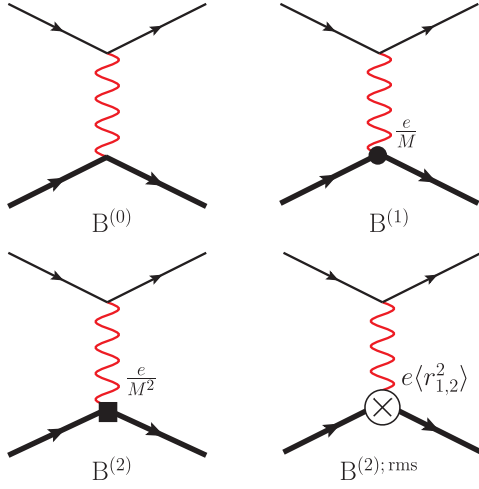


FIG. 1. Born diagrams  $B^{(0,1,2)}$  for  $\ell$ -p elastic scattering at leading-order [i.e.,  $\mathcal{O}(e^2)$ ], next-to-leading-order [i.e.,  $\mathcal{O}(e^2 Q/M)$ ], and next-to-next-to-leading-order [i.e.,  $\mathcal{O}(e^2 Q^2/M^2)$ ] in chiral expansion [see Eqs. (9)–(11)]. The effective Born diagram  $B^{(2);rms}$  also contributing at next-to-next-to-leading-order [see Eqs. (13) and (14)] parametrizes the proton’s structure effects (pion loops and LECs) via insertions of the Dirac and Pauli mean-squared radii  $\langle r_{1,2}^2 \rangle$  (crossed blob). The dark filled blob and square represent the proton-photon vertex insertion of order  $1/M$  and  $1/M^2$ , respectively.

so-called *small scale* or  $\delta$ - *expansion* [51,52,55,56]. In addition, we refer to Refs. [33,37–39] regarding some recently developed techniques of the so-called *dispersively improved*  $\chi$ PT, for a consistent inclusion of resonance contributions.

The predominant portion of this work deals with the evaluation the first two orders of our “chiral-radiative” corrections, namely, the *radiative leading-order* whose amplitudes are denoted as “ $LO_\alpha$ ,” i.e.,  $\mathcal{O}(e^2 \alpha) \simeq \mathcal{O}(e^2 \cdot 0.007)$ , and the *radiative next-to-leading-order* corrections, denoted as “ $NLO_\alpha$ ,” i.e.,  $\mathcal{O}(e^2 \alpha Q/M) \simeq \mathcal{O}(e^2 \cdot 0.0015)$ . The next-higher-order chiral-radiative amplitudes, i.e.,  $\mathcal{O}(e^2 \alpha Q^2/M^2) \simeq \mathcal{O}(e^2 \cdot 0.0003)$ , are expected to yield only a tiny contribution.

To the best of our knowledge, the current work represents the first attempt at using a model-independent EFT framework, namely, HB $\chi$ PT, to simultaneously evaluate the chiral and the radiative corrections in a unified framework. The EFT radiative evaluation includes all one-loop virtual correction, viz., the self-energies (SEs), vertex corrections (VC), vacuum polarization (VP), and the *two-photon exchange* (TPE) contributions to the  $\ell$ -p elastic scattering process. Moreover, in our work, the contributions from single soft photon ( $\gamma_{\text{soft}}^*$ ) emission are required in order to demonstrate the cancellation of the *infrared* (IR) divergences arising from the virtual processes. The *modus operandi* adopted in this paper is reminiscent of the seminal work of Yennie *et al.* (YFS) of Ref. [57], developed within a QED approach with relativistic pointlike Dirac particles.

In order to render the radiative corrections IR-finite, we need to include the  $LO_\alpha$  and  $NLO_\alpha$  soft photon bremsstrahlung amplitudes of  $\mathcal{O}(e^3)$  and  $\mathcal{O}(e^3 Q/M)$ , respectively. In the ensuing analysis, the  $LO_\alpha$  fractional radiative corrections are denoted by  $\delta_{2\gamma}^{(0)} \sim \mathcal{O}(\alpha)$ , and likewise the  $NLO_\alpha$  corrections are denoted by  $\delta_{2\gamma}^{(1)} \sim \mathcal{O}(\alpha Q/M)$ , with respect to the elastic LO (Born) cross section of  $\mathcal{O}(\alpha^2)$ . The interference of the NNLO $_\chi$  terms with the  $LO_\alpha$  radiative corrections is included together with other nonfactorizable NNLO $_\alpha$  corrections in  $\delta_{2\gamma}^{(2)} \sim \mathcal{O}(\alpha Q^2/M^2)$ , and  $\delta_{2\gamma}^{(2)}$  will be used in our uncertainty assessment; see Eq. (99). Thus, our result for the total fractional radiative correction to the  $\ell$ -p elastic LO (Born) cross section can be symbolically expressed in the form  $\delta_{2\gamma} = \delta_{2\gamma}^{(0)} + \delta_{2\gamma}^{(1)} + \delta_{2\gamma}^{(2)}$ .

In one of our previous work, Ref. [58], we evaluated the TPE contributions to the  $\ell$ -p elastic process at  $NLO_\alpha$  accuracy in HB $\chi$ PT invoking a soft photon approximation (SPA), e.g., the approach as pursued in Ref. [1] (see the discussion relating to the use of SPA later in this paper). We demonstrated that the TPE amplitudes diverge in the vanishing limit of the photon momenta, *vis-à-vis* IR divergences. The present work is an essential follow-up of that analysis [58]. Here, we shall detail the systematical stepwise evaluation of the radiative corrections at  $LO_\alpha$  and  $NLO_\alpha$ . In this work, the NNLO $_\alpha$  corrections are only partially included (for brevity, the analytical NNLO $_\alpha$  results are not displayed explicitly) and contribute to our estimate of the theoretical error. We explicitly demonstrate how the chiral power counting allows an order by order cancellation of all the IR divergences arising from the one-loop virtual and the single-photon bremsstrahlung processes.

We assign the real bremsstrahlung photon as being either “soft” or “hard” in comparison to some fixed but frame-dependent small energy scale  $\Delta E$ . The  $\Delta E$  as associated with the outgoing detected lepton, practically fixes the upper limit of the energy integration of the (undetected) emitted *soft* photon when evaluating the bremsstrahlung cross section. Especially, in the context of laboratory (lab) frame kinematics,  $\Delta E = \Delta_{\gamma^*}$ , where  $\Delta_{\gamma^*}$  is the so-called detector *acceptance*.<sup>2</sup> In particular, to integrate over this soft elastic radiative tail, we adopt Tsai’s formalism [59,60] of boosting to the so-called *S*-frame, where the otherwise complicated phase-space integration involving the photon emission angles becomes rather simplified, as

<sup>2</sup>In the present radiative analysis of  $\ell$ -p elastic scattering in the lab frame, we include only the soft photons whose energies lie below the detector threshold  $\Delta_{\gamma^*}$ . The *hard* photons with energies larger than  $\Delta_{\gamma^*}$  will not be considered since they contribute to the inelastic radiative process,  $\ell + p \rightarrow \ell + p + \gamma^*$ . The soft photons go undetected in a typical experiment, and therefore it is necessary to integrate the part of the elastic radiative tail distribution for photon energies between 0 and  $\Delta_{\gamma^*}$ , in order to compare with the measured differential cross section.

demonstrated in the Appendixes. Our results for the radiative corrections will depend on the resolution factor  $\Delta_{\gamma^*}$ , which constitutes a free parameter in our theoretical framework specified by the design of a given experimental arrangement. In this work, for the sake of numerical evaluations, we have chosen the value of this parameter to be approximately 1% of the incoming lepton energy.

The evaluation of the radiative correction diagrams involve virtual or real photons, which yield matrix elements containing UV and/or IR divergences. In this work, both the chiral and the QED divergences will be treated by employing *dimensional regularization* (DR).<sup>3</sup> While the UV-divergent terms are renormalized using LECs and QED counterterms in the Lagrangian, the IR divergences, as demonstrated in this paper, systematically cancel at each order in the chiral expansion. The ultimate objective of this paper is to obtain a finite analytical expression for the fractional chiral-radiative correction  $\delta_{2\gamma}$  to the elastic  $\ell$ -p differential cross section in the lab frame, namely,

$$\left. \frac{d\sigma_{el}}{d\Omega'_l} \right|_{\text{lab}} = \left[ \frac{d\sigma_{el}}{d\Omega'_l} \right]_{\gamma} \{1 + \delta_{2\gamma}(Q^2)\}, \quad (1)$$

where the prefactor on the right side includes all our  $\mathcal{O}(\alpha^2 Q^2/M^2)$  (i.e., NNLO $_{\chi}$ ) hadronic chiral corrections to the elastic Born differential cross section (cf. Sec. II for details).

The paper is outlined as follows. The details of our methodology are presented in Sec. II, where we display the pertinent terms of the effective Lagrangian (QED + HB $\chi$ PT). Based on the aforementioned chiral power counting scheme, we determine the analytical expressions for the two chiral corrections to the LO Born cross section, namely, the NLO $_{\chi}$  and NNLO $_{\chi}$  terms in HB $\chi$ PT. The details of the chiral-radiative corrections, namely, at LO $_{\alpha}$  and NLO $_{\alpha}$ , involving evaluations of the corresponding one-loop virtual and single real soft photon emission diagrams, are presented in Secs. III and IV, respectively. In Sec. V, we discuss and compare the numerical estimates of the various contributions in regard to the MUSE kinematical region [47,48]. We also outline the major sources of theoretical uncertainties in this section. Finally, Sec. VI summarizes the key features of our analysis and concludes with prospects of possible future extensions of this work. Technical details regarding the utilization of the  $S$ -frame

kinematics to perform the bremsstrahlung phase-space integrals are relegated to the Appendixes.

## II. HB $\chi$ PT: FORMALISM

The most general effective Lagrangian consistent with the low-energy symmetries is the sum of the QED Lagrangian for the lepton fields  $\psi_l$  and the hadronic  $\pi N$  effective Lagrangian, namely,

$$\begin{aligned} \mathcal{L}_{IN\gamma} = & -\frac{1}{4} F_{\mu\nu} F^{\mu\nu} + \frac{1}{2\xi_A} (\partial \cdot A)^2 \\ & + \sum_{l=e,\mu} \bar{\psi}_l (i\not{D} - m_l) \psi_l + \mathcal{L}_{\pi N}^{\text{eff}}, \end{aligned} \quad (2)$$

where  $F_{\mu\nu} = \partial_\mu A_\nu - \partial_\nu A_\mu$  is the electromagnetic field tensor with  $A_\mu$  being the photon field and  $\xi_A$  is the gauge parameter, which in the Feynman gauge is  $\xi_A = 1$ . The gauge covariant derivatives appearing in the Lagrangian are defined as  $D_\mu = \partial_\mu - ieA_\mu$ . The hadronic part of the effective Lagrangian is expressed here as the sum of the lowest-order pionic Lagrangian  $\mathcal{L}_{\pi}^{(2)}$  and the  $\pi N$  Lagrangian expanded in an infinite sequence of operator terms characterized by the chiral dimension  $\nu = 0, 1, 2, \dots$ , namely,

$$\mathcal{L}_{\pi N}^{\text{eff}} = \mathcal{L}_{\pi}^{(2)} + \sum_{\nu=0} \mathcal{L}_{\pi N}^{(\nu)},$$

where<sup>4</sup>

$$\begin{aligned} \mathcal{L}_{\pi}^{(2)} = & \frac{f_\pi}{4} \text{Tr}[\nabla_\mu U^\dagger \nabla^\mu U + \chi^\dagger U + \chi U^\dagger]; \\ U = & \sqrt{1 - \frac{\vec{\pi}^2}{f_\pi^2}} + \frac{i}{f_\pi} \vec{\tau} \cdot \vec{\pi}, \\ \chi = & 2B \begin{pmatrix} m_u & 0 \\ 0 & m_d \end{pmatrix}. \end{aligned} \quad (3)$$

Here, we use the so-called *sigma gauge* parametrization of the nonlinear pion field  $U$ , and the constant  $B$  is related to the scalar current quark condensate  $\langle 0|\bar{q}q|0\rangle$ , the order parameter of spontaneously broken chiral symmetry. The chiral covariant derivative  $\nabla_\mu$  is given in Eq. (7). Below, we explicitly specify only the  $\nu = 0$  (LO $_{\chi}$ ) and  $\nu = 1$  (NLO $_{\chi}$ ) terms of the  $\pi N$  Lagrangian. The  $\nu = 2$  (NNLO $_{\chi}$ ) chiral Lagrangian contains many additional LECs as well as  $1/M^2$ -order “fixed” terms and counterterms, some of which contribute to the lowest-order proton’s form factors, including the rms radii (see, e.g., Ref. [54]). Owing to the large

<sup>3</sup>Most works in the literature prefer to use a nonzero photon mass,  $\lambda$  (see, e.g., Refs. [1,60]), which leads to IR-divergent terms in the form of logarithms, e.g.,  $\ln(\frac{\lambda^2}{-Q^2})$ . We follow the DR treatment of IR divergences, e.g., Refs. [61–64]). A naive comparison of the IR treatments leads to the correspondence  $\frac{1}{|\epsilon_{\text{IR}}|} + \gamma_E - \ln\left(\frac{4\pi\mu^2}{-Q^2}\right) \leftrightarrow -\ln\left(\frac{\lambda^2}{-Q^2}\right)$ , where  $\mu$  is the subtraction scale (typically chosen as the momentum scale associated with the scattering process).

<sup>4</sup>In principle, the LECs in the Lagrangian should be taken in the chiral limit, e.g.,  $\mathring{f}$  and  $\mathring{g}_A$ . However, they will be renormalized to their respective physical values,  $f_\pi$  and  $g_A$ , at a given chiral-order.

number of operator terms in  $\mathcal{L}_{\pi N}^{(2)}$ , we just refer the reader to, e.g., Refs. [52,53], where the complete expression can be found. The lowest chiral order  $\pi N$  Lagrangian is given as

$$\mathcal{L}_{\pi N}^{(0)} = \bar{N}_v (i v \cdot \mathcal{D} + g_A S \cdot u) N_v; \quad N_v \equiv \begin{pmatrix} \mathbf{p}_v \\ \mathbf{n}_v \end{pmatrix}, \quad (4)$$

where in HB $\chi$ PT the nucleon velocity and spin four-vectors can be chosen as  $v_\mu = (1, \vec{0})$  and  $S_\mu = (0, \vec{\sigma}/2)$  respectively, satisfying the condition  $v \cdot S = 0$ . The pion fields enter  $\mathcal{L}_{\pi N}^{(0)}$  through the term  $u = \sqrt{U}$ , where  $u_\mu = i u^\dagger \nabla_\mu U u^\dagger$  is the chiral vielbein. The LEC  $g_A \simeq 1.26$  is the axial-vector coupling constant. The velocity-dependent heavy nucleon field  $N_v$  represents the ‘‘large’’ components of the nucleon isospinor field with the proton ( $\mathbf{p}_v$ ) and neutron ( $\mathbf{n}_v$ ) projections. The next sub-leading chiral-order  $\pi N$  Lagrangian is given by

$$\begin{aligned} \mathcal{L}_{\pi N}^{(1)} = & \bar{N}_v \left[ \left( \frac{(v \cdot \mathcal{D})^2 - \mathcal{D} \cdot \mathcal{D}}{2M} \right) - \frac{i g_A}{2M} \{ S \cdot \mathcal{D}, v \cdot u \} \right. \\ & + c_1 \text{Tr}(\chi_+) + \left( c_2 - \frac{g_A^2}{8M} \right) (v \cdot u)^2 + c_3 u \cdot u \\ & + \left( c_4 + \frac{1}{4M} \right) [S^\mu, S^\nu] u_\mu u_\nu + c_5 \text{Tr}(\tilde{\chi}_+) \\ & \left. - \frac{i}{4M} [S^\mu, S^\nu] [(1 + c_6) f_{\mu\nu}^+ + c_7 \text{Tr}(f_{\mu\nu}^+)] \right] N_v, \quad (5) \end{aligned}$$

where in our case we have

$$\begin{aligned} \chi_+ &= u^\dagger \chi u + u \chi^\dagger u, \quad \tilde{\chi}_+ = \chi_+ - \frac{\mathbb{I}}{2} \text{Tr}(\chi_+), \\ f_{\mu\nu}^+ &= u^\dagger (f_{\mu\nu}^R + v_{\mu\nu}^{(s)}) u + u (f_{\mu\nu}^L + v_{\mu\nu}^{(s)}) u^\dagger \\ &= e F_{\mu\nu} (u \mathcal{Q} u^\dagger + u^\dagger \mathcal{Q} u), \\ f_{\mu\nu}^R &= \partial_\mu r_\nu - \partial_\nu r_\mu - i [r_\mu, r_\nu] = e \frac{\tau^3}{2} F_{\mu\nu}, \\ f_{\mu\nu}^L &= \partial_\mu l_\nu - \partial_\nu l_\mu - i [l_\mu, l_\nu] = e \frac{\tau^3}{2} F_{\mu\nu}, \\ v_{\mu\nu}^{(s)} &= e \frac{\mathbb{I}}{2} (\partial_\mu A_\nu - \partial_\nu A_\mu), \quad \text{and} \\ \mathcal{Q} &= \frac{1}{2} (\mathbb{I} + \tau_3) = \begin{pmatrix} 1 & 0 \\ 0 & 0 \end{pmatrix}. \quad (6) \end{aligned}$$

Apart from the  $1/M$ -order terms, the  $\nu = 1$  chiral dimension Lagrangian contains the seven LECs,  $c_i$ ,  $i = 1, 2, \dots, 7$ , whose values are phenomenologically determined [50,53]. The speciality of these dimension-0 and -1 LECs are that they are finite and unaffected by pion loop effects, which start at chiral-order 2. In particular, the LECs  $c_6 = \kappa_v$  and  $c_7 = (\kappa_s - \kappa_v)/2$ , where the nucleon isovector and isoscalar anomalous magnetic moments are  $\kappa_v = 3.71$

and  $\kappa_s = -0.12$ , respectively [54]. The field tensor  $f_{\mu\nu}^+$  represents the external isoscalar and isovector sources. As shown in Eq. (6), the external isoscalar field is  $v_\mu^{(s)} = -e \frac{\mathbb{I}}{2} A_\mu$ , and the isovector right-handed ( $r_\mu$ ) and left-handed ( $l_\mu$ ) external sources are given as  $l_\mu = r_\mu = -e \frac{\tau^3}{2} A_\mu$ , where  $\mathbb{I}$  is the identity matrix and  $\tau^3$  is the diagonal Pauli matrix in isospin SU(2). In this work, we have ignored all sources of isospin violation. Consequently, there is no contribution from the term proportional to  $c_5$ , since  $\tilde{\chi}_+ \rightarrow 0$  in the limit  $m_d \rightarrow m_u$ . Finally, the covariant derivatives used in the HB $\chi$ PT Lagrangian are

$$\begin{aligned} \mathcal{D}_\mu &= \partial_\mu + \Gamma_\mu - i v_\mu^{(s)}, \quad \text{and} \\ \nabla_\mu U &= \partial_\mu U - i r_\mu U + i U l_\mu, \quad (7) \end{aligned}$$

where

$$\Gamma_\mu = \frac{1}{2} [u^\dagger (\partial_\mu - i r_\mu) u + u (\partial_\mu - i l_\mu) u^\dagger]. \quad (8)$$

In Fig. 1, we display the LO $_\chi$ , NLO $_\chi$ , and NNLO $_\chi$  Born amplitudes (diagrams B<sup>(0,1,2)</sup>) for the elastic lepton-proton scattering process. As mentioned, we prefer to represent the proton form factor (rms radii) contributions at NNLO $_\chi$  via the effective Born amplitude  $\mathcal{M}_\gamma^{(2); \text{rms}}$  (diagram B<sup>(2); rms</sup>). The LO Born amplitude is given as

$$\mathcal{M}_\gamma^{(0)} = -\frac{e^2}{Q^2} [\bar{u}_l(p') \gamma^\mu u_l(p)] [\chi^\dagger(p'_p) v_\mu \chi(p_p)], \quad (9)$$

where  $\chi$  is the two-component Pauli spinor for the nonrelativistic proton, while  $u_l$  is the Dirac spinors for the relativistic leptons. The subleading Born amplitudes needed in this work are given as

$$\begin{aligned} \mathcal{M}_\gamma^{(1)} &= \mathcal{M}_\gamma^{(1); \text{a}} + \mathcal{M}_\gamma^{(1); \text{b}}; \\ \mathcal{M}_\gamma^{(1); \text{a}} &= -\frac{e^2}{2M Q^2} [\bar{u}_l(p') \gamma^\mu u_l(p)] [\chi^\dagger(p'_p) \\ &\quad \times \{ (p_p + p'_p)_\mu - v_\mu v \cdot (p_p + p'_p) \} \chi(p_p)], \\ \mathcal{M}_\gamma^{(1); \text{b}} &= -\frac{e^2}{2M Q^2} [\bar{u}_l(p') \gamma^\mu u_l(p)] [\chi^\dagger(p'_p) \\ &\quad \times (2 + \kappa_s + \kappa_v) [S_\mu \cdot S \cdot \mathcal{Q}] \chi(p_p)], \quad (10) \end{aligned}$$

where  $\mathcal{M}_\gamma^{(1); \text{a}}$  and  $\mathcal{M}_\gamma^{(1); \text{b}}$  are the spin-independent and spin-dependent parts of the NLO $_\chi$  amplitude  $\mathcal{M}_\gamma^{(1)}$ , respectively. Including the  $\nu = 2$  chiral-order interactions, the  $1/M^2$ -order Born amplitude is given as

$$\begin{aligned} \mathcal{M}_\gamma^{(2)} &= -\frac{e^2}{8M^2 Q^2} [\bar{u}_l(p') \gamma^\mu u_l(p)] [\chi^\dagger(p'_p) \\ &\quad \times \{ (2(v \cdot Q)^2 - Q^2) v_\mu - Q_\mu v \cdot Q \} \chi(p_p)]. \quad (11) \end{aligned}$$

Furthermore, the proton's Dirac and Pauli form factors up to  $\mathcal{O}(\mathcal{Q}^2/M^2)$  get contributions from the pion loops and various LECs. Expressed in terms of the mean square radii  $\langle r_1^2 \rangle$  and  $\langle r_2^2 \rangle$ , respectively, they are viable in the following low-energy expansions in  $\mathcal{Q}^2$ :

$$F_1^p(\mathcal{Q}^2) = 1 + \frac{\mathcal{Q}^2}{6} \langle r_1^2 \rangle + \mathcal{O}(M^{-3}), \quad \text{and}$$

$$F_2^p(\mathcal{Q}^2) = \kappa_p + \frac{\mathcal{Q}^2}{6} \langle r_2^2 \rangle + \mathcal{O}(M^{-3}). \quad (12)$$

Including these form factors, we derive the general form for the effective Born amplitude, diagram  $B^{(2);\text{rms}}$ , namely,

$$\mathcal{M}_\gamma^{(2);\text{rms}} = -\frac{e^2}{\mathcal{Q}^2} [\bar{u}_l(p') \gamma^\mu u_l(p)] [\chi^\dagger(p'_p) \mathcal{V}_\mu^{(2)} \chi(p_p)], \quad (13)$$

where the effective proton-photon vertex, due to form factor corrections from pion loops and LECs at NNLO $_\chi$ , is given as

$$\mathcal{V}_\mu^{(2)} = (F_1^p - 1)v_\mu + \frac{1}{M} \left\{ (F_1^p - 1) \left( \mathcal{Q}_\mu + \frac{\mathcal{Q}^2}{2M} v_\mu \right) + 2(F_1^p + F_2^p - 1 - \kappa_p) [S_\mu, S \cdot \mathcal{Q}] \right\} - \frac{\mathcal{Q}^2}{8M^2} (F_1^p - 2F_2^p - 1)v_\mu + \mathcal{O}\left(\frac{1}{M^3}\right). \quad (14)$$

Here,  $\kappa_p = (\kappa_v + \kappa_s)/2 = 1.795$  is the anomalous magnetic moment of the proton. Analytical expressions for the form factors evaluated to NNLO $_\chi$  in HB $\chi$ PT already exist in the literature [54] and may be used to determine the scattering cross section. However, in this work, we shall only consider some representative input for the proton's rms charge radius among the recently measured values from scattering as well as atomic-spectroscopy measurements [10,12,15–22].

In this paper, we define the four-momentum transfer  $\mathcal{Q}_\mu = p_\mu - p'_\mu = (p'_p)_\mu - (p_p)_\mu$  of the  $\ell$ -p elastic scattering process,  $\ell(p) + p(p_p) \rightarrow \ell(p') + p(p'_p)$ , where  $\mathcal{Q}^2 < 0$ . The incoming and outgoing lepton four-momenta are  $p = (E, \vec{p})$  and  $p' = (E', \vec{p}')$ . The initial and final proton four-momenta in the lab frame are  $P = (M, 0)$ ,  $P' = (E'_p, \vec{p}'_p)$ . In the heavy baryon formalism, the initial and final state proton four-momenta are  $P^\mu = Mv^\mu + p_p^\mu$  and  $P'^\mu = Mv^\mu + p'_p{}^\mu$ , respectively. We have in the lab frame,  $v \cdot p_p = 0$ , and  $v \cdot p'_p = -\frac{(p'_p)^2}{2M} + \mathcal{O}(M^{-2})$ .

The full (chirally corrected) effective Born cross section in the lab frame is determined by evaluating the phase-space integral of the expression

$$[d\sigma_{el}]_\gamma = \frac{(2\pi)^4 \delta^4(p + P - p' - P')}{4ME} \times \frac{d^3\vec{p}'}{(2\pi)^3 2E'} \frac{d^3\vec{P}'}{(2\pi)^3 2E'_p} \frac{1}{4} \sum_{\text{spins}} |\mathcal{M}_\gamma|^2, \quad (15)$$

where the squared amplitude is

$$|\mathcal{M}_\gamma|^2 = |\mathcal{M}_\gamma^{(0)} + \mathcal{M}_\gamma^{(1)} + \mathcal{M}_\gamma^{(2)} + \mathcal{M}_\gamma^{(2);\text{rms}}|^2. \quad (16)$$

It is notable that, due to the sum over spins, only the spin-independent parts of  $\mathcal{M}_\gamma^{(1)}$  and  $\mathcal{M}_\gamma^{(2);\text{rms}}$  contribute to the interference with the LO Born amplitude  $\mathcal{M}_\gamma^{(0)}$ . The lowest-order Born contribution is well known, namely,

$$\frac{1}{4} \sum_{\text{spins}} |\mathcal{M}_\gamma^{(0)}|^2 = \frac{4e^4}{\mathcal{Q}^2} M^2 \left(1 - \frac{\mathcal{Q}^2}{4M^2}\right) \left[1 + \frac{4EE'}{\mathcal{Q}^2}\right]. \quad (17)$$

The following are the relevant fractional contributions needed at  $1/M^2$ -order accuracy involving the NLO $_\chi$  amplitudes, where we introduce the compact notation  $\mathcal{R}_\mathcal{Q} \equiv \frac{\mathcal{Q}^2}{2M^2}$  for later convenience,

$$\frac{2\text{Re} \sum_{\text{spins}} (\mathcal{M}_\gamma^{(0)\dagger} \mathcal{M}_\gamma^{(1)})}{\sum_{\text{spins}} |\mathcal{M}_\gamma^{(0)}|^2} = \frac{2\text{Re} \sum_{\text{spins}} (\mathcal{M}_\gamma^{(0)\dagger} \mathcal{M}_\gamma^{(1);a})}{\sum_{\text{spins}} |\mathcal{M}_\gamma^{(0)}|^2} = \frac{\mathcal{Q}^2}{2M^2} \equiv \mathcal{R}_\mathcal{Q},$$

$$\frac{\sum_{\text{spins}} |\mathcal{M}_\gamma^{(1)}|^2}{\sum_{\text{spins}} |\mathcal{M}_\gamma^{(0)}|^2} = \frac{\sum_{\text{spins}} |\mathcal{M}_\gamma^{(1);b}|^2}{\sum_{\text{spins}} |\mathcal{M}_\gamma^{(0)}|^2} = \frac{1}{2} (1 + \kappa_p)^2 \mathcal{R}_\mathcal{Q} \left( \frac{\mathcal{Q}^2 + 4(m_l^2 - EE')}{\mathcal{Q}^2 + 4EE'} \right) + \mathcal{O}\left(\frac{\mathcal{Q}^4}{M^4}\right), \quad (18)$$

and those involving the NNLO $_\chi$  amplitudes:

$$\frac{2\text{Re} \sum_{\text{spins}} (\mathcal{M}_\gamma^{(0)\dagger} \mathcal{M}_\gamma^{(2);\text{rms}})}{\sum_{\text{spins}} |\mathcal{M}_\gamma^{(0)}|^2} = \frac{\mathcal{Q}^2}{3} \langle r_1^2 \rangle + \mathcal{O}\left(\frac{\mathcal{Q}^3}{M^3}\right),$$

$$\frac{2\text{Re} \sum_{\text{spins}} (\mathcal{M}_\gamma^{(0)\dagger} \mathcal{M}_\gamma^{(2)})}{\sum_{\text{spins}} |\mathcal{M}_\gamma^{(0)}|^2} = -\frac{1}{2} \mathcal{R}_\mathcal{Q} + \mathcal{O}\left(\frac{\mathcal{Q}^4}{M^4}\right). \quad (19)$$

In fact, the effective Born differential cross section including up to NNLO $_{\chi}$  corrections may be expressed in terms of the proton form factors  $F_{1,2}^p$  and the incoming and outgoing lepton velocities,

$$\beta = \frac{|\vec{p}|}{E} \quad \text{and}$$

$$\beta' = \frac{|\vec{p}'|}{E'} = \sqrt{1 - \left(\frac{\eta m_l}{E}\right)^2},$$

respectively, in the generic form

$$\left[\frac{d\sigma_{el}(Q^2)}{d\Omega'_l}\right]_{\gamma} = \int \frac{|\vec{p}'|dE'}{(2\pi)^2 16M^2 E} \delta\{E + M - E' - E'_p\} \frac{1}{4} \sum_{\text{spins}} |\mathcal{M}_{\gamma}|^2 = \frac{1}{64\pi^2 M^2} \left(\frac{\beta'}{\eta\beta}\right) \frac{1}{4} \sum_{\text{spins}} |\mathcal{M}_{\gamma}|^2, \quad (20)$$

where

$$\eta \equiv \frac{E}{E'} = \frac{E}{E + Q^2/2M} = 1 + \frac{E}{M}(1 - \cos\theta) \quad (21)$$

is the proton recoil factor which may either be expressed in terms the four-momentum transfer  $Q^2$  or, equivalently, in terms of the lab frame lepton scattering angle  $\theta$ . The spin-averaged squared amplitude is

$$\begin{aligned} \frac{1}{4} \sum_{\text{spins}} |\mathcal{M}_{\gamma}|^2 &= \frac{1}{4} \sum_{\text{spins}} \left[ \{|\mathcal{M}_{\gamma}^{(0)}|^2 + |\mathcal{M}_{\gamma}^{(1);a}|^2 + 2\text{Re}(\mathcal{M}_{\gamma}^{(0)\dagger} \mathcal{M}_{\gamma}^{(1);a})\} (F_1^p(Q^2))^2 + \frac{1}{(1 + \kappa_p)^2} |\mathcal{M}_{\gamma}^{(1);b}|^2 \right. \\ &\quad \left. \times (F_1^p(Q^2) + F_2^p(Q^2))^2 + 2\text{Re}(\mathcal{M}_{\gamma}^{(0)\dagger} \mathcal{M}_{\gamma}^{(2)}) (F_1^p(Q^2) - 2F_2^p(Q^2)) F_1^p(Q^2) + \mathcal{O}\left(\alpha^2 \frac{Q^3}{M^3}\right) \right]. \quad (22) \end{aligned}$$

The prefactor  $\eta$ , which arises from the phase-space integration over the energy conservation  $\delta$ -function, exactly cancels out while considering the different ratios of the chirally or radiatively corrected  $\ell$ -p scattering cross sections to the LO Born contribution,

$$\left[\frac{d\sigma_{el}(Q^2)}{d\Omega'_l}\right]_0 = \frac{\alpha^2 \beta'}{\eta\beta Q^2} \left(1 - \frac{Q^2}{4M^2}\right) \left[1 + \frac{4E^2}{\eta Q^2}\right]. \quad (23)$$

First, we note that  $|\mathcal{M}_{\gamma}^{(0)}|^2$  contains terms up to and including  $\mathcal{O}(M^{-2})$ . Retaining its complete expression generates the above LO Born cross section. Second, the term  $\sum |\mathcal{M}_{\gamma}^{(1);a}|^2 \sim \sum |\mathcal{M}_{\gamma}^{(0)}|^2 \mathcal{O}(M^{-4})$  and is therefore ignored. Thus, we obtain the full chirally corrected NNLO $_{\chi}$  result for the elastic differential cross section of the form

$$\left[\frac{d\sigma_{el}(Q^2)}{d\Omega'_l}\right]_{\gamma} = \left[\frac{d\sigma_{el}(Q^2)}{d\Omega'_l}\right]_0 \{1 + \delta_{\chi}^{(2)}(Q^2)\}, \quad (24)$$

where the  $\mathcal{O}(Q^2/M^2)$  fractional contributions due to the pure hadronic chiral effects are represented as

$$\delta_{\chi}^{(2)}(Q^2) = \delta_{\chi}^{(\text{rms})}(Q^2) + \delta_{\chi}^{(1/M^2)}(Q^2). \quad (25)$$

Here,

$$\begin{aligned} \delta_{\chi}^{(\text{rms})}(Q^2) &= \frac{Q^2}{3} \langle r_1^2 \rangle + \mathcal{O}\left(\frac{Q^3}{M^3}\right) \\ &= \frac{Q^2}{3} \left[ \langle r_E^2 \rangle - \frac{3\kappa_p}{2M^2} \right] + \mathcal{O}\left(\frac{Q^3}{M^3}\right) \quad (26) \end{aligned}$$

stands for the NNLO $_{\chi}$  corrections due to the proton's rms electric charge radius,  $r_p = \sqrt{\langle r_E^2 \rangle}$ , and

$$\begin{aligned} \delta_{\chi}^{(1/M^2)}(Q^2) &= \frac{1}{2} \mathcal{R}_Q \left[ 1 + 2\kappa_p + (1 + \kappa_p)^2 \right. \\ &\quad \left. \times \left( \frac{\eta Q^2 + 4(\eta m_l^2 - E^2)}{\eta Q^2 + 4E^2} \right) \right] + \mathcal{O}\left(\frac{Q^3}{M^3}\right) \quad (27) \end{aligned}$$

are  $\mathcal{O}(Q^2/M^2)$  contributions. Figure 2 displays separately the proton's NNLO $_{\chi}$  recoil and structure-dependent corrections to the LO Born  $e$ -p and  $\mu$ -p elastic scattering cross sections in the MUSE kinematic region [47,48]. These two NNLO $_{\chi}$  terms are the largest of the corrections to the LO Born contributions, each increasing to about 40% at the largest  $Q^2$  values. However, due to their opposite signs,

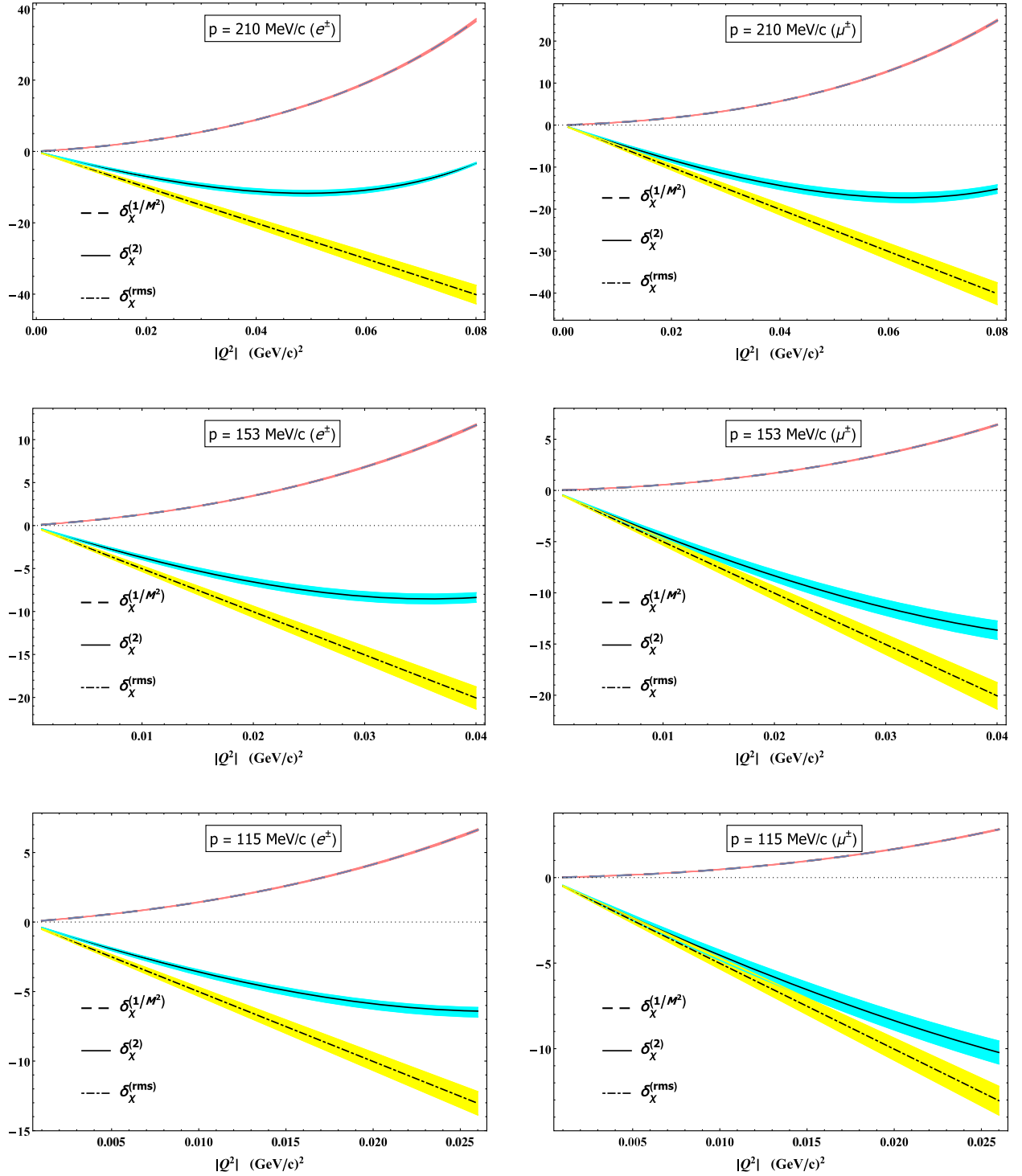


FIG. 2. The fractional chiral corrections (in percentage) to the leading-order Born elastic cross section [Eq. (23)] for  $e$ - $p$  (left panel) and  $\mu$ - $p$  (right panel) at  $\text{NNLO}_\chi$  in  $\text{HB}\chi\text{PT}$ , see Eq. (25), as a function of the squared four-momentum transfer  $|Q^2|$ . The contributions due to the proton's rms radius  $\delta_\chi^{(\text{rms})}$  [dashed-dotted (yellow) curve], recoil contributions  $\delta_\chi^{(1/M^2)}$  [dashed (red) curve], and their sum  $\delta_\chi^{(2)}$  [solid (cyan) curve] are separately displayed. Each plot covers the MUSE kinematic range of  $|Q^2|$  where the scattering angle lies within the range  $\theta \in [20^\circ, 100^\circ]$  at specific incoming lepton momenta,  $|\vec{p}| = p = 115, 153, 210$  MeV/c. The curves for the proton's rms charge radius in the above plots are varied within the range corresponding to the extracted values from the recent precision  $e$ - $p$  scattering measurements by the PRad Collaboration [21] and that from the erstwhile high-precision muonic hydrogen atomic-spectroscopy measurements by the CREMA Collaboration [11,12]. The theoretical uncertainty due to the input variation of the rms radius along with the  $\text{N}^3\text{LO}$  error are depicted by the widths of the colored bands.



there are large cancellations as observed in Fig. 2. Although the proton rms radius-dependent effects are independent of the lepton mass, the  $1/M^2$ -order effects are about one-half times smaller in muon as compared to electron scattering. The overall contributions are only somewhat sensitive to lepton mass dependence. To check the sensitivity of our chiral corrections to the input  $r_p$  value, we vary  $r_p$  within the range corresponding to the extracted value from recent precision  $e$ -p scattering measurements at the Jefferson Laboratory (PRad Collaboration) [21] and that from the high-precision muonic hydrogen atomic-spectroscopy measurements at PSI (CREMA Collaboration) [11,12]. The resulting plots for  $\delta_\chi^{(\text{rms})}$  show a sensitivity of about  $\pm 6.4\%$ . We have included both the experimental and theoretical uncertainties in quadrature (see footnote 8). These uncertainties are represented by the error bands in yellow. For the purpose of estimating the theoretical error, we have, in addition, varied each of the two chiral corrections in Fig. 2 by  $\pm 1\%$  to incorporate the uncertainties due to the  $\text{N}^3\text{LO}_\chi$  [i.e.,  $\mathcal{O}(\mathcal{Q}^3/M^3) \sim 0.008$ ] effects excluded in our analysis. The error bands in cyan associated with the total chiral corrections  $\delta_\chi^{(2)}$  [with the error bands in pink representing the  $\delta_\chi^{(1/M^2)}$  terms] yield about 7% uncertainty relative to their central estimates, after combining the two errors.

In the next section, we demonstrate that the radiative (QED) contributions are smaller in comparison to the individual chiral corrections. However, owing to the subtlety of the large chiral cancellations noted in case of  $e$ -p scattering, the otherwise power counting subdominant QED effects get effectively promoted as a serious correction to the Born cross section. Thus, estimating the crucial radiative effects along with the chiral corrections becomes a necessary precursor before attempting a precision extraction of the proton's rms charge radius.

### III. RADIATIVE CORRECTION AT $\text{LO}_\alpha$

The lowest-order radiative ( $\text{LO}_\alpha$ ) corrections to the  $\ell$ -p elastic scattering process constitute diagrams with amplitudes either of  $\mathcal{O}(e^2\alpha)$ , which arise from one-loop virtual corrections, or of  $\mathcal{O}(e^3)$ , associated with the emission of a single undetectable real soft photon. In this section, we outline all UV and IR divergences in DR arising in the analytical evaluation of the  $\text{LO}_\alpha$  contributions,  $\delta_{2\gamma}^{(0)} \sim \mathcal{O}(\alpha)$ .

The UV-divergent terms are renormalized by the Bogoliubov, Parasiuk, Hepp, and Zimmermann renormalization method [65,66] using Lagrangian counterterms to render UV-finite results. To this end, all bare Lagrangian masses, charges, coupling constants, etc., are replaced by the corresponding physical ones in the standard way. As in our previous work [58], we analytically evaluate the one-loop virtual diagrams in order to project out the complete IR-singularity structures ensuring exact cancellation with

the soft bremsstrahlung IR divergences. Note that, unlike the SPA which was invoked to allow analytical evaluation of the TPE *box amplitudes* in Ref. [58], the other one-loop virtual amplitudes in this paper will be analytically performed without any approximations. However, for the purpose of extracting the IR-singularities from the soft photon bremsstrahlung diagrams, we need to rely on SPA as a basic precept of the YFS methodology [57]. In what follows, we consider each of the *virtual* and *real* (bremsstrahlung) contributions separately.

#### A. One-loop virtual corrections at $\text{LO}_\alpha$

The one-loop diagrams contributing to the virtual radiative corrections are displayed in Fig. 3. It is notable that the SE loops renormalize the bare masses and wave functions of the external lepton and proton, but on the mass shell, such SE diagrams themselves vanish upon renormalization (these corrections are nonvanishing for internal off-shell propagator lines). Nonetheless, their expressions are needed to determine the respective wavefunction renormalization constants  $Z_2^{l,p}$ , which by virtue of *Ward-Takahashi identity* in QED is equal to the corresponding vertex renormalization constants  $Z_1^{l,p}$ . Furthermore, as previously discussed in Ref. [58], the sum of the real parts of TPE “direct” and “crossed” box diagrams at  $\text{LO}_\alpha$  in  $\text{HB}\chi\text{PT}$  (cf. diagrams in the last row of Fig. 3) vanishes with or without SPA.<sup>5</sup> The remaining one-loop contributions listed in Fig. 3 are evaluated without invoking SPA and will be discussed in the following:

##### 1. Lepton-photon vertex correction

The one-loop lepton-photon VC amplitude from the  $\text{VC}^{(0)}$  diagram in Fig. 3 using DR is well known (see, e.g., Refs. [61,66]). The VC amplitude  $\text{VC}^{(0)}$  is

$$\begin{aligned} \mathcal{M}_{\gamma\gamma;\text{vertex}}^{(0)} &= -\frac{e^2}{Q^2} [\bar{u}_l(p') \delta\Gamma_1^\mu(p, p') u_l(p)] \\ &\quad \times [\chi^\dagger(p'_p) v_\mu \chi(p_p)], \end{aligned} \quad (28)$$

and the radiative corrections to the lepton-photon vertex in terms of the Dirac and Pauli form factors,  $F_1^l = 1 + \delta F_1^l$  and Pauli  $F_2^l$ , respectively, is expressed in the general form

$$\delta\Gamma_1^\mu(p, p') = \gamma^\mu \delta F_1^l(Q^2) + \frac{i\sigma^{\mu\nu} Q_\nu}{2m_l} F_2^l(Q^2). \quad (29)$$

The evaluation of diagram  $\text{VC}^{(0)}$  yields both UV and IR divergences for the form factor  $F_1^l$ , while  $F_2^l$  is finite

<sup>5</sup>The imaginary part of the sum of the  $\text{LO}_\alpha$  TPE box amplitudes is, however, nonvanishing even after invoking SPA, but it is irrelevant in this work since it does not contribute to the unpolarized elastic cross section.

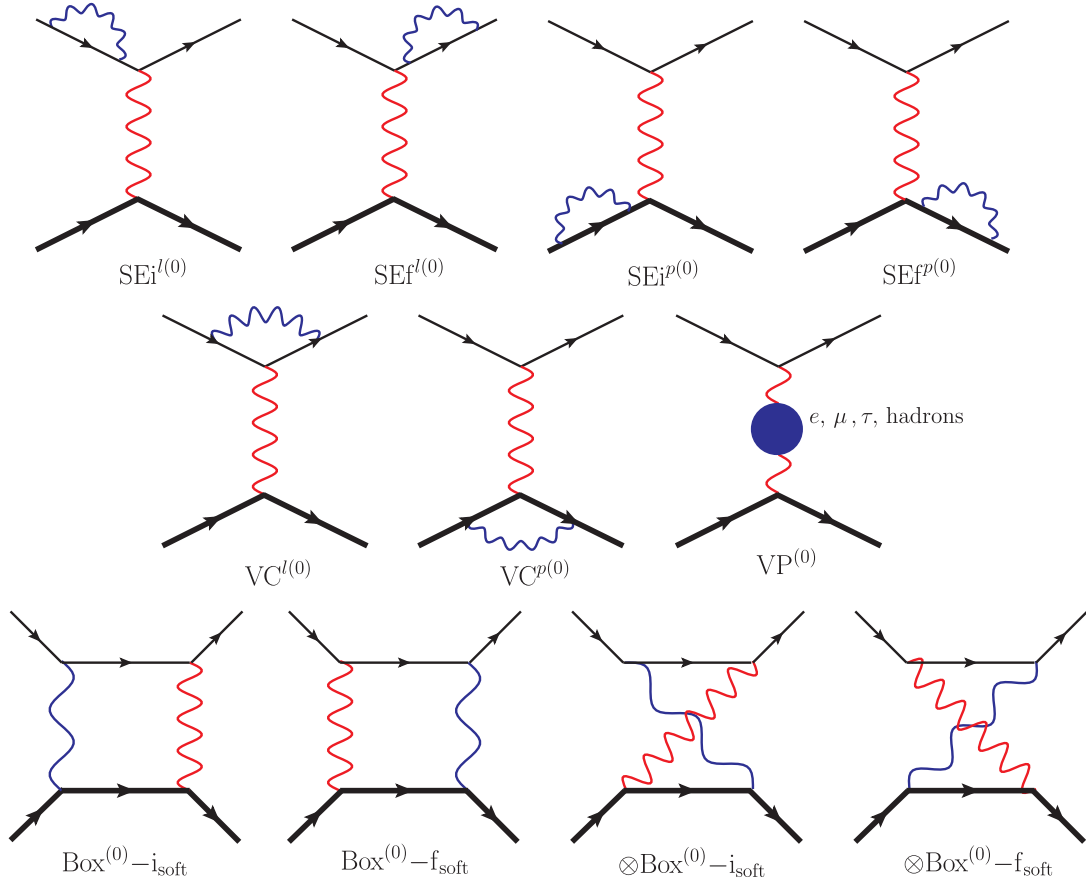


FIG. 3. The one-loop  $\mathcal{O}(e^2\alpha)$  diagrams at  $\text{LO}_\alpha$  in  $\text{HB}\chi\text{PT}$ , contributing to the virtual radiative corrections to the elastic leading-order Born  $\ell$ -p scattering amplitude [see Eq. (9)]. The blob in the diagram  $\text{VP}^{(0)}$  represents one-loop leptonic and hadronic vacuum polarization contributions. For the sake of illustration, each leading-order two-photon exchange (direct and crossed) box diagram is shown with one hard photon (red) and one soft photon (blue) exchange.

at  $\mathcal{O}(\alpha)$ . It is noteworthy that, while the ‘‘Dirac’’ part of amplitude factorizes into the Born amplitude  $\mathcal{M}_\gamma^{(0)}$ , the ‘‘Pauli’’ part does not manifest itself in the same way, namely,

$$\mathcal{M}_{\gamma\gamma;\text{vertex}}^{l(0)} = \mathcal{M}_\gamma^{(0)} \delta F_1^l(Q^2) + \overline{\mathcal{M}}_\gamma^{(0)} F_2^l(Q^2),$$

$$\text{with } \overline{\mathcal{M}}_\gamma^{(0)} = -\frac{e^2}{2m_l Q^2} [\bar{u}_l(p') i\sigma^{\mu\nu} Q_\nu u_l(p)] \times [\chi^\dagger(p'_p) v_\mu \chi(p_p)]. \quad (30)$$

As discussed, we use DR in order to simultaneously extract the UV and IR divergences from the loop diagrams. The UV divergence in space-time dimensions  $d = 4 - 2\epsilon_{\text{UV}}$  (with  $\epsilon_{\text{UV}} > 0$ ) is characterized by the pole-term proportional to  $1/\epsilon_{\text{UV}}$  and a log-dependent subtraction scale  $\mu$ . Likewise, for space-time dimensions  $d = 4 - 2\epsilon_{\text{IR}}$  (with  $\epsilon_{\text{IR}} < 0$ ), the IR-singularity appears as a pole term proportional to  $1/\epsilon_{\text{IR}}$ . The one-loop  $\text{LO}_\alpha$  expressions for the Dirac and Pauli form factor evaluated using DR are, respectively, given as [61,62]

$$\begin{aligned} \delta F_1^l(Q^2) = & \frac{\alpha}{4\pi} \left[ \left[ \frac{1}{\epsilon_{\text{UV}}} - \gamma_E + \ln\left(\frac{4\pi\mu^2}{m_l^2}\right) \right] \right. \\ & - \left. \left[ \frac{1}{|\epsilon_{\text{IR}}|} + \gamma_E - \ln\left(\frac{4\pi\mu^2}{m_l^2}\right) \right] \frac{\nu^2 + 1}{\nu} \right. \\ & \times \ln\left[\frac{\nu + 1}{\nu - 1}\right] + \frac{\nu^2 + 1}{2\nu} \ln\left[\frac{\nu + 1}{\nu - 1}\right] \\ & \times \ln\left[\frac{\nu^2 - 1}{4\nu^2}\right] + \frac{2\nu^2 + 1}{\nu} \ln\left[\frac{\nu + 1}{\nu - 1}\right] \\ & \left. - \frac{\nu^2 + 1}{\nu} \left\{ \text{Sp}\left(\frac{\nu + 1}{2\nu}\right) - \text{Sp}\left(\frac{\nu - 1}{2\nu}\right) \right\} \right], \end{aligned}$$

and

$$F_2^l(Q^2) = \frac{\alpha}{4\pi} \frac{\nu^2 - 1}{\nu} \ln\left[\frac{\nu + 1}{\nu - 1}\right], \quad (31)$$

where  $\nu = \sqrt{1 - 4m_l^2/Q^2}$  and ‘‘Sp’’ denotes the Spence function, defined as

$$\text{Sp}(x) = \int_0^x dt \frac{\ln|1-t|}{t}; \quad x < 1, \quad (32)$$

and  $\gamma_E = 0.577216\dots$  is the Euler-Mascheroni constant. Note that our definition of the Spence function differs from the standard one (e.g., as used in Ref. [61]) by an overall sign.

The UV divergence is renormalized in the standard way by adding the counterterm vertex  $(Z_1^l - 1)\gamma^\mu$  to the vertex function  $\Gamma_l^\mu$ , requiring that the total vertex function,  $\tilde{\Gamma}_l^\mu = \Gamma_l^\mu + (Z_1^l - 1)\gamma^\mu$ , defines the physical charge at  $Q^2 = 0$  according to the renormalization condition, i.e.,  $\tilde{\Gamma}_l^\mu(Q^2 = 0) = \gamma^\mu$ . The wave-function renormalization constant  $Z_2^l$  is defined by the derivative of the lepton SE function  $\Sigma_l(p)$  in the on-shell limit, namely,

$$\begin{aligned} Z_2^l &= 1 + \left. \frac{\partial \Sigma^l(p)}{\partial \not{p}} \right|_{\not{p}=m_l} + \mathcal{O}(\alpha^2) \\ &\equiv Z_1^l = 1 - \delta F_1^l(Q^2 = 0). \end{aligned} \quad (33)$$

Taking the limit  $Q^2 \rightarrow 0$  (or  $\nu \rightarrow \infty$ ), i.e.,

$$\lim_{\nu \rightarrow \infty} \frac{\nu^2 \pm 1}{\nu} \ln \left[ \frac{\nu + 1}{\nu - 1} \right] = 2, \quad (34)$$

we obtain

$$\begin{aligned} \left. \frac{\partial \Sigma^l(p)}{\partial \not{p}} \right|_{\not{p}=m_l} &= -\frac{\alpha}{4\pi} \left[ \frac{1}{\epsilon_{\text{UV}}} - \gamma_E + \ln \left( \frac{4\pi\mu^2}{m_l^2} \right) \right] \\ &+ \frac{\alpha}{2\pi} \left[ \frac{1}{\epsilon_{\text{IR}}} + \gamma_E - \ln \left( \frac{4\pi\mu^2}{m_l^2} \right) - 2 \right]. \end{aligned} \quad (35)$$

Thus, by adding the counterterm  $-\delta F_1^l(0)\gamma^\mu$ , the renormalized amplitude is given by

$$[\mathcal{M}_{\gamma\gamma;\text{vertex}}^{l(0)}]_{\text{ren}} = \mathcal{M}_\gamma^{(0)}[\delta F_1^l(Q^2) - \delta F_1^l(0)] + \bar{\mathcal{M}}_\gamma^{(0)} F_2^l(Q^2), \quad (36)$$

where  $\bar{\mathcal{M}}_\gamma^{(0)}$  is given in Eq. (30), and the renormalized one-loop expression for the Dirac form factor of the lepton is given as [61,62]

$$\begin{aligned} F_1^{l,\text{ren}}(Q^2) &= 1 + \delta F_1^l(Q^2) - \delta F_1^l(0) \\ &= 1 + \frac{\alpha}{2\pi} \left[ -\left[ \frac{1}{\epsilon_{\text{IR}}} + \gamma_E - \ln \left( \frac{4\pi\mu^2}{m_l^2} \right) \right] \left[ \frac{\nu^2 + 1}{2\nu} \ln \left[ \frac{\nu + 1}{\nu - 1} \right] - 1 \right] + \frac{\nu^2 + 1}{4\nu} \ln \left[ \frac{\nu + 1}{\nu - 1} \right] \ln \left[ \frac{\nu^2 - 1}{4\nu^2} \right] \right. \\ &\quad \left. + \frac{2\nu^2 + 1}{2\nu} \ln \left[ \frac{\nu + 1}{\nu - 1} \right] - 2 - \frac{\nu^2 + 1}{2\nu} \left\{ \text{Sp} \left( \frac{\nu + 1}{2\nu} \right) - \text{Sp} \left( \frac{\nu - 1}{2\nu} \right) \right\} \right]. \end{aligned} \quad (37)$$

Besides, the finite Pauli form factor  $F_2^l$  contributes to the lepton's spin magnetic moment as [61]

$$\vec{\mu}_S^l = \frac{e\vec{S}}{2m_l} [1 + F_2^l(Q^2 = 0)] = \frac{e\vec{S}}{2m_l} \left( 1 + \frac{\alpha}{2\pi} \right). \quad (38)$$

For  $|Q^2| \gg m_l^2$  (i.e.,  $\nu \rightarrow 1$ ) it implies that  $F_2^l \rightarrow 0$ . Hence,  $F_2^l$ 's contribution to the unpolarized scattering cross section can safely be ignored relative to  $F_1^l$  for the case of electron scattering. However, for low-energy muon scattering, e.g., at MUSE kinematics, the Pauli form factor could give significant contributions.

## 2. Proton-photon vertex correction

In the literature, the proton-photon vertex has often been modeled using phenomenological form factors, e.g., as done in Refs. [1,60]. As discussed earlier, HB $\chi$ PT allows a systematic order by order estimation of this vertex using the gauge invariant couplings of the photon with the hadrons involved. In general, one parametrizes the proton-photon vertex in terms of the nonrelativistic electric  $G_E^p$  and

magnetic  $G_M^p$  Sachs form factors which are related to the standard relativistic Dirac and Pauli form factors via

$$\begin{aligned} G_E^p(Q^2) &= F_1^p(Q^2) + \frac{Q^2}{4M^2} F_2^p(Q^2), \\ G_M^p(Q^2) &= F_1^p(Q^2) + F_2^p(Q^2). \end{aligned} \quad (39)$$

The matrix element of the electromagnetic quark current between proton states is given by

$$\begin{aligned} \langle p(P') | \bar{q}\gamma^\mu q | p(P) \rangle \\ \rightarrow \chi^\dagger(p'_p) \left[ v^\mu G_E^p(Q^2) + \frac{[S^\mu, S \cdot Q]}{M} G_M^p(Q^2) \right] \chi(p_p). \end{aligned} \quad (40)$$

In our heavy baryon formulation when including  $\mathcal{O}(\alpha)$  radiative corrections, only the proton's electric form factor  $G_E^p$  is expected to contribute, while the magnetic form factor  $G_M^p$  contributes at a higher chiral-order. This is already apparent in our  $\mathcal{O}(Q^2/M^2)$  chiral corrections to the LO Born cross section presented in Sec. II (also see

Ref. [54] for details regarding  $\chi$ PT expressions of the proton form factors). As revealed in our analysis in the next section, even the inclusion of the chiral-radiative corrections of  $\mathcal{O}(\alpha\mathcal{Q}/M)$  does not renormalize the form factors. To this end, we write  $G_E^p = G_E^{p(0)} + \delta G_E^{p(0)}$ , where  $\delta G_E^{p(0)}$  incorporates the radiative corrections to the electric form factor. Subsequently, the possible UV divergences, arising from the  $\text{LO}_\alpha$  one-loop photon corrections to the vertex function, namely,  $v^\mu G_E^{p(0)}$ , are renormalized by adding the counterterm  $(Z_1^p - 1)v^\mu$ , with the requirement that the total renormalized vertex function,  $\mathcal{V}_p^\mu = v^\mu G_E^{p(0)} + (Z_1^p - 1)v^\mu$ , defines the physical proton charge at  $Q^2 = 0$ , i.e.,  $\mathcal{V}_p^\mu(Q^2 = 0) = v^\mu$ . Similarly to the lepton counterpart, the proton wave-function renormalization constant  $Z_2^p$  can be defined as

$$\begin{aligned} Z_2^{p(0)} &= 1 + \left. \frac{\partial \Sigma^p(p_p)}{\partial (v \cdot p_p)} \right|_{v \cdot p_p = 0} + \mathcal{O}\left(\alpha^2, \frac{1}{M}\right) \\ &\equiv Z_1^{p(0)} = 1 - \delta G_E^{p(0)}(Q^2 = 0), \end{aligned}$$

where

$$\left. \frac{\partial \Sigma^p(p_p)}{\partial (v \cdot p_p)} \right|_{v \cdot p_p = 0} = -\delta G_E^{p(0)}(Q^2 = 0). \quad (41)$$

With the on-shell conditions for the external protons,  $v \cdot p_p = 0$  and  $v \cdot p'_p = -\frac{(p'_p)^2}{2M} + \mathcal{O}(M^{-2})$ , the amplitude of the diagram  $\text{VC}^{p(0)}$  in Fig. 3 is

$$\begin{aligned} \mathcal{M}_{\gamma\gamma;\text{vertex}}^{p(0)} &= \frac{ie^4}{Q^2} [\bar{u}_l(p') \gamma^\mu(p, p') u_l(p)] \\ &\times \int \frac{d^4 k}{(2\pi)^4} \frac{[\chi^\dagger(p'_p) v_\mu \chi(p_p)]}{(k^2 + i0)(-v \cdot k + i0)^2} \\ &\times \left( 1 - \frac{(p'_p)^2}{2M(v \cdot k)} + \dots \right) \\ &\equiv \mathcal{M}_\gamma^{(0)} \delta G_E^{p(0)\text{DR}}. \end{aligned} \quad (42)$$

Here, we used the fact that all scaleless loop integrals of the type

$$\mathcal{I}(m, n) = \int \frac{d^d k}{(2\pi)^d} \frac{(k^2)^m}{(-v \cdot k + i0)^n} \quad (43)$$

vanish in DR (see, e.g., Ref. [67]). Consequently, there is no contribution to the proton VC at  $\text{LO}_\alpha$ . In fact, this result is intuitively anticipated from the fact that in  $\text{HB}\chi\text{PT}$  there is no proton bremsstrahlung at this order [68]. In other words, at  $\text{LO}_\alpha$  the proton is static and unaffected by radiative correction.

### 3. Vacuum polarization

The one-loop VP contribution from diagram  $\text{VP}^{(0)}$  in Fig. 3 at  $\text{LO}_\alpha$  in  $\text{HB}\chi\text{PT}$  is IR-finite. However, it contains a logarithmic UV divergence. Its unrenormalized amplitude in terms of the bare electric charge  $e_0$  is given by

$$\begin{aligned} \mathcal{M}_{\gamma\gamma;\text{v.p.}}^{(0)} &= [\bar{u}_l(p') e_0 \gamma_\mu u_l(p)] D^{\mu\nu}(Q) \\ &\times [\chi^\dagger(p'_p) e_0 v_\nu \chi(p_p)]. \end{aligned} \quad (44)$$

The full (interacting) photon propagator expressed in terms of the polarization tensor,  $\Pi^{\mu\nu} = (Q^2 g^{\mu\nu} - Q^\mu Q^\nu) \Pi(Q^2)$ , is

$$\begin{aligned} iD^{\mu\nu}(Q) &= \frac{-ig^{\mu\nu}}{Q^2} + iD^{\mu\rho}(Q) i\Pi_{\rho\sigma}(Q) \left( \frac{-ig^{\sigma\nu}}{Q^2} \right) \\ &= \frac{-ig^{\mu\nu}}{Q^2 [1 - \Pi(Q^2)]} + \text{terms with } Q^\mu Q^\nu \\ &\simeq \frac{-ig^{\mu\nu}}{Q^2 [1 - \Pi(0)] [1 - (\Pi(Q^2) - \Pi(0))]} + \dots \end{aligned} \quad (45)$$

The UV divergence is as usual renormalized by adding the counterterm  $-(Q^2 g^{\mu\nu} - Q^\mu Q^\nu)(Z_3 - 1)$  to  $\Pi^{\mu\nu}$ , which renormalizes the photon propagator,

$$i\tilde{D}^{\mu\nu}(Q) = \frac{-ig^{\mu\nu}}{Q^2 [1 - \Pi(Q^2) + (Z_3 - 1)]} + \dots, \quad (46)$$

where the ellipses denote the ‘‘gauge terms’’ containing  $Q_\mu Q_\nu$  which do not contribute in any gauge invariant result [61]. The requirement that  $\tilde{D}^{\mu\nu}$  has a pole at  $Q^2 = 0$  with residue 1 yields  $Z_3 = 1 + \Pi(0)$ , which renormalizes the bare QED coupling,  $\alpha_0 = \alpha/Z_3$ , where  $\alpha = e^2/(4\pi) \approx 1/137$  is the physical QED coupling. Finally, the renormalized amplitude factorizes into the LO Born amplitude as

$$[\mathcal{M}_{\gamma\gamma;\text{v.p.}}^{(0)}]_{\text{ren}} = \mathcal{M}_\gamma^{(0)} \Delta\Pi(Q^2), \quad (47)$$

with the renormalized polarization function

$$\begin{aligned} \Delta\Pi(Q^2) &= \Pi(Q^2) - \Pi(0) \\ &= \Delta\Pi_{\text{lepton}}(Q^2) + \Delta\Pi_{\text{hadron}}(Q^2), \end{aligned} \quad (48)$$

receiving both leptonic  $\Delta\Pi_{\text{lepton}}$  and hadronic  $\Delta\Pi_{\text{hadron}}$  contributions at the one-loop level. Using DR, one can readily obtain the well-known expression for the one-loop leptonic vacuum polarization (LVP) contribution [61,69,70]:

$$\begin{aligned} \Delta\Pi_{\text{lepton}}(Q^2) &= \frac{\alpha}{2\pi} \sum_{f=e,\mu,\tau} \left\{ \frac{2}{3} \left( \nu_f^2 - \frac{8}{3} \right) \right. \\ &\quad \left. + \nu_f \left( \frac{3 - \nu_f^2}{3} \right) \ln \left[ \frac{\nu_f + 1}{\nu_f - 1} \right] \right\}. \end{aligned} \quad (49)$$

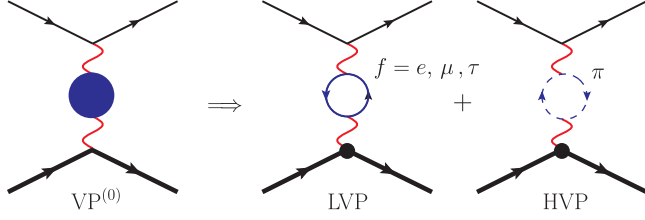


FIG. 4. The one-loop vacuum polarization diagram at  $\text{LO}_\alpha$  receives contributions from both leptonic (LVP) and hadronic (HVP) particle-antiparticle pairs. We only consider the dominant HVP due to structureless pions.

Here,  $\nu_f = \sqrt{1 - 4m_f^2/Q^2}$ , with index  $f = e, \mu, \tau$  that is used to distinguish between the different lepton flavors contributing to the fermion loop. The hadronic vacuum polarization (HVP) contribution is illustrated in Fig. 4. It only shows the contribution arising from structureless, noninteracting pions in the loop. There is no unique method to determine the contributions for the HVP contributions, and we consider a simplistic one-loop *estimate* of HVP that arises due to a  $\pi^+\pi^-$  pair, evaluated using scalar QED. In this regard, we quote the renormalized expression obtained by Tsai [71],

$$\begin{aligned} \Delta\Pi_{\text{hadron}}(Q^2) &\rightarrow \Delta\Pi_{\pi^+\pi^-}(Q^2) \\ &= \frac{\alpha}{2\pi} \left\{ -\frac{2}{3} \left( \nu_\pi^2 + \frac{1}{3} \right) + \frac{\nu_\pi^3}{3} \ln \left[ \frac{\nu_\pi + 1}{\nu_\pi - 1} \right] \right\}, \end{aligned} \quad (50)$$

where  $\nu_\pi = \sqrt{1 - 4m_\pi^2/Q^2}$ . In Fig. 5, we display the  $\mathcal{O}(\alpha)$  fractional leptonic and pionic one-loop VP contributions at

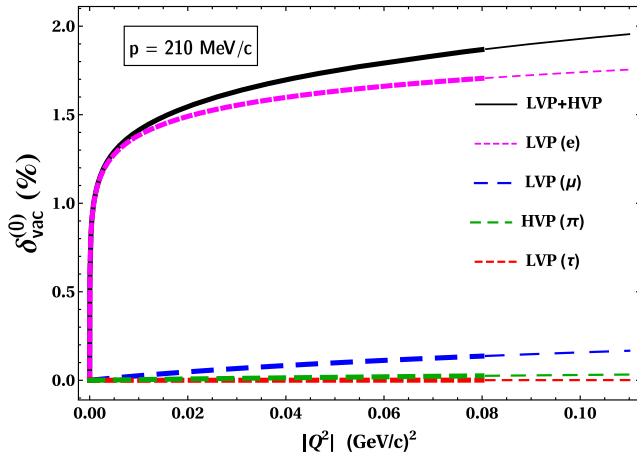


FIG. 5. The one-loop leptonic and hadronic vacuum polarization corrections  $\delta_{\text{vac};e,\mu,\tau,\pi}^{(0)}$  and their sum  $\delta_{\text{vac}}^{(0)}$ , contributing to the  $\ell$ - $p$  elastic cross section at  $\text{LO}_\alpha$ , as a function of the squared four-momentum transfer  $|Q^2|$ . The plot covers the full kinematic scattering range,  $0 < |Q^2| < |Q_{\text{max}}^2|$ , when  $\theta \in [0, \pi]$ . The thickened section of each curve corresponds to the MUSE kinematic cut, where  $\theta \in [20^\circ, 100^\circ]$ .

$\text{LO}_\alpha$ ,  $\delta_{\text{vac};f,\pi}^{(0)} = 2\Delta\Pi_{f,\pi}$ , with respect to the  $\ell$ - $p$  elastic Born cross section, Eq. (23). The results are shown for the largest incoming momentum  $p = 210 \text{ MeV}/c$  for MUSE. We note that these corrections are independent of the flavor of the incident lepton ( $\ell = e, \mu$ ) and the beam energy  $E$ . As expected, the  $e^+e^-$  loop gives the dominant contribution due to the small electron mass and is an order larger than the other VP contributions combined. It amounts to about 1.7% in the MUSE kinematic range. The  $\mu^+\mu^-$ ,  $\tau^+\tau^-$ , and  $\pi^+\pi^-$  pairs contribute about 0.15%, 0.002%, and 0.03%, respectively. Thus, the total UV finite VP contribution (i.e., LVP + HVP) at  $\text{LO}_\alpha$  is

$$\delta_{\text{vac}}^{(0)}(Q^2) = 2\Delta\Pi(Q^2) = \sum_{f=e,\mu,\tau} \delta_{\text{vac};f}^{(0)}(Q^2) + \delta_{\text{vac};\pi}^{(0)}(Q^2), \quad (51)$$

which amounts to about 2% of the elastic Born differential cross section.

#### 4. Complete one-loop virtual contribution

Adding all the nonvanishing renormalized virtual contributions from the one-loop diagrams of Fig. 3 yields the total UV-finite elastic scattering amplitude at  $\text{LO}_\alpha$ :

$$\begin{aligned} \mathcal{M}_{\gamma\gamma}^{(0)} &= \mathcal{M}_\gamma^{(0)} + [\mathcal{M}_{\gamma\gamma;\text{vertex}}^{l(0)}]_{\text{ren}} + [\mathcal{M}_{\gamma\gamma;\text{v.p.}}^{(0)}]_{\text{ren}} \\ &= \mathcal{M}_\gamma^{(0)} + \mathcal{M}_\gamma^{(0)} [F_1^{l;\text{ren}}(Q^2) - 1 + \Delta\Pi(Q^2)] \\ &\quad + \overline{\mathcal{M}}_\gamma^{(0)} F_2^l(Q^2). \end{aligned} \quad (52)$$

Here,  $F_1^{l;\text{ren}}$  is the UV renormalized one-loop leptonic Dirac form factor given in Eq. (37), and  $F_2^l$  is the one-loop *finite* leptonic Pauli form factor given in Eq. (31). The renormalized VP corrections  $\Delta\Pi$  are obtained from Eqs. (49) and (50), and the amplitude  $\overline{\mathcal{M}}_\gamma^{(0)}$  is given in Eq. (30). The IR divergences arising from the photon loops are contained in the factor multiplying the Born amplitude  $\mathcal{M}_\gamma^{(0)}$ . The lab frame  $\text{LO}_\alpha$  radiative correction to the elastic differential cross section becomes

$$\Delta \left[ \frac{d\sigma_{el}^{(\text{LO})}(Q^2)}{d\Omega'_l} \right]_{\gamma\gamma} = \left[ \frac{d\sigma_{el}(Q^2)}{d\Omega'_l} \right]_0 \delta_{\gamma\gamma}^{(0)}(Q^2), \quad (53)$$

with

$$\begin{aligned} \delta_{\gamma\gamma}^{(0)}(Q^2) &= \frac{2\text{Re} \sum_{\text{spins}} (\mathcal{M}_\gamma^{(0)\dagger} \mathcal{M}_{\gamma\gamma}^{(0)})}{\sum_{\text{spins}} |\mathcal{M}_\gamma^{(0)}|^2} - 2 \\ &= \mathbf{IR}_{\gamma\gamma}^{(0)}(Q^2) + \overline{\delta}_{\gamma\gamma}^{(0)}(Q^2), \end{aligned} \quad (54)$$

representing the  $\mathcal{O}(\alpha)$  fractional contribution from the virtual photon loops at  $\text{LO}_\alpha$ . The IR-divergent part is contained in  $\mathbf{IR}_{\gamma\gamma}^{(0)}(Q^2)$ . The corresponding finite part

$\bar{\delta}_{\gamma\gamma}^{(0)}$  includes the  $\text{LO}_\alpha$  lepton-photon VC contributions  $\bar{\delta}_{\gamma\gamma;1,2}^{(0)}$ , as extracted from Eq. (52), namely, the contribution from the lepton Dirac form factor,

$$\bar{\delta}_{\gamma\gamma;1}^{(0)}(Q^2) = 2[F_1^{l;\text{ren}}(Q^2) - 1] - \mathbf{IR}_{\gamma\gamma}^{(0)}(Q^2), \quad (55)$$

and that from the lepton Pauli form factor,

$$\begin{aligned} \delta_{\gamma\gamma;2}^{(0)}(Q^2) &= \frac{2\text{Re}\sum_{\text{spins}}(\mathcal{M}_\gamma^{(0)\dagger}\overline{\mathcal{M}}_\gamma^{(0)})}{\sum_{\text{spins}}|\mathcal{M}_\gamma^{(0)}|^2} F_2^l(Q^2) = -\left(\frac{2\eta Q^2}{\eta Q^2 + 4E^2}\right) \left(1 - \frac{Q^2}{4M^2}\right) F_2^l(Q^2) \\ &= \frac{\alpha}{\pi\nu} \left(\frac{2\eta m_l^2}{\eta Q^2 + 4E^2}\right) \ln\left[\frac{\nu+1}{\nu-1}\right] + \mathcal{O}\left(\alpha\frac{Q^2}{M^2}\right), \end{aligned} \quad (56)$$

where the above  $1/M^2$ -order term is dropped from our central result presented below. However, these  $1/M^2$ -order terms will be included as a part of the theoretical error estimate. The finite part includes the total  $\text{LO}_\alpha$  VP contribution,  $\delta_{\text{vac}}^{(0)} = 2\Delta\Pi(Q^2)$ , obtained earlier in this section. Thus, the total finite fractional virtual radiative corrections at  $\text{LO}_\alpha$  read

$$\begin{aligned} \bar{\delta}_{\gamma\gamma}^{(0)}(Q^2) &= \bar{\delta}_{\gamma\gamma;1}^{(0)}(Q^2) + \delta_{\gamma\gamma;2}^{(0)}(Q^2) + \sum_{f=e,\mu,\tau} \delta_{\text{vac};f}^{(0)}(Q^2) + \delta_{\text{vac};\pi}^{(0)}(Q^2) \\ &= \frac{\alpha}{\pi} \left[ \frac{\nu^2+1}{4\nu} \ln\left[\frac{\nu+1}{\nu-1}\right] \ln\left[\frac{\nu^2-1}{4\nu^2}\right] + \ln\left(\frac{-Q^2}{m_l^2}\right) \left[ \frac{\nu^2+1}{2\nu} \ln\left[\frac{\nu+1}{\nu-1}\right] - 1 \right] + \frac{2\nu^2+1}{2\nu} \ln\left[\frac{\nu+1}{\nu-1}\right] \right. \\ &\quad \left. - 2 - \frac{\nu^2+1}{2\nu} \left\{ \text{Sp}\left(\frac{\nu+1}{2\nu}\right) - \text{Sp}\left(\frac{\nu-1}{2\nu}\right) \right\} + \sum_{f=e,\mu,\tau} \left\{ \frac{2}{3} \left(\nu_f^2 - \frac{8}{3}\right) + \nu_f \left(\frac{3-\nu_f^2}{3}\right) \ln\left[\frac{\nu_f+1}{\nu_f-1}\right] \right\} \right. \\ &\quad \left. - \frac{2}{3} \left(\nu_\pi^2 + \frac{1}{3}\right) + \frac{\nu_\pi^3}{3} \ln\left[\frac{\nu_\pi+1}{\nu_\pi-1}\right] + \frac{1}{\nu} \left(\frac{2\eta m_l^2}{\eta Q^2 + 4E^2}\right) \ln\left[\frac{\nu+1}{\nu-1}\right] \right] + \mathcal{O}\left(\alpha\frac{Q^2}{M^2}\right). \end{aligned} \quad (57)$$

The IR-divergent part of Eqs. (54) and (55),  $\mathbf{IR}_{\gamma\gamma}^{(0)}(Q^2)$ , which essentially stems from the ‘‘Dirac’’ contribution to the one-loop lepton-photon VC at  $\text{LO}_\alpha$ , Eq. (37), is given as

$$\mathbf{IR}_{\gamma\gamma}^{(0)}(Q^2) \equiv \mathbf{IR}_{\gamma\gamma;\text{vertex}}^{l(0)}(Q^2) = -\frac{\alpha}{\pi} \left[ \frac{1}{|\epsilon_{\text{IR}}|} + \gamma_E - \ln\left(\frac{4\pi\mu^2}{-Q^2}\right) \right] \left[ \frac{\nu^2+1}{2\nu} \ln\left[\frac{\nu+1}{\nu-1}\right] - 1 \right]. \quad (58)$$

In Sec. III B, we show that this IR divergence is canceled by the IR divergence from the soft-bremsstrahlung process at  $\text{LO}_\alpha$ . Figure 6 displays the  $\text{LO}_\alpha$  fractional contributions from the lepton-photon VC terms,  $\bar{\delta}_{\gamma\gamma;1}^{(0)}$  and  $\delta_{\gamma\gamma;2}^{(0)}$ , stemming from the form factors  $F_1^{l;\text{ren}}$  and  $F_2^l$ , respectively, for the full kinematic elastic scattering range  $0 < |Q^2| < |Q_{\text{max}}^2|$  of the MUSE specified incoming lepton momenta. A summary of our observations is in order:

- (i) All the radiative corrections vanish in the limit  $Q^2 \rightarrow 0$ , as dictated by gauge invariance.
- (ii) There is no  $\text{LO}_\alpha$  contribution from the TPE box diagrams, even without invoking SPA.
- (iii) The lepton Dirac form factor contribution is basically independent of the lepton beam energy.
- (iv) In contrast, the lepton Pauli form factor contribution depends strongly on the beam momentum. For electron scattering in the MUSE momentum range, the contributions are practically negligible, about  $10^{-5}\%$ . However, for muon scattering, the

relative corrections turn out to be much larger, about  $10^{-1}\%$ .

- (v) The electronic and muonic Dirac form factor contributions in the region of low momentum transfers,  $|Q^2| < 0.1 (\text{GeV}/c)^2$ , differ by almost 2 orders of magnitudes. The reason is that the electronic Dirac term  $\bar{\delta}_{\gamma\gamma;1}^{l(0)}$  is enhanced in the soft and *collinear* region of the loop-momentum integration resulting from the so-called *Sudakov* double-logarithms, namely,

$$\begin{aligned} &\frac{\nu^2+1}{4\nu} \ln\left[\frac{\nu+1}{\nu-1}\right] \ln\left[\frac{\nu^2-1}{4\nu^2}\right] \\ &+ \frac{\nu^2+1}{2\nu} \ln\left(\frac{-Q^2}{m_l^2}\right) \ln\left[\frac{\nu+1}{\nu-1}\right] \approx \frac{1}{2} \ln^2\left(\frac{-Q^2}{m_l^2}\right), \end{aligned}$$

in the limit of a small lepton mass (i.e.,  $m_l^2 \ll |Q^2|$ ). However, for muon scattering at MUSE kinematics where  $m_\mu^2 = 0.01 \text{ GeV}^2 \approx |Q^2|$ , no such enhancements are manifest.

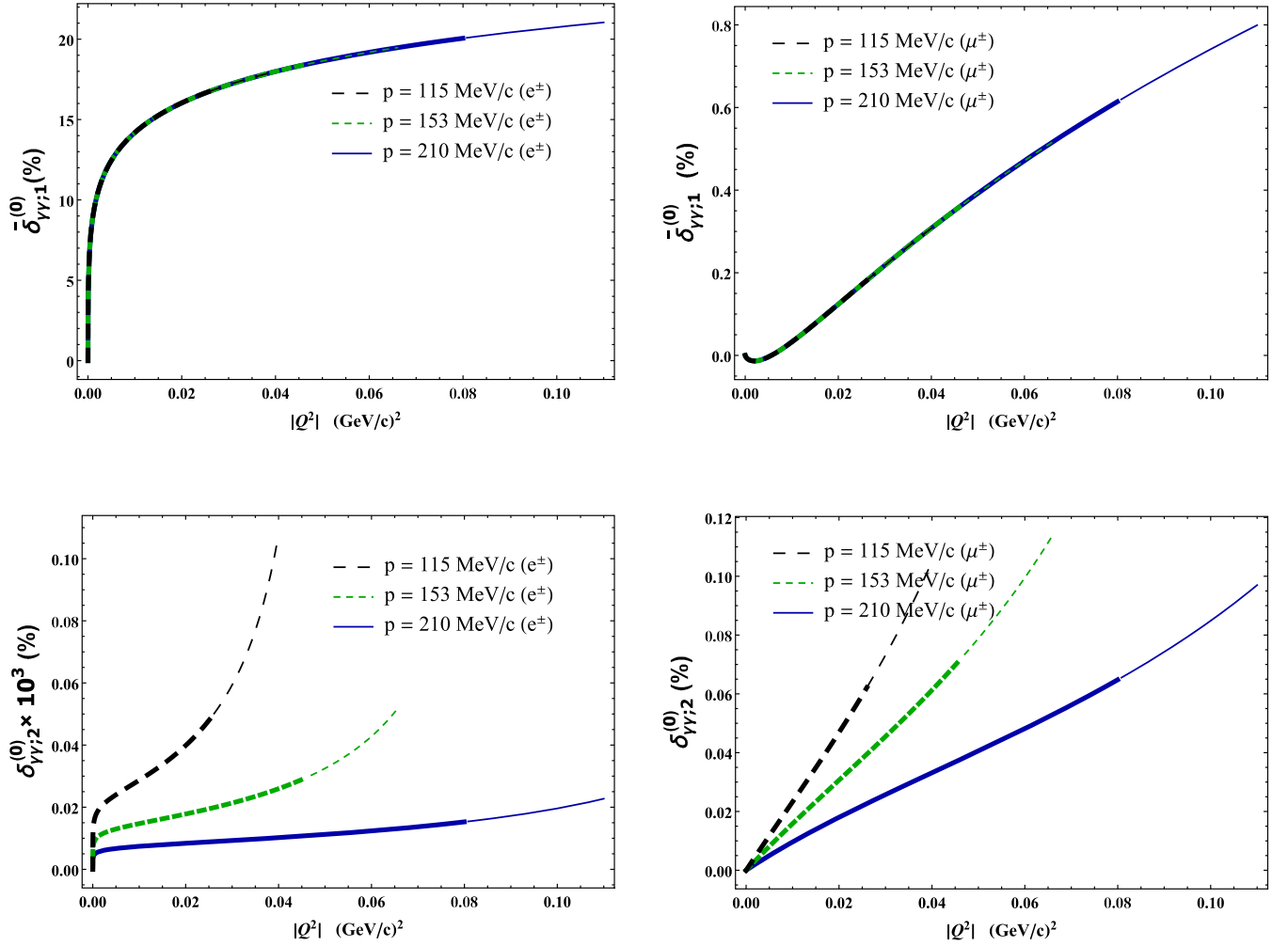


FIG. 6. The one-loop  $\text{LO}_\alpha$  contributions  $\bar{\delta}_{\gamma\gamma,1}^{(0)}$  (upper panel) and  $\delta_{\gamma\gamma,2}^{(0)}$  (lower panel) to the  $e$ - $p$  (left panel) and  $\mu$ - $p$  (right panel) elastic cross sections (in percentage) from the finite lepton-photon vertex corrections terms containing the (UV and IR-finite) form factors  $F_{1,\text{ren}}^l$  and  $F_2^l$ . Each plot covers the full kinematic scattering range,  $0 < |Q^2| < |Q_{\text{max}}^2|$ , when  $\theta \in [0, \pi]$  at the incoming lepton momenta,  $|\vec{p}| = p = 115, 153, 210$  MeV/c. The thickened section of each curve corresponds to the MUSE kinematic cut, where  $\theta \in [20^\circ, 100^\circ]$ .

### B. Soft bremsstrahlung corrections at $\text{LO}_\alpha$

A review of known results using standard field theoretical techniques can be found in, e.g., Refs. [1,59–62]. We reevaluated the bremsstrahlung process,  $\ell p \rightarrow \ell p \gamma^*$ , in our HB $\chi$ PT work of Ref. [68]. By virtue of transversality of real photons with polarization four-vector  $\varepsilon_\mu$ , namely,  $k \cdot \varepsilon = 0$ , the Coulomb gauge condition,  $v \cdot \varepsilon = 0$ , is naturally satisfied for the bremsstrahlung process.

Consequently, with the  $\text{LO}_\alpha$  proton-photon vertex in heavy baryon formalism proportional to  $v \cdot \varepsilon^*$ , the “static” proton does not radiate at the leading chiral-order. Therefore, in this case, the lowest-order soft bremsstrahlung process consists of a single soft photon that is emitted from either the incoming lepton, diagram  $\text{Ri}^{l(0)}$ , or the outgoing one, diagram  $\text{Rf}^{l(0)}$ , as displayed in Fig. 7, with amplitudes given as

$$\begin{aligned} \mathcal{M}_{\gamma\gamma^*}^{l(0);i} &= -e^3 \int \frac{d^4 k}{(2\pi)^4} \left[ \bar{u}_l(p'') \gamma^\mu \frac{(\not{p} - \not{k} + m)}{(p-k)^2 - m_l^2} \not{\varepsilon}^* u_l(p) \right] \frac{1}{(Q-k)^2} [\chi^\dagger(p'_p) v_\mu \chi(p_p)], \quad \text{and} \\ \mathcal{M}_{\gamma\gamma^*}^{l(0);f} &= -e^3 \int \frac{d^4 k}{(2\pi)^4} \left[ \bar{u}_l(p'') \not{\varepsilon}^* \frac{(\not{p}'' + \not{k} + m)}{(p''+k)^2 - m_l^2} \gamma^\mu u_l(p) \right] \frac{1}{(Q-k)^2} [\chi^\dagger(p'_p) v_\mu \chi(p_p)]. \end{aligned} \quad (59)$$

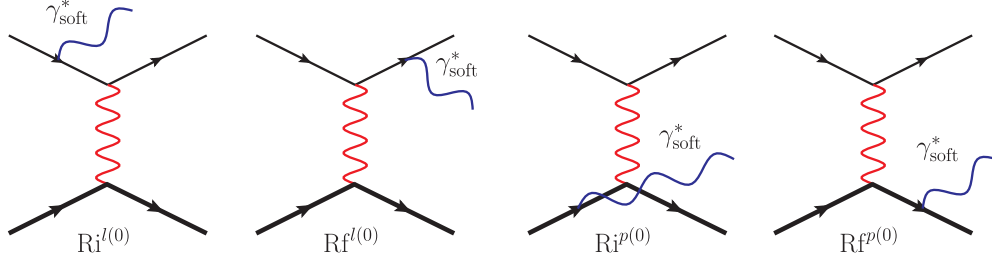


FIG. 7. Soft bremsstrahlung diagrams at  $\text{LO}_\alpha$  [i.e.,  $\mathcal{O}(e^3)$ ] in  $\text{HB}\chi\text{PT}$  contributing to the radiative corrections to the elastic leading-order (Born)  $\ell$ - $p$  scattering amplitude [see Eq. (9)]. The proton radiating diagrams vanish.

In the above expressions,  $k_\mu$  is the four-momentum of the bremsstrahlung photon, and  $p''_\mu$  is the four-momentum of the inelastically scattered outgoing lepton. In this paper, we are only concerned with the undetectable soft photon emissions. Thus, by the YFS methodology [57], the real photon emission amplitudes are evaluated using SPA, where SPA regards  $p''_\mu$  as the physical four-momentum of the *elastically* scattered lepton. Henceforth, for reasons of brevity, we drop all distinctions between the  $p'_\mu$  and  $p''_\mu$ , unless explicitly mentioned. In SPA, the photon momentum of the propagator numerator is taken to be zero, i.e.,  $k_\mu \rightarrow 0$ , with the crucial assumption that the soft emissions does not alter the elastic kinematics. In other words, in this limit, the four-momentum transfer for the bremsstrahlung process,  $q_\mu = (Q - k)_\mu$ , is practically indistinguishable from its elastic counterpart,  $Q_\mu = (p - p')_\mu = (P' - P)_\mu$ . Then, the matrix elements

get factorized into the LO (Born) amplitude  $\mathcal{M}_\gamma^{(0)}$ , namely,

$$\begin{aligned} \mathcal{M}_{\gamma\gamma^*}^{l(0);i} \xrightarrow{\gamma_{\text{soft}}^*} \widetilde{\mathcal{M}}_{\gamma\gamma^*}^{l(0);i} &= e\mathcal{M}_\gamma^{(0)} \left( \frac{p \cdot \varepsilon^*}{p \cdot k} \right), \\ \mathcal{M}_{\gamma\gamma^*}^{l(0);f} \xrightarrow{\gamma_{\text{soft}}^*} \widetilde{\mathcal{M}}_{\gamma\gamma^*}^{l(0);f} &= -e\mathcal{M}_\gamma^{(0)} \left( \frac{p' \cdot \varepsilon^*}{p' \cdot k} \right). \end{aligned} \quad (60)$$

Taking the square of the total  $\text{LO}_\alpha$  bremsstrahlung matrix element,  $\mathcal{M}_{\gamma\gamma^*}^{(0)} = \mathcal{M}_{\gamma\gamma^*}^{l(0);i} + \mathcal{M}_{\gamma\gamma^*}^{l(0);f}$ , in SPA yields a cross section in accordance with the well-known Low's soft photon theorem [72]. This implies that in terms of the bremsstrahlung soft photon energy, the first two terms in the expansion of the unpolarized radiative cross section depend only on the corresponding nonradiative unpolarized cross section. Thus, the lab frame differential cross section for the  $\text{LO}_\alpha$  bremsstrahlung process is given by the expression

$$[\text{d}\sigma_{\text{br}}^{(\text{LO}_\alpha)}]_{\gamma\gamma^*} = \frac{\text{d}^3\vec{p}'}{(2\pi)^3 2E'} \frac{\text{d}^3\vec{P}'}{(2\pi)^3 2E'_p} \frac{\text{d}^3\vec{k}}{(2\pi)^3 2E_\gamma} \frac{(2\pi)^4 \delta^4(p + P - p' - P' - k)}{4ME} \frac{1}{4} \sum_{\text{spins}} |\mathcal{M}_{\gamma\gamma^*}^{(0)}|^2, \quad (61)$$

where

$$\begin{aligned} \sum_{\text{spin}} |\mathcal{M}_{\gamma\gamma^*}^{(0)}|^2 &\equiv |\mathcal{M}_{\gamma\gamma^*}^{l(0);i} + \mathcal{M}_{\gamma\gamma^*}^{l(0);f}|^2 \xrightarrow{\gamma_{\text{soft}}^*} |\widetilde{\mathcal{M}}_{\gamma\gamma^*}^{l(0);i} + \widetilde{\mathcal{M}}_{\gamma\gamma^*}^{l(0);f}|^2 \\ &= -e^2 \sum_{\text{spins}} |\mathcal{M}_\gamma^{(0)}|^2 \left( \frac{m_l^2}{(p \cdot k)^2} + \frac{m_l^2}{(p' \cdot k)^2} - \frac{2p' \cdot p}{(p \cdot k)(p' \cdot k)} \right). \end{aligned} \quad (62)$$

The phase-space integrated cross section also factorizes into the Born cross section, Eq. (23), and reads

$$\begin{aligned} \Delta \left[ \frac{\text{d}\sigma_{\text{br}}^{(\text{LO})}(Q^2)}{\text{d}\Omega'_l} \right]_{\gamma\gamma^*} &\xrightarrow{\gamma_{\text{soft}}^*} \frac{\alpha}{2\pi^2} \left[ \frac{\text{d}\sigma_{\text{el}}(Q^2)}{\text{d}\Omega'_l} \right]_0 \\ &\times (-L_{\text{ii}} - L_{\text{ff}} + L_{\text{if}}). \end{aligned} \quad (63)$$

The integrals,  $L_{\text{ii}}$ ,  $L_{\text{ff}}$ , and  $L_{\text{if}}$ , are three-momentum integrals involving the soft photons radiated by the leptons. They are evaluated in Appendix B using the method of,

e.g., Refs. [1,59–62]. The integrals,  $L_{\text{ii}}$ ,  $L_{\text{ff}}$ , and  $L_{\text{if}}$ , are all IR-divergent. As demonstrated in the Appendix B, we isolate the corresponding finite contributions,  $\tilde{L}_{\text{ii}}$ ,  $\tilde{L}_{\text{ff}}$ , and  $\tilde{L}_{\text{if}}$ , using DR. This yields the lab frame  $\text{LO}_\alpha$  bremsstrahlung correction to the elastic differential cross section with all possible soft photon emissions with energies less than  $\Delta_{\gamma^*}$ ,

$$\Delta \left[ \frac{\text{d}\sigma_{\text{br}}^{(\text{LO})}(Q^2)}{\text{d}\Omega'_l} \right]_{\gamma\gamma^*}^{(E_{\gamma^*} < \Delta_{\gamma^*})} = \left[ \frac{\text{d}\sigma_{\text{el}}(Q^2)}{\text{d}\Omega'_l} \right]_0 \delta_{\gamma\gamma^*}^{(0)}(Q^2), \quad (64)$$



where the  $\mathcal{O}(\alpha)$  fractional bremsstrahlung contribution  $\delta_{\gamma\gamma^*}^{(0)}$  at  $\text{LO}_\alpha$  reads [1,61]

$$\delta_{\gamma\gamma^*}^{(0)}(Q^2) = \mathbf{IR}_{\gamma\gamma^*}^{(0)}(Q^2) + \bar{\delta}_{\gamma\gamma^*}^{(0)}(Q^2), \quad (65)$$

with

$$\mathbf{IR}_{\gamma\gamma^*}^{(0)}(Q^2) \equiv \mathbf{IR}_{\gamma\gamma^*}^{l(0)}(Q^2) = \frac{\alpha}{\pi} \left[ \frac{1}{|\epsilon_{\text{IR}}|} + \gamma_E - \ln\left(\frac{4\pi\mu^2}{-Q^2}\right) \right] \left[ \frac{\nu^2 + 1}{2\nu} \ln\left[\frac{\nu + 1}{\nu - 1}\right] - 1 \right] \quad (66)$$

being the IR-divergent term, and the finite part of the  $\text{LO}_\alpha$  bremsstrahlung contribution is represented by

$$\begin{aligned} \bar{\delta}_{\gamma\gamma^*}^{(0)}(Q^2) &= \frac{\alpha}{\pi} (-\tilde{L}_{\text{ii}} - \tilde{L}_{\text{ff}} + \tilde{L}_{\text{if}}) \\ &= \frac{\alpha}{\pi} \left[ \ln\left(\frac{4\eta^2\Delta_{\gamma^*}^2}{-Q^2}\right) \left[ \frac{\nu^2 + 1}{2\nu} \ln\left[\frac{\nu + 1}{\nu - 1}\right] - 1 \right] + \frac{1}{4\beta} \ln\sqrt{\frac{1+\beta}{1-\beta}} + \frac{1}{4\beta'} \ln\sqrt{\frac{1+\beta'}{1-\beta'}} \right. \\ &\quad - \frac{\nu^2 + 1}{2\nu} \left\{ \ln^2\sqrt{\frac{1+\beta}{1-\beta}} - \ln^2\sqrt{\frac{1+\beta'}{1-\beta'}} + \text{Sp}\left(1 - \frac{\lambda_\nu - \eta}{(1-\beta')\xi_\nu}\right) + \text{Sp}\left(1 - \frac{\lambda_\nu - \eta}{(1+\beta')\xi_\nu}\right) \right. \\ &\quad \left. \left. - \text{Sp}\left(1 - \frac{\lambda_\nu - \eta}{(1-\beta)\eta\lambda_\nu\xi_\nu}\right) - \text{Sp}\left(1 - \frac{\lambda_\nu - \eta}{(1+\beta)\eta\lambda_\nu\xi_\nu}\right) \right\} \right], \quad (67) \end{aligned}$$

where  $\nu$  is defined below Eq. (31), and  $\xi_\nu = \frac{2\nu}{(\nu+1)(\nu-1)}$  and  $\lambda_\nu = \frac{3\nu-1}{\nu-1}$  are  $Q^2$ -dependent kinematic variables. The IR-divergent term  $\mathbf{IR}_{\gamma\gamma^*}^{(0)}$  from the  $\text{LO}_\alpha$  bremsstrahlung diagrams, being equal and opposite to the  $\text{LO}_\alpha$  one-loop IR-divergent counterpart  $\mathbf{IR}_{\gamma\gamma}^{(0)}$  [cf. Eq. (58)], exactly cancels out in the sum of the  $\text{LO}_\alpha$  real and virtual radiative contributions. Thus, the resulting finite contribution is

$$\delta_{2\gamma}^{(0)}(Q^2) = \delta_{\gamma\gamma}^{(0)}(Q^2) + \delta_{\gamma\gamma^*}^{(0)}(Q^2) \equiv \bar{\delta}_{\gamma\gamma}^{(0)}(Q^2) + \bar{\delta}_{\gamma\gamma^*}^{(0)}(Q^2). \quad (68)$$

### C. Total radiative corrections at $\text{LO}_\alpha$

After eliminating all the UV and IR divergences, we obtain the desired analytical result for the complete radiative contributions at  $\text{LO}_\alpha$  in HB $\chi$ PT. The finite one-loop  $\mathcal{O}(\alpha)$  expression for the  $\text{LO}_\alpha$  fractional radiative corrections to the  $\ell$ -p elastic differential cross section is given by the expression

$$\begin{aligned} \delta_{2\gamma}^{(0)} &= \frac{\alpha}{\pi} \left[ \frac{\nu^2 + 1}{4\nu} \ln\left[\frac{\nu + 1}{\nu - 1}\right] \ln\left[\frac{\nu^2 - 1}{4\nu^2}\right] + \frac{2\nu^2 + 1}{2\nu} \ln\left[\frac{\nu + 1}{\nu - 1}\right] - \frac{\nu^2 + 1}{2\nu} \left\{ \text{Sp}\left(\frac{\nu + 1}{2\nu}\right) - \text{Sp}\left(\frac{\nu - 1}{2\nu}\right) \right\} \right. \\ &\quad - 2 + \sum_{f=e,\mu,\tau} \left\{ \frac{2}{3} \left( \nu_f^2 - \frac{8}{3} \right) + \nu_f \left( \frac{3 - \nu_f^2}{3} \right) \ln\left[\frac{\nu_f + 1}{\nu_f - 1}\right] \right\} - \frac{2}{3} \left( \nu_\pi^2 + \frac{1}{3} \right) + \frac{\nu_\pi^3}{3} \ln\left[\frac{\nu_\pi + 1}{\nu_\pi - 1}\right] \\ &\quad + \frac{1}{\nu} \left( \frac{2\eta m_l^2}{\eta Q^2 + 4E^2} \right) \ln\left[\frac{\nu + 1}{\nu - 1}\right] + \ln\left(\frac{4\eta^2\Delta_{\gamma^*}^2}{m_l^2}\right) \left[ \frac{\nu^2 + 1}{2\nu} \ln\left[\frac{\nu + 1}{\nu - 1}\right] - 1 \right] + \frac{1}{4\beta} \ln\sqrt{\frac{1+\beta}{1-\beta}} \\ &\quad + \frac{1}{4\beta'} \ln\sqrt{\frac{1+\beta'}{1-\beta'}} - \frac{\nu^2 + 1}{2\nu} \left\{ \ln^2\sqrt{\frac{1+\beta}{1-\beta}} - \ln^2\sqrt{\frac{1+\beta'}{1-\beta'}} + \text{Sp}\left(1 - \frac{\lambda_\nu - \eta}{(1-\beta')\xi_\nu}\right) \right. \\ &\quad \left. + \text{Sp}\left(1 - \frac{\lambda_\nu - \eta}{(1+\beta')\xi_\nu}\right) - \text{Sp}\left(1 - \frac{\lambda_\nu - \eta}{(1-\beta)\eta\lambda_\nu\xi_\nu}\right) - \text{Sp}\left(1 - \frac{\lambda_\nu - \eta}{(1+\beta)\eta\lambda_\nu\xi_\nu}\right) \right\} \right] + \mathcal{O}\left(\frac{Q^2}{M^2}\right). \quad (69) \end{aligned}$$

Apart from the pionic VP contribution result of Tsai [71] that is included in above expression, the remaining expression is by and large identical to what is found in the literature [1,59–62].

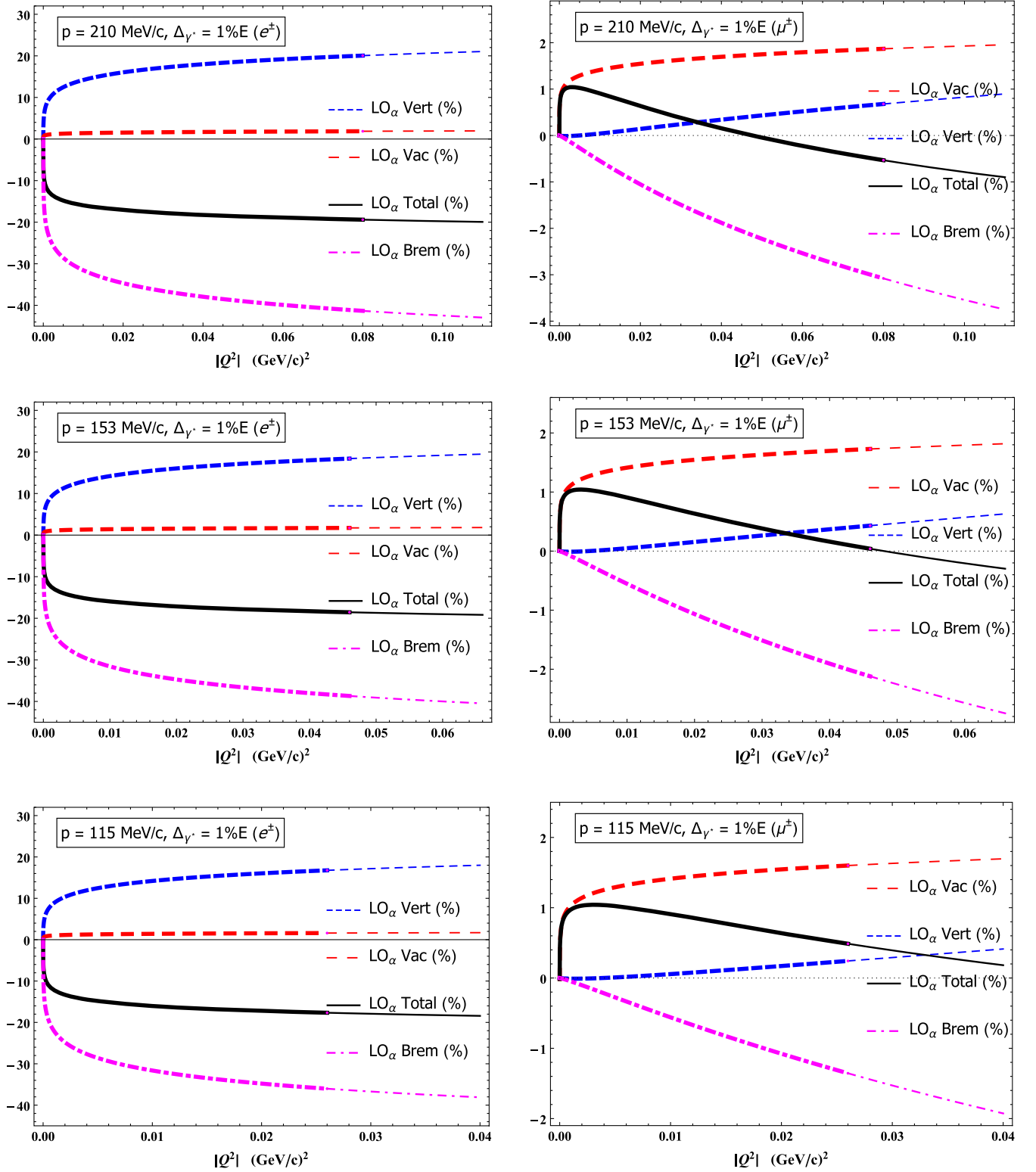


FIG. 8. The individual one-loop LO $_\alpha$  contributions (in percentage), namely, the vacuum polarization correction  $\delta_{\text{vac}}^{(0)}$ , lepton-photon vertex correction  $\delta_{\gamma\gamma;\text{vertex}}^{(0)}$ , and the soft photon bremsstrahlung correction  $\delta_{\gamma\gamma}^{(0)}$ , to the  $e^\pm$ -p (left panels) and  $\mu^\pm$ -p (right panels) elastic cross sections as a function of the squared four-momentum transfer  $|Q^2|$ . The total LO $_\alpha$  contribution  $\bar{\delta}_{\gamma\gamma}^{(0)}$  is displayed as the solid (black) line. Each plot covers the full kinematically allowed scattering range,  $0 < |Q^2| < |Q_{\text{max}}^2|$ , when  $\theta \in [0, \pi]$  (cf. Table I of Ref. [58]). The thickened portion of each curve corresponds to the MUSE kinematic cut, where  $\theta \in [20^\circ, 100^\circ]$ . The lab frame detector acceptance  $\Delta_{\gamma^*}$  is taken to be 1% of the incident lepton beam energy  $E$ .

In Fig. 8, we summarize all the fractional radiative corrections to the  $\ell$ -p elastic cross section at  $\text{LO}_\alpha$  in  $\text{HB}\chi\text{PT}$ , namely, the VP correction,  $\delta_{\text{vac}}^{(0)} = \sum_{f=e,\mu,\tau} \delta_{\text{vac};f}^{(0)} + \delta_{\text{vac};\pi}^{(0)}$ ; the lepton-photon VC,  $\bar{\delta}_{\gamma\gamma;\text{vertex}}^{(0)} = \bar{\delta}_{\gamma\gamma;1}^{(0)} + \delta_{\gamma\gamma;2}^{(0)}$ ; and the soft bremsstrahlung correction  $\bar{\delta}_{\gamma\gamma^*}^{(0)}$ , in the MUSE kinematic range. A *key feature* of these  $\text{LO}_\alpha$  radiative corrections is that they are *charge-symmetric*; viz., the cross sections are identical for both  $\ell^-$ -p and  $\ell^+$ -p scatterings. We find that the negative bremsstrahlung contribution is the most dominant correction in this low- $|Q^2|$  range. In contrast, the lepton-photon VC and VP correction are both positive. The plots in essence suggests very little sensitivity of the radiative corrections to the incoming lepton beam momenta. While the VP contributions are identical in both electron and muon scatterings, the following observations

depict the contrasting nature of the other two  $\text{LO}_\alpha$  radiative corrections, viz., the lepton-photon vertex and soft bremsstrahlung corrections, associated with MUSE kinematics:

- (i) While both electronic VC and the soft photon bremsstrahlung contributions are very large and of comparable magnitudes, the muonic VC is roughly 2 orders of magnitude smaller. One reason for this contrast is evidently the absence of *Sudakov enhancement* in muonic scattering since  $m_\mu^2 \approx |Q^2|$ , as mentioned earlier.
- (ii) The electron and muon bremsstrahlung corrections are both negative, but the latter is over a magnitude smaller. Here, too, the Sudakov enhancement of the term  $\bar{\delta}_{\gamma\gamma^*}^{(0)}$  plays a vital role, which can be seen as follows. In the limit of small lepton mass (i.e.,  $m_l^2 \ll |Q^2|$ ), we obtain

$$\bar{\delta}_{\gamma\gamma^*}^{(0)}(Q^2) \stackrel{Q^2 \gg m_l^2}{\approx} \frac{\alpha}{\pi} \left[ \ln\left(\frac{\eta^3 \Delta_{\gamma^*}^2}{E^2}\right) \left[ \ln\left(\frac{-Q^2}{m_l^2}\right) - 1 \right] - \frac{1}{2} \ln^2\left(\frac{-Q^2}{m_l^2}\right) + \ln\left(\frac{-Q^2}{m_l^2}\right) - \frac{1}{2} \ln^2 \eta - \frac{\pi^2}{3} - \text{Sp}\left(\cos^2 \frac{\theta}{2}\right) \right].$$

In regard to the low- $|Q^2|$  MUSE kinematics, the “high-energy” approximations of  $\bar{\delta}_{\gamma\gamma^*}^{(0)}$  for electron scattering are quite legitimate since  $m_e^2 \ll |Q^2|$  ( $m_e^2 = 0.25 \times 10^{-6} \text{ GeV}^2$ ), which cannot be justified in case of the muon. With  $\Delta_{\gamma^*}$  typically much smaller than the beam energies, the first two double-log terms containing the factor  $-\ln(-Q^2/m_e^2)$  dominates in case of electron scattering, accounting for the large negative sign of the bremsstrahlung contribution. This contrasts the positive sign of electron-photon VC attributed to the dominant positive contributions from the Sudakov terms proportional to  $\ln^2(-Q^2/m_e^2)$ , as elucidated earlier.<sup>6</sup>

- (iii) Large cancellations occur between the VC and bremsstrahlung contributions and lead to approximately 20% correction in electron scattering. For the muon, cancellations between the comparable VP and bremsstrahlung contributions lead to

approximately 1% correction only at the *largest* MUSE beam momenta.

- (iv) At lowest-order in chiral expansion, the proton is essentially an infinitely heavy static object, i.e., leptons scatter off a static Coulomb potential. This naturally explains why all  $\text{LO}_\alpha$  radiative effects on the proton vanish.

#### IV. RADIATIVE CORRECTION AT $\text{NLO}_\alpha$

The next-order radiative corrections are *dynamical* in nature, since they arise from the  $\text{NLO}_\alpha$  interactions in the  $\text{HB}\chi\text{PT}$  Lagrangian. Thus, the power counting scheme allows for diagrams containing either one  $\text{NLO}_\alpha$  vertex or one insertion of an  $\text{NLO}_\chi$  proton propagator. The  $\text{NLO}_\alpha$  diagrams that we consider are the  $\mathcal{O}(e^2 \alpha Q/M)$  one-loop virtual correction amplitudes, along with those of the  $\mathcal{O}(e^3 Q/M)$  soft photon bremsstrahlung amplitudes. Employing the DR scheme, we extract the UV and IR divergences generated at  $\text{NLO}_\alpha$  to obtain the corresponding fractional radiative corrections to the cross section,  $\delta_{2\gamma}^{(1)} \sim \mathcal{O}(\alpha Q/M)$ . The  $\text{NLO}_\alpha$  TPE box diagrams were evaluated analytically invoking SPA in Sec. III of Ref. [58] (we shall make some pertinent comments regarding SPA and its validity in the evaluation of the TPE box diagrams in Secs. V and VI of this paper). In this section, the other virtual  $\text{NLO}_\alpha$  one-loop diagrams shall be evaluated exactly; i.e., we make no approximations in our evaluation of the one-loop diagrams. Below, we elucidate the details of the

<sup>6</sup>It should be noted that the above expression differs by a factor  $\ln\left(\frac{-Q^2}{m_l^2}\right) \left[ \ln\left(\frac{-Q^2}{m_l^2}\right) - 1 \right]$  compared to the standard expression known in the existing literature (see, e.g., Refs. [1]). This difference is due to the DR scheme we have adopted in order to separate the IR-divergent part from the finite contribution. Specifically, in DR, we prefer to retain the factor  $\ln\left(\frac{4\pi\mu^2}{-Q^2}\right)$  in the IR-singular part  $\mathbf{IR}_{\gamma\gamma^*}^{(0)}$ , instead of  $\ln\left(\frac{4\pi\mu^2}{m_l^2}\right)$ , which is a more standard representation in the literature. For the same reason, our leptonic VC result [cf. Eq. (57)] differs by the same factor.

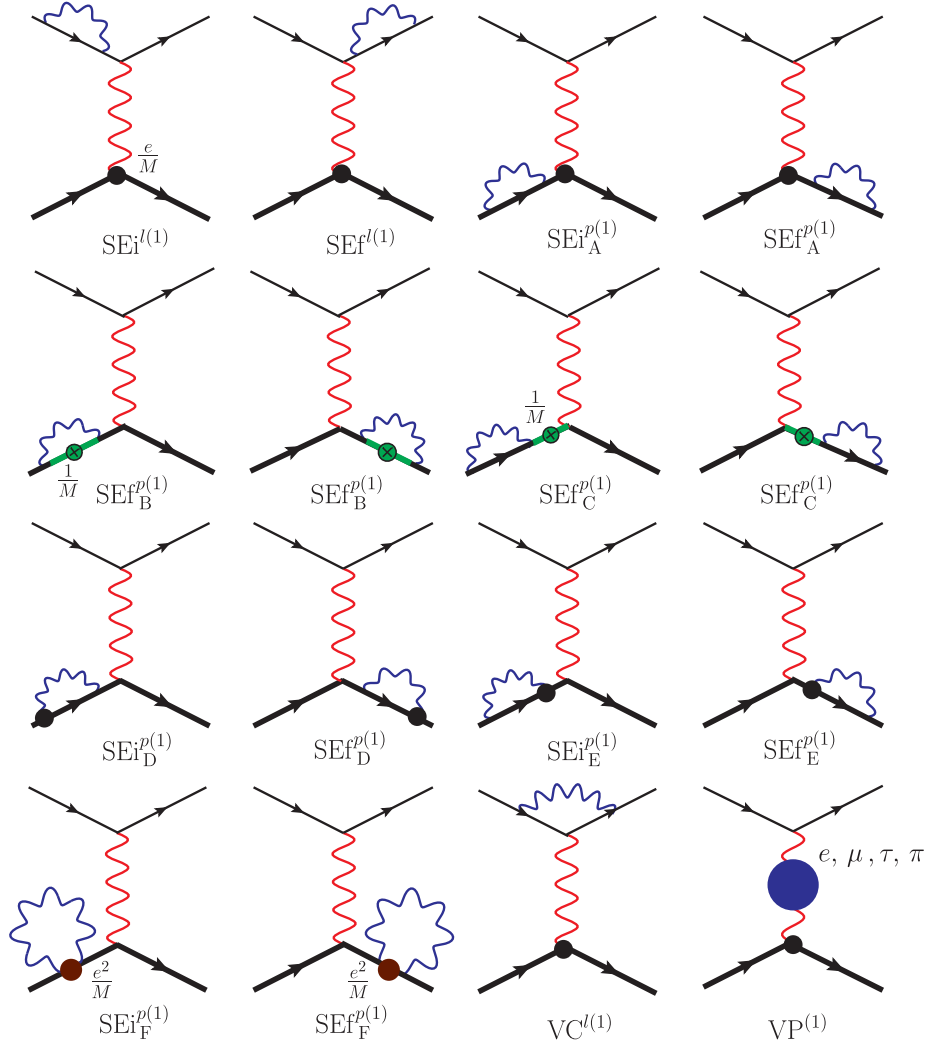


FIG. 9. The one-loop lepton and proton self-energies, lepton-proton vertex corrections, and the vacuum polarizations at  $\text{NLO}_\alpha$  in HB $\chi$ PT [i.e.,  $\mathcal{O}(e^2\alpha Q/M)$ ], contributing to the radiative corrections to the LO (Born)  $\ell$ -p elastic scattering amplitude [see Eq. (9)]. The filled blobs represent  $1/M$ -order proton-photon vertex insertions. In particular, the proton self-energy “tadpoles” (diagrams  $\text{SEi}_i, \text{f}_F^{p(1)}$ ) have  $e^2/M$ -order vertices. The proton propagators with the crossed blobs “ $\otimes$ ” represent  $1/M$ -order propagator insertions. While all the self-energy diagrams vanish in the on-shell limit of the external particles, the lepton vertex correction and vacuum polarization diagrams do not contribute at  $\text{NLO}_\alpha$  since they are kinematically suppressed to  $1/M^2$ -order.

$\text{NLO}_\alpha$  virtual and real contributions and the subsequent cancellation of the IR divergences.

### A. One-loop virtual corrections at $\text{NLO}_\alpha$

In case of the external on-shell particles, the lepton and proton SE amplitude terms (diagrams  $\text{SEi}_i, \text{f}_F^{l(1)}$  and  $\text{SEi}_i, \text{f}_{A,\dots,F}^{p(1)}$  shown in Fig. 9) do not contribute directly to the elastic scattering amplitude as they vanish due to the on-shell renormalization condition. The respective SE loops, however, renormalize the off-shell bare masses in the propagators. In addition, their derivatives contribute at  $\text{NLO}_\alpha$  to the respective wave-function renormalization constants  $Z_1^{l,p(1)}$ . In the following, we discuss the

evaluations of the other one-loop  $\text{NLO}_\alpha$  amplitudes at  $\mathcal{O}(e^2\alpha Q/M)$ , which include the lepton-photon VC diagram ( $\text{VC}^{l(1)}$  in Fig. 9), the VP diagram ( $\text{VP}^{(1)}$  in Fig. 9), and the proton VC diagrams ( $\text{VC}_{A,\dots,G}^{p(1)}$  in Fig. 10). Furthermore, the  $\text{NLO}_\alpha$  TPE amplitudes, which were already evaluated invoking SPA in our previous work [58], are used in this work to determine the complete one-loop virtual radiative contribution at  $\text{NLO}_\alpha$ .

#### 1. Lepton-photon vertex and vacuum polarization corrections

Formally, the only nontrivial  $\text{NLO}_\alpha$  contributions in Fig. 9 are expected to arise from the last two diagrams, namely, the lepton-photon VC (diagram  $\text{VC}^{l(1)}$ ) and the VP

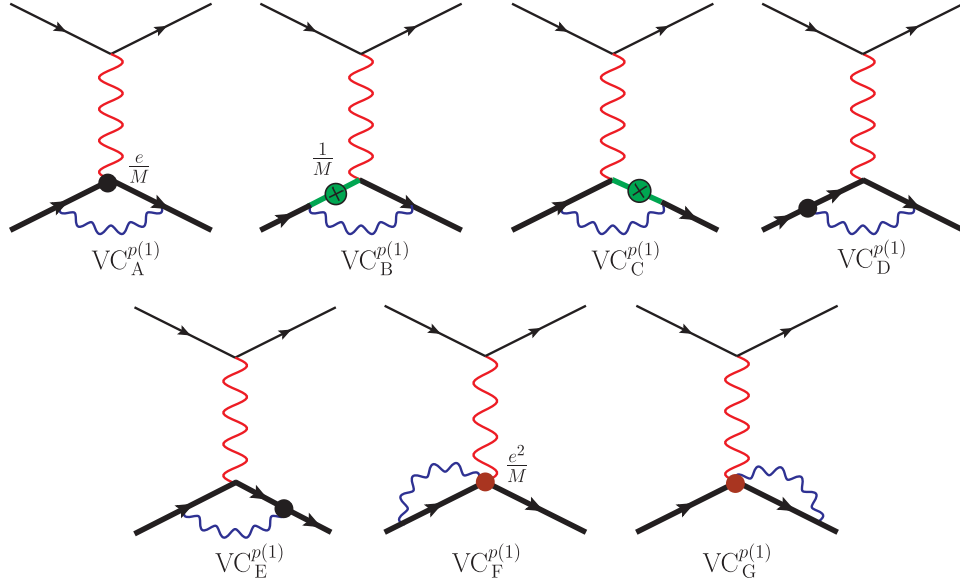


FIG. 10. One-loop proton-photon vertex correction diagrams at  $\text{NLO}_\alpha$  in  $\text{HB}\chi\text{PT}$  [i.e.,  $\mathcal{O}(e^2\alpha Q/M)$ ], contributing to the radiative corrections to the LO (Born)  $\ell$ - $p$  elastic scattering amplitude [see Eq. (9)]. The filled blobs represent  $1/M$ -order proton-photon vertex insertions. In particular, the two-photon proton vertices (diagrams  $\text{VC}_{\text{F,G}}^{p(1)}$ ) are of order  $e^2/M$ . The proton propagators with the crossed blobs  $\otimes$  represent  $1/M$ -order propagator insertions (diagrams  $\text{VC}_{\text{B,C}}^{p(1)}$ ). None of these diagrams contributes to the cross section at  $\text{NLO}_\alpha$  (see the text).

(diagram  $\text{VP}^{(1)}$ ) contributions. The result closely resembles the corresponding  $\text{LO}_\alpha$  result, Eq. (52), in that the amplitude of each of the above  $\text{NLO}_\alpha$  diagrams, apart from the vertex term proportional to  $F_2^l$ , factorizes into the  $\text{NLO}_\chi$  Born amplitude  $\mathcal{M}_\gamma^{(1)}$  [see Eq. (11)], namely,

$$\begin{aligned} \mathcal{M}_{\gamma\gamma}^{l(1)} &= \mathcal{M}_\gamma^{(1)} + \mathcal{M}_\gamma^{(1)} [F_1^{l:\text{ren}}(Q^2) - 1 + \Delta\Pi(Q^2)] \\ &\quad + \overline{\mathcal{M}}_\gamma^{(1)} F_2^l(Q^2), \end{aligned} \quad (70)$$

where

$$\begin{aligned} \overline{\mathcal{M}}_\gamma^{(1)} &= \overline{\mathcal{M}}_\gamma^{(1):\text{a}} + \overline{\mathcal{M}}_\gamma^{(1):\text{b}}; \\ \overline{\mathcal{M}}_\gamma^{(1):\text{a}} &= -\frac{e^2}{4m_l M Q^2} [\bar{u}_l(p') i\sigma^{\mu\nu} Q_\nu u_l(p)] [\chi^\dagger(p_p) \{ (p_p + p_p')_\mu - v_\mu v \cdot (p_p + p_p') \} \chi(p_p)], \\ \overline{\mathcal{M}}_\gamma^{(1):\text{b}} &= -\frac{e^2}{4m_l M Q^2} [\bar{u}_l(p') i\sigma^{\mu\nu} Q_\nu u_l(p)] [\chi^\dagger(p_p') (2 + \kappa_s + \kappa_v) [S_\mu, S \cdot Q] \chi(p_p)]. \end{aligned} \quad (71)$$

Here,  $F_1^{l:\text{ren}}$  is the renormalized Dirac form factor of the lepton, Eq. (37). In Sec. II, it was demonstrated that the interference of the LO and  $\text{NLO}_\chi$  Born amplitudes is proportional to  $\mathcal{R}_Q \sim \mathcal{O}(M^{-2})$  [see Eq. (18)]. Consequently, with  $F_1^{l:\text{ren}}(Q^2) - 1$ ,  $\Delta\Pi(Q^2)$ , and  $F_2^l(Q^2)$  of  $\mathcal{O}(\alpha)$ , the relevant  $\text{NLO}_\alpha$  terms which arise from the interference of the amplitudes, Eqs. (52) and (70), and which should formally contribute here, are *de facto* kinematically suppressed to  $\mathcal{O}(\alpha Q^2/M^2)$ , i.e., in essence  $\text{NNLO}_\alpha$  in  $\text{HB}\chi\text{PT}$ . Thus, we have

$$\begin{aligned} \delta_{\gamma\gamma}^{l(1)}(Q^2) &= \frac{\sum_{\text{spins}} [|\mathcal{M}_{\gamma\gamma}^{(0)} + \mathcal{M}_{\gamma\gamma}^{l(1)}|^2 - |\mathcal{M}_{\gamma\gamma}^{(0)}|^2 - 2\text{Re}(\mathcal{M}_{\gamma\gamma}^{(0)\dagger} \mathcal{M}_{\gamma\gamma}^{(1)} + \mathcal{M}_{\gamma\gamma}^{(0)\dagger} \mathcal{M}_{\gamma\gamma}^{(0)})]}{\sum_{\text{spins}} |\mathcal{M}_{\gamma\gamma}^{(0)}|^2} + 1 \\ &= 2[F_1^{l:\text{ren}}(Q^2) - 1 + \Delta\Pi(Q^2)] \left( \mathcal{R}_Q + \frac{\sum_{\text{spins}} |\mathcal{M}_\gamma^{(1)}|^2}{\sum_{\text{spins}} |\mathcal{M}_\gamma^{(0)}|^2} \right) \\ &\quad + \frac{2\text{Re} \sum_{\text{spins}} (\mathcal{M}_\gamma^{(0)\dagger} \overline{\mathcal{M}}_\gamma^{(1)} + \mathcal{M}_\gamma^{(1)\dagger} \overline{\mathcal{M}}_\gamma^{(0)} + \mathcal{M}_\gamma^{(1)\dagger} \overline{\mathcal{M}}_\gamma^{(1)})}{\sum_{\text{spins}} |\mathcal{M}_\gamma^{(0)}|^2} F_2^l(Q^2) + \mathcal{O}(\alpha^2) \end{aligned}$$

$$\begin{aligned}
&= \mathcal{R}_Q[\mathbf{IR}_{\gamma\gamma}^{(0)}(Q^2) + \bar{\delta}_{\gamma\gamma}^{(0)}(Q^2)] \left\{ 1 + \frac{1}{2}(1 + \kappa_p)^2 \left( \frac{Q^2 + 4(m_l^2 - E^2)}{Q^2 + 4E^2} \right) \right\} \\
&\quad + (1 + \kappa_p)^2 \mathcal{R}_Q \delta_{\gamma\gamma;2}^{(0)}(Q^2) \left\{ 1 - \frac{1}{2} \left( \frac{Q^2 + 4(m_l^2 - E^2)}{Q^2 + 4E^2} \right) \right\} + \mathcal{O}(\alpha^2) \sim \mathcal{O}\left(\alpha \frac{Q^2}{M^2}\right)
\end{aligned} \tag{72}$$

by using the results of Eqs. (18), (55)–(57) as well as the two estimates

$$\begin{aligned}
&\frac{2\mathcal{R}e \sum_{\text{spins}} (\mathcal{M}_\gamma^{(0)\dagger} \overline{\mathcal{M}}_\gamma^{(1);a} + \mathcal{M}_\gamma^{(1);a\dagger} \overline{\mathcal{M}}_\gamma^{(0)})}{\sum_{\text{spins}} |\mathcal{M}_\gamma^{(0)}|^2} F_2^l(Q^2) = \mathcal{R}_Q \delta_{\gamma\gamma;2}^{(0)}(Q^2), \quad \text{and} \\
&\frac{2\mathcal{R}e \sum_{\text{spins}} (\mathcal{M}_\gamma^{(1);a\dagger} \overline{\mathcal{M}}_\gamma^{(1);a} + \mathcal{M}_\gamma^{(1);b\dagger} \overline{\mathcal{M}}_\gamma^{(1);b})}{\sum_{\text{spins}} |\mathcal{M}_\gamma^{(0)}|^2} F_2^l(Q^2) = (1 + \kappa_p)^2 \mathcal{R}_Q \delta_{\gamma\gamma;2}^{(0)}(Q^2) + o\left(\alpha \frac{Q^4}{M^4}\right),
\end{aligned} \tag{73}$$

where the symbol  $o(\alpha Q^4/M^4)$  denotes further terms of order  $1/M^4$ , which we ignore. Please note that  $\delta_{\gamma\gamma;2}^{(0)}$  already contains  $1/M^2$ -order terms [cf. Eq. (56)]. As illustrated above, a notable feature regarding these subleading chiral-order radiative corrections is that they generally do not completely factorize as a simple product of the  $\mathcal{O}(Q^2/M^2)$  pure chiral correction, e.g.,  $\delta_\chi^{(1/M^2)}$  [cf. Eq. (25)], and the  $\mathcal{O}(\alpha)$  leading virtual radiative correction  $\bar{\delta}_{\gamma\gamma}^{(0)}$ . At our accuracy of  $\mathcal{O}(\alpha Q/M)$ , however, we eventually drop all  $1/M^2$ -order terms in our final expressions for the fractional contributions. These NNLO $_\alpha$  terms of  $\mathcal{O}(\alpha Q^2/M^2)$  above, as mentioned earlier, will be useful in estimating our

theoretical uncertainties. We then conclude that none of the diagrams displayed in Fig. 9 contributes to the scattering cross section at NLO $_\alpha$ .

## 2. Proton-photon vertex corrections

As displayed in Fig. 10, a total of seven diagrams,  $\text{VC}_A^{p(1)}, \dots, \text{VC}_G^{p(1)}$ , contribute to the proton-photon VC at NLO $_\alpha$  in HB $\chi$ PT. Five of these diagrams involve  $1/M$ -order proton-photon vertex insertions, and the remaining two involve  $1/M$ -order ‘‘heavy’’ proton propagator insertions. The amplitudes of these diagrams  $\mathcal{M}_{\gamma\gamma;\text{vertex}}^{p(1);A,\dots,G}$  can be expressed as follows:

$$\begin{aligned}
\mathcal{M}_{\gamma\gamma;\text{vertex}}^{p(1);A} &= \frac{ie^4}{2MQ^2} [\bar{u}_l(p') \gamma^\mu u_l(p)] \int \frac{d^4k}{(2\pi)^4} \frac{[\chi^\dagger(p'_p) \{ (p_p + p'_p - 2k)_\mu - [v \cdot (p_p + p'_p - 2k)] v_\mu \} \chi(p_p)]}{(k^2 + i0)[v \cdot (p_p - k) + i0][v \cdot (p'_p - k) + i0]}, \\
\mathcal{M}_{\gamma\gamma;\text{vertex}}^{p(1);B} &= \frac{ie^4}{2MQ^2} [\bar{u}_l(p') \gamma^\mu u_l(p)] \int \frac{d^4k}{(2\pi)^4} \frac{[\chi^\dagger(p'_p) v_\mu \chi(p_p)]}{(k^2 + i0)[v \cdot (p'_p - k) + i0]} \left( 1 + \frac{p_p^2}{(v \cdot k)^2} - \frac{(p_p - k)^2}{(v \cdot k)^2} \right), \\
\mathcal{M}_{\gamma\gamma;\text{vertex}}^{p(1);C} &= \frac{ie^4}{2MQ^2} [\bar{u}_l(p') \gamma^\mu u_l(p)] \int \frac{d^4k}{(2\pi)^4} \frac{[\chi^\dagger(p'_p) v_\mu \chi(p_p)]}{(k^2 + i0)[v \cdot (p_p - k) + i0]} \left( 1 + \frac{(p'_p)^2}{(v \cdot k)^2} - \frac{(p'_p - k)^2}{(v \cdot k)^2} \right), \\
\mathcal{M}_{\gamma\gamma;\text{vertex}}^{p(1);D} &= \frac{ie^4}{2MQ^2} [\bar{u}_l(p') \gamma^\mu u_l(p)] \int \frac{d^4k}{(2\pi)^4} \frac{[\chi^\dagger(p'_p) v_\mu \{ [v \cdot (2p_p - k)] - [v \cdot (2p_p - k)] v^2 \} \chi(p_p)]}{(k^2 + i0)[v \cdot (p_p - k) + i0][v \cdot (p'_p - k) + i0]} = 0, \\
\mathcal{M}_{\gamma\gamma;\text{vertex}}^{p(1);E} &= \frac{ie^4}{2MQ^2} [\bar{u}_l(p') \gamma^\mu u_l(p)] \int \frac{d^4k}{(2\pi)^4} \frac{[\chi^\dagger(p'_p) v_\mu \{ [v \cdot (2p'_p - k)] - [v \cdot (2p'_p - k)] v^2 \} \chi(p_p)]}{(k^2 + i0)[v \cdot (p_p - k) + i0][v \cdot (p'_p - k) + i0]} = 0, \\
\mathcal{M}_{\gamma\gamma;\text{vertex}}^{p(1);F} &= \frac{ie^4}{2MQ^2} [\bar{u}_l(p') \gamma^\mu u_l(p)] \int \frac{d^4k}{(2\pi)^4} \frac{[\chi^\dagger(p'_p) v_\mu (1 - v^2) \chi(p_p)]}{(k^2 + i0)[v \cdot (p_p - k) + i0]} = 0, \\
\mathcal{M}_{\gamma\gamma;\text{vertex}}^{p(1);G} &= \frac{ie^4}{2MQ^2} [\bar{u}_l(p') \gamma^\mu u_l(p)] \int \frac{d^4k}{(2\pi)^4} \frac{[\chi^\dagger(p'_p) v_\mu (1 - v^2) \chi(p_p)]}{(k^2 + i0)[v \cdot (p'_p - k) + i0]} = 0.
\end{aligned} \tag{74}$$

Since  $v^2 = 1$ , the last four amplitudes  $\mathcal{M}_{\gamma\gamma;\text{vertex}}^{p(1);D,E,F,G}$  vanish as indicated. To evaluate the remaining three amplitudes  $\mathcal{M}_{\gamma\gamma;\text{vertex}}^{p(1);A,B,C}$ , as earlier, we first use (in the lab frame) the on-shell relations,  $v \cdot p_p = 0$  and  $v \cdot p'_p = -\frac{(p'_p)^2}{2M} + \mathcal{O}(M^{-2})$ , in the denominators of the leading chiral-order proton propagators. Second, we incorporate a  $1/M$  expansion and retain terms up

to  $\mathcal{O}(e^2\alpha Q/M)$  in the  $\text{NLO}_\alpha$  proton-photon VC amplitudes. Using DM this eventually leads to vanishing contribution, namely,

$$\begin{aligned}
 \mathcal{M}_{\gamma\gamma;\text{vertex}}^{p(1)} &= \mathcal{M}_{\gamma\gamma;\text{vertex}}^{p(1);A} + \mathcal{M}_{\gamma\gamma;\text{vertex}}^{p(1);B} + \mathcal{M}_{\gamma\gamma;\text{vertex}}^{p(1);C} \\
 &= \frac{ie^4}{2MQ^2} [\bar{u}_l(p')\gamma^\mu u_l(p)] \int \frac{d^4k}{(2\pi)^4} \frac{[\chi^\dagger(p'_p)(p_p + p'_p - 2k)_\mu \chi(p_p)]}{(k^2 + i0)(-v \cdot k + i0)^2} \left(1 - \frac{(p'_p)^2}{2M(v \cdot k)} + \dots\right) \\
 &\quad + \frac{ie^4}{2MQ^2} [\bar{u}_l(p')\gamma^\mu u_l(p)] \int \frac{d^4k}{(2\pi)^4} \frac{[\chi^\dagger(p'_p)v_\mu \chi(p_p)]}{(k^2 + i0)(-v \cdot k + i0)} \left(1 - \frac{k^2}{(v \cdot k)^2}\right) \left(2 - \frac{(p'_p)^2}{2M(v \cdot k)} + \dots\right) \\
 &\stackrel{\text{DR}}{\mapsto} 0.
 \end{aligned} \tag{75}$$

In the last step, we again used the fact that all scaleless loop integrals of the type  $\mathcal{I}(m, n)$ , Eq. (43), vanish in DR [67]. Consequently, none of the  $\text{NLO}_\alpha$  proton-photon vertex correction diagrams shown in Fig. 10 contributes to the radiative corrections. The nonvanishing radiative corrections from  $\text{NNLO}_\alpha$  vertices (excluded in this work) are potentially expected to renormalize the proton's Sachs form factors. This leaves us only with the TPE diagrams which do contribute to the  $\text{NLO}_\alpha$  one-loop radiative corrections for the LO Born lepton-proton elastic scattering cross section.

### 3. Two-photon exchange corrections

The  $\text{NLO}_\alpha$  TPE diagrams of  $\mathcal{O}(e^2\alpha Q/M)$ , comprising the *direct-box*, *crossed-box*, and *seagull* amplitudes, contribute to the fractional radiative correction,  $\delta_{\gamma\gamma}^{(1)} \sim \mathcal{O}(\alpha Q/M)$ . The TPE box amplitudes are IR-divergent, and their exact analytical evaluation involves an intricate system of scalar and tensor *three- and four-point integral* functions and their derivatives. In contrast to the relativistic treatment of the proton propagator within the TPE loops in  $d$  dimensions, the integrals involving the nonrelativistic “heavy nucleon” propagator is a challenge in  $d$  dimensions. To the best of our knowledge, an exact analytical evaluation of such “heavy baryon TPE loop” functions in order to isolate the IR divergences has not been pursued in the literature. However, we remark that efforts are currently underway [73] to analytically isolate the IR-singularities from the box integrals in the context of a cutoff

regularization scheme. A direct numerical evaluation of the TPE loops without approximation *per se* may not be feasible unless the IR-divergent parts are first analytically isolated. We therefore rely on an approximate analytical method to evaluate the TPE box amplitudes in order to project out the IR-singular parts, as outlined in details in the work of Ref. [58]. Notably, the IR-finite TPE seagull amplitude can be straightforwardly evaluated analytically without any approximations.

Following the seminal review of Mo and Tsai [60], and as later advocated in the work of Koshchii and Afanasev [45], Ref. [58] evaluated the TPE box diagrams invoking SPA. A “less drastic” variant of this approximation was advocated for in the work of Maximon and Tjon [1]. The use of SPA has the advantage that the seemingly intractable four-point functions get reduced to scalar three-point integrals which can be readily evaluated in analytical form. The disadvantage of this methodology is that, while the vital IR-divergent parts are evaluated correctly, the numerically small finite parts are estimated only partially up to terms that preclude the TPE kinematical region of simultaneous propagation of two hard photons (see, e.g., Ref. [42]). As demonstrated in Ref. [58], using SPA the TPE box amplitudes get factorized into the LO Born amplitude  $\mathcal{M}_\gamma^{(0)}$ . Our  $\text{NLO}_\alpha$  TPE contribution is given by the sum of the factorizable IR-singular TPE box amplitudes and the nonfactorizable IR-finite “residual part” of the TPE seagull amplitude (see Ref. [58] for details),

$$\begin{aligned}
 \mathcal{M}_{\gamma\gamma;\text{TPE}}^{lp(1)} &= \frac{e^2 Q^2}{16\pi^2 M E} \mathcal{M}_\gamma^{(0)} \left\{ \left[ \frac{1}{|\epsilon_{\text{IR}}|} + \gamma_E - \ln\left(\frac{4\pi\mu^2}{-Q^2}\right) \right] \left[ \frac{1}{\beta} \ln \sqrt{\frac{1+\beta}{1-\beta}} + \frac{\eta}{\beta'} \ln \sqrt{\frac{1+\beta'}{1-\beta'}} \right] \right. \\
 &\quad \left. - \frac{1}{\beta} \left[ \frac{\pi^2}{2} - \ln^2 \sqrt{\frac{1+\beta}{1-\beta}} - \text{Sp}\left(\frac{2\beta}{1+\beta}\right) \right] - \frac{\eta}{\beta'} \left[ \frac{\pi^2}{2} - \ln^2 \sqrt{\frac{1+\beta'}{1-\beta'}} - \text{Sp}\left(\frac{2\beta'}{1+\beta'}\right) \right] \right\}_{\text{box}} \\
 &\quad + \frac{e^4}{16\pi^2 m_l^2 M} \left\{ \mathcal{N}_1 \mathcal{I}_1 - \mathcal{N}_2 \left( \mathcal{I}_2 + \frac{Q^2}{m_l^2} \mathcal{I}_3 \right) - \mathcal{N}_3 \left( \mathcal{I}_6 - \frac{Q^2}{m_l^2} \mathcal{I}_5 \right) - \mathcal{N}_4 \frac{Q^2}{m_l^2} \mathcal{I}_4 \right\}_{\text{seagull}}, \tag{76}
 \end{aligned}$$

where the TPE seagull amplitude is expressed in terms of the nonfactorizable amplitudes,  $\mathcal{N}_i \propto \mathcal{M}_\gamma^{(0)}$  ( $i = 1, \dots, 4$ ), namely,

$$\begin{aligned}\mathcal{N}_1 &= [\bar{u}(p')\gamma^\mu(m_l + \not{p})\gamma_\mu u(p)][\chi^\dagger(p'_p)\chi(p_p)], \\ \mathcal{N}_2 &= [\bar{u}(p')\gamma^\mu(\not{p} - \not{Q})\gamma_\mu u(p)][\chi^\dagger(p'_p)\chi(p_p)], \\ \mathcal{N}_3 &= [\bar{u}(p')\gamma^\mu \not{Q}\gamma_\mu u(p)][\chi^\dagger(p'_p)\chi(p_p)], \\ \mathcal{N}_4 &= [\bar{u}(p')\gamma^\mu(2\not{Q} - \not{p})\gamma_\mu u(p)][\chi^\dagger(p'_p)\chi(p_p)].\end{aligned}\quad (77)$$

For brevity, the analytic expressions for the  $Q^2$ -dependent integrals  $\mathcal{I}_{i=1,\dots,4}$  are given in Ref. [58].

#### 4. Complete one-loop virtual contribution

Using the result for the TPE amplitude, we find that the total one-loop NLO $_\alpha$  radiative amplitude is

$$\mathcal{M}_{\gamma\gamma}^{(1)} = \mathcal{M}_{\gamma\gamma}^{l(1)} + \mathcal{M}_{\gamma\gamma;\text{TPE}}^{lp(1)}, \quad (78)$$

where  $\mathcal{M}_{\gamma\gamma}^{l(1)}$  is determined from the lepton-photon VC and the VP contributions at NLO $_\alpha$ , Eqs. (70) and (71). This yields the lab frame one-loop radiative correction to the LO Born differential cross section

$$\Delta \left[ \frac{d\sigma_{el}^{(\text{NLO})}}{d\Omega'_l}(Q^2) \right]_{\gamma\gamma} = \left[ \frac{d\sigma_{el}(Q^2)}{d\Omega'_l} \right]_0 \delta_{\gamma\gamma}^{(1)}(Q^2), \quad (79)$$

where the fractional contribution  $\delta_{\gamma\gamma}^{(1)}$  including the kinematically suppressed  $\mathcal{O}(\alpha Q^2/M^2)$  terms (contributing to the theoretical error) reads

$$\begin{aligned}\delta_{\gamma\gamma}^{(1)}(Q^2) &= \frac{\sum_{\text{spins}} [|\mathcal{M}_{\gamma\gamma}^{(0)} + \mathcal{M}_{\gamma\gamma}^{(1)}|^2 - |\mathcal{M}_{\gamma\gamma}^{(0)}|^2 - 2\text{Re}(\mathcal{M}_{\gamma\gamma}^{(0)\dagger} \mathcal{M}_{\gamma\gamma}^{(1)} + \mathcal{M}_{\gamma\gamma}^{(0)\dagger} \mathcal{M}_{\gamma\gamma}^{(0)})]}{\sum_{\text{spins}} |\mathcal{M}_{\gamma\gamma}^{(0)}|^2} + 1 \\ &= \mathbf{IR}_{\gamma\gamma}^{(1)}(Q^2) + \bar{\delta}_{\gamma\gamma}^{(\text{box})}(Q^2) + \delta_{\gamma\gamma}^{(\text{seagull})}(Q^2) + \mathcal{R}_Q \bar{\delta}_{\gamma\gamma}^{(0)}(Q^2) \left\{ 1 + \frac{1}{2}(1 + \kappa_p)^2 \left( \frac{Q^2 + 4(m_l^2 - E^2)}{Q^2 + 4E^2} \right) \right\} \\ &\quad + (1 + \kappa_p)^2 \mathcal{R}_Q \delta_{\gamma\gamma;2}^{(0)}(Q^2) \left\{ 1 - \frac{1}{2} \left( \frac{Q^2 + 4(m_l^2 - E^2)}{Q^2 + 4E^2} \right) \right\} + o\left(\alpha \frac{Q^2}{M^2}\right).\end{aligned}\quad (80)$$

Here again, the symbol  $o(\alpha Q^2/M^2)$  denotes other possible virtual radiative corrections (from additional LECs and pion loops) of  $1/M^2$ -order that are not explicitly accounted for in our analysis. The insofar obtained IR divergences stemming from the NLO $_\alpha$  one-loop lepton VC and TPE box diagrams are contained in

$$\begin{aligned}\mathbf{IR}_{\gamma\gamma}^{(1)}(Q^2) &= \mathbf{IR}_{\gamma\gamma;\text{TPE}}^{lp(1)}(Q^2) + \mathbf{IR}_{\gamma\gamma}^{(0)}(Q^2) \mathcal{R}_Q \left\{ 1 + \frac{1}{2}(1 + \kappa_p)^2 \left( \frac{Q^2 + 4(m_l^2 - E^2)}{Q^2 + 4E^2} \right) \right\}; \\ \mathbf{IR}_{\gamma\gamma;\text{TPE}}^{lp(1)}(Q^2) &= \frac{\alpha Q^2}{2\pi M E \beta} \left[ \frac{1}{|\epsilon_{\text{IR}}|} + \gamma_E - \ln\left(\frac{4\pi\mu^2}{-Q^2}\right) \right] \left[ \ln \sqrt{\frac{1+\beta}{1-\beta}} + \frac{\eta\beta}{\beta'} \ln \sqrt{\frac{1+\beta'}{1-\beta'}} \right],\end{aligned}\quad (81)$$

where the term  $\mathbf{IR}_{\gamma\gamma}^{(0)}$  is displayed in Eq. (58) and the expression for  $\mathbf{IR}_{\gamma\gamma;\text{TPE}}^{lp(1)}$  is extracted from Ref. [58]. The remaining IR-finite contributions  $\bar{\delta}_{\gamma\gamma}^{(\text{box})}$  and  $\delta_{\gamma\gamma}^{(\text{seagull})}$  originating from the TPE diagrams are, respectively, given as [58]

$$\bar{\delta}_{\gamma\gamma}^{(\text{box})}(Q^2) = -\frac{\alpha Q^2}{2\pi M E \beta} \left\{ \left[ \frac{\pi^2}{2} - \ln^2 \sqrt{\frac{1+\beta}{1-\beta}} - \text{Sp}\left(\frac{2\beta}{1+\beta}\right) \right] + \frac{\eta\beta}{\beta'} \left[ \frac{\pi^2}{2} - \ln^2 \sqrt{\frac{1+\beta'}{1-\beta'}} - \text{Sp}\left(\frac{2\beta'}{1+\beta'}\right) \right] \right\}, \quad (82)$$

and

$$\delta_{\gamma\gamma}^{(\text{seagull})}(Q^2) = -\frac{2\alpha Q^2}{\pi M E} \left[ \frac{E^2(1+\eta)}{\eta Q^2 + 4E^2} \right] \left\{ \mathcal{I}_1(Q^2) + \mathcal{I}_2(Q^2) + \frac{Q^2}{m_l^2} [\mathcal{I}_3(Q^2) - \mathcal{I}_4(Q^2)] \right\}. \quad (83)$$

As already pointed out, all nonvanishing  $\mathcal{O}(e^2\alpha Q/M)$  one-loop diagrams, displayed in Figs. 9 and 10, though formally expected to contribute to the NLO $_\alpha$  virtual corrections,  $\bar{\delta}_{\gamma\gamma}^{(1)} \sim \mathcal{O}(\alpha Q/M)$ , are in effect kinematically

suppressed, contributing at NNLO $_\alpha$ . Therefore, such contributions shall be dropped in presenting our central results. However, here, we prefer to retain the full structure of the IR-divergent terms, i.e., including also the  $1/M^2$



suppressed contributions proportional to  $\mathcal{R}_Q$ , Eq. (81), in order to demonstrate their complete cancellations after including the corresponding  $\text{NLO}_\alpha$  bremsstrahlung

counterpart. Thus, at  $\mathcal{O}(\alpha Q/M)$ , the IR-finite part of the one-loop  $\text{NLO}_\alpha$  radiative corrections, that arises solely from the  $\text{NLO}_\alpha$  TPE contributions, reads

$$\begin{aligned} \bar{\delta}_{\gamma\gamma}^{(1)}(Q^2) &= \bar{\delta}_{\gamma\gamma}^{(\text{box})}(Q^2) + \delta_{\gamma\gamma}^{(\text{seagull})}(Q^2) = -\frac{\alpha Q^2}{\pi M E \beta} \left[ \frac{\pi^2}{2} + \ln\left(\frac{-Q^2}{m_l^2}\right) \ln\sqrt{\frac{1+\beta}{1-\beta}} - \ln^2\sqrt{\frac{1+\beta}{1-\beta}} \right. \\ &\quad \left. - \text{Sp}\left(\frac{2\beta}{1+\beta}\right) + \frac{4E^2\beta}{Q^2 + 4E^2} \left\{ \mathcal{I}_1(Q^2) + \mathcal{I}_2(Q^2) + \frac{Q^2}{m_l^2} [\mathcal{I}_3(Q^2) - \mathcal{I}_4(Q^2)] \right\} \right] + \mathcal{O}\left(\alpha \frac{Q^2}{M^2}\right). \end{aligned} \quad (84)$$

Note that in order to arrive at the above  $\text{NLO}_\alpha$  expression, we removed terms of  $\mathcal{O}(1/M^2)$  by replacing  $E' \rightarrow E$  (i.e.,  $\eta = 1$ ) and  $\beta' \rightarrow \beta$ .

### B. Soft bremsstrahlung corrections at $\text{NLO}_\alpha$

In  $\text{HB}\chi\text{PT}$ , all bremsstrahlung diagrams with leading-order photon emission proton vertex, e.g., diagrams  $\text{Ri}$ ,  $f^{p(0)}$  in Fig. 7 and diagrams  $\bar{\text{Ri}}$ ,  $f^{p(1)}$  and  $\bar{\text{Ri}}$ ,  $f_M^{p(1)}$  in Fig. 11, proportional to  $v \cdot \varepsilon^*$  vanish at the amplitude level. The  $\text{NLO}_\alpha$  bremsstrahlung diagrams with a  $1/M$ -order photon

emission vertex yield the first nonvanishing contributions. The soft bremsstrahlung corrections at  $\text{NLO}_\alpha$  originate from diagrams with either the lepton or proton emitting a single undetectable soft photon ( $\gamma_{\text{soft}}^*$ ), as illustrated in Fig. 11. We use the soft photon limit  $k \rightarrow 0$  to evaluate the IR-divergent contributions to the cross section at  $\text{NLO}_\alpha$ . These contributions arise from the diagrams, namely,  $\text{Ri}^{l(1)}$ ,  $\text{Rf}^{l(1)}$ ,  $\text{Ri}^{p(1)}$ , and  $\text{Rf}^{p(1)}$ , in Fig. 11, which get factorized into the  $\text{LO}_\chi$  and  $\text{NLO}_\chi$  Born amplitudes  $\mathcal{M}_\gamma^{(0,1)}$ . In the  $k \rightarrow 0$  limit, the amplitudes are, respectively, given as

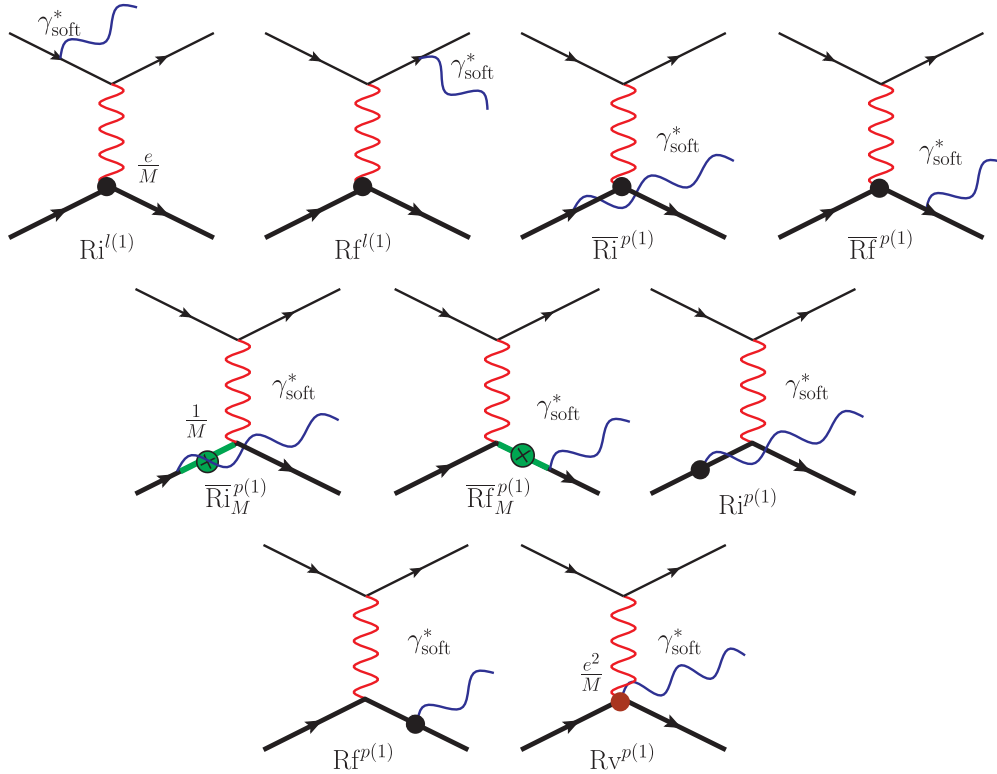


FIG. 11. Soft bremsstrahlung diagrams at  $\text{NLO}_\alpha$  in  $\text{HB}\chi\text{PT}$  [i.e.,  $\mathcal{O}(e^3 Q/M)$ ], contributing to the radiative corrections to the elastic  $\ell$ - $p$  scattering amplitude [see Eq. (9)]. The filled blobs represent  $1/M$ -order proton-photon vertices. In particular, the two-photon proton vertex (diagram  $\text{Rv}^{p(1)}$ ) is of order  $e^2/M$ . The proton propagators with the crossed blobs  $\otimes$  represent  $1/M$ -order propagator insertions. The amplitudes (diagrams  $\bar{\text{Ri}}$ ,  $f^{p(1)}$  and  $\bar{\text{Ri}}$ ,  $f_M^{p(1)}$ ) with the leading-order proton-photon vertices trivially vanish.

$$\begin{aligned}
\mathcal{M}_{\gamma\gamma^*}^{l(1);i} \xrightarrow{\gamma_{\text{soft}}^*} \widetilde{\mathcal{M}}_{\gamma\gamma^*}^{l(1);i} &= e\mathcal{M}_\gamma^{(1)} \left( \frac{p \cdot \epsilon^*}{p \cdot k} \right), \\
\mathcal{M}_{\gamma\gamma^*}^{l(1);f} \xrightarrow{\gamma_{\text{soft}}^*} \widetilde{\mathcal{M}}_{\gamma\gamma^*}^{l(1);f} &= -e\mathcal{M}_\gamma^{(1)} \left( \frac{p' \cdot \epsilon^*}{p' \cdot k} \right), \\
\mathcal{M}_{\gamma\gamma^*}^{p(1);i} \xrightarrow{\gamma_{\text{soft}}^*} \widetilde{\mathcal{M}}_{\gamma\gamma^*}^{p(1);i} &= \frac{e}{M} \mathcal{M}_\gamma^{(0)} \left( \frac{p_p \cdot \epsilon^*}{v \cdot k} \right) = 0, \\
\mathcal{M}_{\gamma\gamma^*}^{p(1);f} \xrightarrow{\gamma_{\text{soft}}^*} \widetilde{\mathcal{M}}_{\gamma\gamma^*}^{p(1);f} &= -\frac{e}{M} \mathcal{M}_\gamma^{(0)} \left( \frac{p'_p \cdot \epsilon^*}{v \cdot k} \right), \quad (85)
\end{aligned}$$

where the otherwise nonzero amplitude  $\mathcal{M}_{\gamma\gamma^*}^{p(1);i}$  trivially vanishes with the initial state proton's residual four-momentum vector as  $p_p = 0$  in the lab frame. Moreover, the proton's spin-dependent terms proportional to the commutator  $[S_\mu, S \cdot k]$  also vanish on the soft photon limit. Evidently, restricting to  $\mathcal{O}(\alpha^3 Q/M)$  the bremsstrahlung cross section gets contributions only from the interference between the  $\text{LO}_\alpha$  and  $\text{NLO}_\alpha$  bremsstrahlung amplitudes. Nevertheless, in order to keep track of the systematic uncertainties, we evaluate all possible  $\mathcal{O}(\alpha^3 Q^2/M^2)$  terms that may arise from the above amplitudes. This requires us to evaluate the squared modulus of the full bremsstrahlung amplitude up to and including  $\text{NLO}_\alpha$ , namely,  $|\mathcal{M}_{\gamma\gamma^*}^{(0)} + \mathcal{M}_{\gamma\gamma^*}^{(1)}|^2$ , and retain  $\mathcal{O}(\alpha^3 Q^2/M^2)$  terms. Notably, the complete  $\mathcal{O}(\alpha^3 Q^2/M^2)$  expression for

the cross section will need additional  $1/M^2$  or  $\text{NNLO}_\alpha$  bremsstrahlung diagrams, which we currently exclude commensurate with the  $\text{NLO}_\alpha$  virtual corrections. In contrast to the aforementioned factorizable amplitudes (diagrams  $\text{Ri}, f^{l(0,1)}$  and  $\text{Ri}, f^{p(1)}$ ) which potentially give rise to IR divergences, the diagram  $\text{Rv}^{p(1)}$  with a proton–two photon  $\text{NLO}_\alpha$  vertex and a nonfactorizable amplitude, namely,

$$\mathcal{M}_{\gamma\gamma^*}^{p(1);v} = -\frac{e^3}{MQ^2} [\bar{u}_l(p') \not{\epsilon} u_l(p)] [\chi^\dagger(p'_p) \chi(p_p)], \quad (86)$$

yields IR-finite contributions only. The corresponding cross section terms are evaluated without explicitly taking the  $k \rightarrow 0$  limit, as reminiscent of the IR-finite one-loop virtual counterpart arising from the TPE seagull diagram having the same  $\text{NLO}_\alpha$  vertex. To this end, the total bremsstrahlung amplitude using the appropriate soft photon limits is given by the sum

$$\begin{aligned}
\widetilde{\mathcal{M}}_{\gamma\gamma^*}^{(0)} + \widetilde{\mathcal{M}}_{\gamma\gamma^*}^{(1)} &= \widetilde{\mathcal{M}}_{\gamma\gamma^*}^{l(0);i} + \widetilde{\mathcal{M}}_{\gamma\gamma^*}^{l(0);f} + \widetilde{\mathcal{M}}_{\gamma\gamma^*}^{l(1);i} \\
&\quad + \widetilde{\mathcal{M}}_{\gamma\gamma^*}^{l(1);f} + \widetilde{\mathcal{M}}_{\gamma\gamma^*}^{p(1);f} + \mathcal{M}_{\gamma\gamma^*}^{p(1);v}. \quad (87)
\end{aligned}$$

Next, the relevant contributions to the squared modulus of the full  $\text{NLO}_\alpha$  amplitude read

$$\begin{aligned}
&\sum_{\text{spins}} \left[ |\widetilde{\mathcal{M}}_{\gamma\gamma^*}^{(0)} + \widetilde{\mathcal{M}}_{\gamma\gamma^*}^{(1)}|^2 - |\widetilde{\mathcal{M}}_{\gamma\gamma^*}^{(0)}|^2 \right] \equiv \sum_{\text{spins}} \left[ |\widetilde{\mathcal{M}}_{\gamma\gamma^*}^{(1)}|^2 + 2\text{Re}(\widetilde{\mathcal{M}}_{\gamma\gamma^*}^{(0)\dagger} \widetilde{\mathcal{M}}_{\gamma\gamma^*}^{(1)}) \right] \\
&= -e^2 \sum_{\text{spins}} |\mathcal{M}_\gamma^{(0)}|^2 \left[ \left( \mathcal{R}_Q + \frac{\sum_{\text{spins}} |\mathcal{M}_\gamma^{(1)}|^2}{\sum_{\text{spins}} |\mathcal{M}_\gamma^{(0)}|^2} \right) \left( \frac{m_l^2}{(p \cdot k)^2} + \frac{m_l^2}{(p' \cdot k)^2} - \frac{2p' \cdot p}{(p \cdot k)(p' \cdot k)} \right) \right. \\
&\quad \left. + \frac{Q^2}{M} \left( \frac{1}{(v \cdot k)(p \cdot k)} + \frac{1}{(v \cdot k)(p' \cdot k)} \right) + \mathcal{R}_Q \frac{2}{(v \cdot k)^2} + \mathcal{O}\left(\frac{Q^3}{M^3}\right) \right] \\
&\quad + \sum_{\text{spin}} \left[ 2\text{Re}(\mathcal{M}_{\gamma\gamma^*}^{(0)} + \mathcal{M}_{\gamma\gamma^*}^{(1)})^\dagger \mathcal{M}_{\gamma\gamma^*}^{p(1);v} - |\mathcal{M}_{\gamma\gamma^*}^{p(1);v}|^2 \right]. \quad (88)
\end{aligned}$$

The first set of terms, namely, those due to the lepton-lepton and lepton-proton bremsstrahlung, are factorizable, being proportional to the squared modulus of the LO Born amplitude  $\mathcal{M}_\gamma^{(0)}$ . The first of these terms are analogous to the  $\text{LO}_\alpha$  bremsstrahlung contribution, Eq. (62), apart from the extra  $1/M^2$ -order prefactors. All such  $1/M^2$ -order IR-finite terms may be dropped from our analytical expressions, as their primary purpose in this work is to contribute to the theoretical error. Nevertheless, we prefer to retain all IR-singular contributions up to  $1/M^2$ -order to demonstrate their order by order cancellations with the corresponding IR-divergent one-loop counterparts. The latter set of interference terms with the proton–two photon vertex diagram leads to IR-finite nonfactorizable contributions and may be readily evaluated, namely,

$$\begin{aligned}
\sum_{\text{spin}} |\mathcal{M}_{\gamma\gamma^*}^{p(1);v}|^2 &= -\frac{32e^6}{Q^6} M \left\{ \frac{\Delta_{p(1)v-p(1)v}^{(1/M)}}{M} \right\} + \mathcal{O}\left(\alpha^3 \frac{Q}{M}\right), \\
\sum_{\text{spin}} 2\text{Re}(\mathcal{M}_{\gamma\gamma^*}^{l(0);i\dagger} \mathcal{M}_{\gamma\gamma^*}^{p(1);v}) &= -\frac{64e^6}{Q^2 q^2 (p \cdot k)} M \left\{ m_l^2 (E + E') - E(p' \cdot k) + E'(p \cdot k) + (v \cdot k) \left( \frac{1}{2} Q^2 - m_l^2 \right) \right. \\
&\quad \left. + \frac{\Delta_{l(0)i-p(1)v}^{(1/M)}}{M} \right\} + \mathcal{O}\left(\alpha^3 \frac{Q}{M}\right),
\end{aligned}$$

$$\begin{aligned}
\sum_{\text{spin}} 2\text{Re}(\mathcal{M}_{\gamma\gamma^*}^{l(0);f\dagger} \mathcal{M}_{\gamma\gamma^*}^{p(1);v}) &= \frac{64e^6}{Q^2 q^2 (p' \cdot k)} M \left\{ m_l^2 (E + E') - E(p' \cdot k) + E'(p \cdot k) - (v \cdot k) \left( \frac{1}{2} Q^2 - m_l^2 \right) \right. \\
&\quad \left. + \frac{\Delta_{l(0)f-p(1)v}^{(1/M)}}{M} \right\} + \mathcal{O}\left(\alpha^3 \frac{Q}{M}\right), \\
\sum_{\text{spin}} 2\text{Re}(\mathcal{M}_{\gamma\gamma^*}^{l(1);i\dagger} \mathcal{M}_{\gamma\gamma^*}^{p(1);v}) &= -\frac{32e^6}{Q^2 q^2 (p \cdot k)} M \left\{ \frac{\Delta_{l(1)i-p(1)v}^{(1/M)}}{M} \right\} + \mathcal{O}\left(\alpha^3 \frac{Q}{M}\right), \\
\sum_{\text{spin}} 2\text{Re}(\mathcal{M}_{\gamma\gamma^*}^{l(1);f\dagger} \mathcal{M}_{\gamma\gamma^*}^{p(1);v}) &= -\frac{32e^6}{Q^2 q^2 (p' \cdot k)} M \left\{ \frac{\Delta_{l(1)f-p(1)v}^{(1/M)}}{M} \right\} + \mathcal{O}\left(\alpha^3 \frac{Q}{M}\right), \\
\sum_{\text{spin}} 2\text{Re}(\mathcal{M}_{\gamma\gamma^*}^{p(1);i\dagger} \mathcal{M}_{\gamma\gamma^*}^{p(1);v}) &= \sum_{\text{spin}} 2\text{Re}(\mathcal{M}_{\gamma\gamma^*}^{p(1);f\dagger} \mathcal{M}_{\gamma\gamma^*}^{p(1);v}) = 0.
\end{aligned} \tag{89}$$

The last two terms exactly vanish, and the  $\Delta^{(1/M)}$ s are finite terms contributing to the cross section at NNLO $_\alpha$ . Hence, in Eq. (89), apart from the interference terms with the LO $_\alpha$  lepton bremsstrahlung amplitude, all the remaining terms are needed only to estimate the theoretical error incurred in our NLO $_\alpha$  results. We may explicitly spell out these terms (replacing  $E' \rightarrow E$  at this order), namely,

$$\begin{aligned}
\Delta_{p(1)v-p(1)v}^{(1/M)} &= 2Q^2 \left( \frac{1}{2} Q^2 + m_l^2 \right), \\
\Delta_{l(0)i-p(1)v}^{(1/M)} &= -\frac{1}{2} (v \cdot k) E [2m_l^2 + Q \cdot k] - \frac{1}{2} (v \cdot k)^2 \left( \frac{1}{2} Q^2 - m_l^2 \right), \\
\Delta_{l(0)f-p(1)v}^{(1/M)} &= -\frac{1}{2} (v \cdot k) E [2m_l^2 + Q \cdot k] + \frac{1}{2} (v \cdot k)^2 \left( \frac{1}{2} Q^2 - m_l^2 \right), \\
\Delta_{l(1)i-p(1)v}^{(1/M)} &= -2(p' \cdot k) \left( \frac{1}{2} Q^2 - m_l^2 \right) - 2m_l^2 (Q \cdot k), \\
\Delta_{l(1)f-p(1)v}^{(1/M)} &= 2(p' \cdot k) \left( \frac{1}{2} Q^2 + m_l^2 \right) + \frac{1}{2} m_l^2 Q^2.
\end{aligned} \tag{90}$$

Notably, with  $|\mathcal{M}_\gamma^{(0)}|^2 \propto M^2$  contributing to the LO Born cross section, for the error estimate, it is sufficient to retain at the most  $M^0$ -order terms as displayed above. Next, the lab frame soft bremsstrahlung correction to the elastic LO differential cross section at NLO $_\alpha$  accuracy in HB $\chi$ PT is expressed as

$$\begin{aligned}
\Delta \left[ \frac{d\sigma_{\text{br}}^{(\text{NLO})}(Q^2)}{d\Omega'_i} \right]_{\gamma\gamma^*} &\stackrel{\gamma^*_{\text{soft}}}{\rightsquigarrow} \frac{\alpha}{2\pi^2} \left[ \frac{d\sigma_{el}(Q^2)}{d\Omega'_i} \right]_0 \\
&\times \left[ (-L_{\text{ii}} - L_{\text{ff}} + L_{\text{if}}) \mathcal{R}_Q \left\{ 1 + \frac{1}{2} (1 + \kappa_p)^2 \left( \frac{Q^2 + 4(m_l^2 - E^2)}{Q^2 + 4E^2} \right) \right\} \right. \\
&\quad \left. - \frac{Q^2}{M} (L_i + L_f) \right] + \left[ \frac{d\sigma_{\text{br}}(Q^2)}{d\Omega'_i} \right]_{\gamma\gamma^*}^{lp(1);v}.
\end{aligned} \tag{91}$$

The IR-divergent integrals,  $L_{\text{ii}}$ ,  $L_{\text{ff}}$ , and  $L_{\text{if}}$ , are identical to the ones we obtained in our LO $_\alpha$  bremsstrahlung evaluations. The two new integrals,  $L_i$  and  $L_f$ , appearing at this order stem from the factorizable lepton-proton interference contribution. All these integrals are IR divergent and conveniently evaluated using DR, as detailed in Appendix B. In particular, to evaluate Eq. (91) at NLO $_\alpha$  accuracy, the exact expression of these integrals displayed

in the Appendix could be approximated with  $E' \rightarrow E$ ,  $\beta' \rightarrow \beta$ , leading to  $L_{\text{ii}} = L_{\text{ff}}$  and  $L_i = L_f$ . The last non-factorizable contribution, namely,  $\left[ \frac{d\sigma_{\text{br}}}{d\Omega'_i} \right]_{\gamma\gamma^*}^{lp(1);v}$ , is IR-finite and readily evaluated using Eq. (89) [see Eq. (B16) in Appendix B]. The resulting expression in the lab frame yields the correction due to soft photon emission with energy less than  $\Delta_{\gamma^*}$ , namely,

$$\Delta \left[ \frac{d\sigma_{\text{br}}^{(\text{NLO})}(Q^2)}{d\Omega'_l} \right]^{(E_{\gamma^*} < \Delta_{\gamma^*})} = \left[ \frac{d\sigma_{\text{el}}(Q^2)}{d\Omega'_l} \right]_0 \delta_{\gamma\gamma^*}^{(1)}(Q^2), \quad (92)$$

where the fractional NLO<sub>α</sub> bremsstrahlung contribution is given as

$$\delta_{\gamma\gamma^*}^{(1)}(Q^2) = \mathbf{IR}_{\gamma\gamma^*}^{(1)}(Q^2) + \bar{\delta}_{\gamma\gamma^*}^{(1)}(Q^2). \quad (93)$$

Using  $\tilde{L}_{\text{ff}} = \tilde{L}_{\text{ii}}$  and  $\tilde{L}_f = \tilde{L}_i$  at NLO<sub>α</sub> accuracy, the finite part of the contribution is expressed as

$$\bar{\delta}_{\gamma\gamma^*}^{(1)}(Q^2) = \frac{\alpha}{\pi} \left[ (-2\tilde{L}_{\text{ii}} + \tilde{L}_{\text{if}}) \mathcal{R}_Q \left\{ 1 + \frac{1}{2} (1 + \kappa_p)^2 \left( \frac{Q^2 + 4(m_l^2 - E^2)}{Q^2 + 4E^2} \right) \right\} - \frac{2Q^2}{M} \tilde{L}_i \right] + \delta_{\gamma\gamma^*}^{lp(1);v}(Q^2),$$

with

$$\delta_{\gamma\gamma^*}^{lp(1);v}(Q^2) = \left[ \frac{d\sigma_{\text{br}}(Q^2)}{d\Omega'_l} \right]_{\gamma\gamma^*}^{lp(1);v} / \left[ \frac{d\sigma_{\text{el}}(Q^2)}{d\Omega'_l} \right]_0, \quad (94)$$

whose explicit expression due to the various interference terms involving the diagram  $\text{Rv}^{p(1)}$  is worked out in Appendix B. The term

$$\begin{aligned} \mathbf{IR}_{\gamma\gamma^*}^{(1)}(Q^2) &= \mathbf{IR}_{\gamma\gamma^*}^{lp(1)}(Q^2) + \mathbf{IR}_{\gamma\gamma^*}^{(0)}(Q^2) \mathcal{R}_Q \left\{ 1 + \frac{1}{2} (1 + \kappa_p)^2 \left( \frac{Q^2 + 4(m_l^2 - E^2)}{Q^2 + 4E^2} \right) \right\} \\ &= -\mathbf{IR}_{\gamma\gamma^*}^{lp(1);\text{TPE}}(Q^2) - \mathbf{IR}_{\gamma\gamma^*}^{(0)}(Q^2) \mathcal{R}_Q \left\{ 1 + \frac{1}{2} (1 + \kappa_p)^2 \left( \frac{Q^2 + 4(m_l^2 - E^2)}{Q^2 + 4E^2} \right) \right\} \end{aligned} \quad (95)$$

collects the IR divergences formally arising from the soft bremsstrahlung contributions of the LO<sub>α</sub> and NLO<sub>α</sub> diagrams with  $\mathbf{IR}_{\gamma\gamma^*}^{(0)} = -\mathbf{IR}_{\gamma\gamma}^{(0)}$  [cf. Eqs. (58) and (66)] and  $\mathbf{IR}_{\gamma\gamma^*}^{lp(1)} = -\mathbf{IR}_{\gamma\gamma^*}^{lp(1);\text{TPE}}$ , [cf. Eq. (81)]. Thus, as anticipated,  $\mathbf{IR}_{\gamma\gamma^*}^{(1)}$  is exactly equal in magnitude but opposite in sign to  $\mathbf{IR}_{\gamma\gamma}^{(1)}$  [cf. Eq. (81)]. Consequently, the sum of the real and virtual radiative corrections at NLO<sub>α</sub>, namely,

$$\delta_{2\gamma}^{(1)}(Q^2) = \delta_{\gamma\gamma}^{(1)}(Q^2) + \delta_{\gamma\gamma^*}^{(1)}(Q^2) \equiv \bar{\delta}_{\gamma\gamma}^{(1)}(Q^2) + \bar{\delta}_{\gamma\gamma^*}^{(1)}(Q^2), \quad (96)$$

is free of IR divergences, where  $\bar{\delta}_{\gamma\gamma}^{(1)}$  represents the finite part of the NLO<sub>α</sub> TPE contributions [cf. Eq. (84)]. Furthermore, the NNLO<sub>α</sub> error terms that we partially considered are also shown to be IR-finite. This, of course, does not preclude the presence of further IR-singularities which may arise from various NNLO<sub>α</sub> contributions not included in this analysis.

Having established the complete cancellation of the IR-singularities among the NLO<sub>α</sub> virtual and real (soft) photon emission diagrams, we explicitly drop all terms of 1/M<sup>2</sup>-order, i.e., terms beyond our intended order of accuracy. Such excluded terms also include “implicit” 1/M<sup>2</sup>-order terms proportional to (E − E′)/M and (β − β′)/M, that is justified following the replacements, E′ → E, η → 1, and β′ → β in all the NLO<sub>α</sub> expression. This yields the finite NLO<sub>α</sub> bremsstrahlung contribution, which modifies the total fractional elastic contribution and is given by

$$\begin{aligned} \bar{\delta}_{\gamma\gamma^*}^{(1)}(Q^2) &= -\frac{\alpha Q^2}{\pi M E \beta} \left[ \ln \left( \frac{4\Delta_{\gamma^*}^2}{-Q^2} \right) \ln \sqrt{\frac{1+\beta}{1-\beta}} + \frac{1}{2} \text{Sp} \left( \frac{2\beta}{\beta+1} \right) - \frac{1}{2} \text{Sp} \left( \frac{2\beta}{\beta-1} \right) \right. \\ &\quad \left. + \frac{32\beta E^2 \Delta_{\gamma^*}^2}{Q^2(Q^2 + 4E^2)} \right] + \mathcal{O} \left( \alpha \frac{Q^2}{M^2} \right). \end{aligned} \quad (97)$$

### C. Total radiative corrections at NLO $_{\alpha}$

By using our analytically derived NLO $_{\alpha}$  expressions for the IR-finite virtual (i.e., TPE) and real contributions [cf. Eqs. (84) and (97)], we obtain the total fractional radiative corrections to the elastic differential cross section accurate up to order  $1/M$ , which reads

$$\begin{aligned} \delta_{2\gamma}^{(1)}(Q^2) = & -\frac{\alpha Q^2}{\pi M E \beta} \left[ \ln\left(\frac{4\Delta_{\gamma^*}^2}{-Q^2}\right) \ln\sqrt{\frac{1+\beta}{1-\beta}} - \frac{1}{2} \text{Sp}\left(\frac{2\beta}{\beta+1}\right) - \frac{1}{2} \text{Sp}\left(\frac{2\beta}{\beta-1}\right) \right. \\ & + \frac{32\beta E^2 \Delta_{\gamma^*}^2}{Q^2(Q^2 + 4E^2)} + \ln\left(\frac{-Q^2}{m_l^2}\right) \ln\sqrt{\frac{1+\beta}{1-\beta}} - \ln^2\sqrt{\frac{1+\beta}{1-\beta}} + \frac{\pi^2}{2} \\ & \left. + \frac{4E^2\beta}{Q^2 + 4E^2} \left\{ \mathcal{I}_1(Q^2) + \mathcal{I}_2(Q^2) + \frac{Q^2}{m_l^2} (\mathcal{I}_3(Q^2) - \mathcal{I}_4(Q^2)) \right\} \right] + \mathcal{O}\left(\alpha \frac{Q^2}{M^2}\right), \end{aligned} \quad (98)$$

where  $\mathcal{I}_{i=1,\dots,4}$  are finite integrals given in Ref. [58].

Our calculated radiative corrections depend on the value of the detector resolution parameter  $\Delta_{\gamma^*}$ . Theoretically,  $\Delta_{\gamma^*}$  determines the maximal energy for the soft bremsstrahlung photon in the lab frame. Anticipating the typical accuracy levels of present-day experiments, in this work, we have chosen a reasonable benchmark estimate,  $\Delta_{\gamma^*} = 1\%$ , of the incoming lepton energy. Figure 12 shows the IR-finite one-loop virtual NLO $_{\alpha}$  radiative (i.e., TPE) corrections  $\bar{\delta}_{\gamma\gamma}^{(1)}$  and the soft photon bremsstrahlung NLO $_{\alpha}$  radiative corrections  $\bar{\delta}_{\gamma\gamma^*}^{(1)}$ , Eqs. (84) and (97), respectively. The following observations describe the features of the NLO $_{\alpha}$  radiative corrections:

- (i) The TPE corrections as expected vanish as  $Q^2 \rightarrow 0$ , while the soft bremsstrahlung corrections become negative, albeit infinitesimally small, at  $Q^2 = 0$  due to nonvanishing of the finite nonfactorizable term  $\delta_{\gamma\gamma^*}^{lp(1);v}$ .

- (ii) Both the real and virtual NLO $_{\alpha}$  corrections display a roughly linear rise with increasing momentum transfer  $|Q^2|$ .
- (iii) Like the LO $_{\alpha}$  chiral-order results, the NLO $_{\alpha}$  corrections do not change rapidly with the increasing lepton beam momenta.
- (iv) Both the NLO $_{\alpha}$  contributions are comparable in magnitudes but of opposite signs. At the *largest* MUSE lepton beam momenta, we observe about 5% and 1% total radiative corrections at NLO $_{\alpha}$  for electron and muon scatterings, respectively.

### V. NUMERICAL RESULTS AND DISCUSSION

In order to determine the total  $\ell$ -p elastic differential cross section, we sum up all the leading (LO $_{\alpha}$ ) and next-to-leading (NLO $_{\alpha}$ ) chiral-order radiative corrections, in addition to the chirally expanded elastic Born terms (i.e., up to NNLO $_{\chi}$ ), as given in Eq. (25), to yield

$$\left. \frac{d\sigma_{el}(Q^2)}{d\Omega'_l} \right|_{\text{lab}} = \left[ \frac{d\sigma_{el}(Q^2)}{d\Omega'_l} \right]_0 \left[ 1 + \delta_{\chi}^{(\text{rms})}(Q^2) + \delta_{\chi}^{(1/M^2)}(Q^2) + \delta_{2\gamma}^{(0)}(Q^2) + \delta_{2\gamma}^{(1)}(Q^2) + \delta_{2\gamma}^{(2)}(Q^2) \right] + \mathcal{O}\left(\frac{Q^3}{M^3}\right), \quad (99)$$

where  $\delta_{2\gamma}^{(0)}$  and  $\delta_{2\gamma}^{(1)}$  are given in Eqs. (69) and (98), respectively. The last term  $\delta_{2\gamma}^{(2)}$  includes the interference terms between the NNLO $_{\chi}$  and the LO $_{\alpha}$  corrections as well as nonfactorizable NNLO $_{\alpha}$  terms, e.g., those in Eqs. (80) and (94), which are beyond the intended accuracy of this work. These higher-order terms, which constitute the  $\mathcal{O}(\alpha Q^2/M^2)$  fractional chiral-radiative corrections to the LO elastic Born cross section, are only partially included in this work and are just used to estimate the systematic error of our methodology.

By comparing the different contributions in Eq. (99), we can obtain a reasonable estimate of the relative magnitudes of the different radiative corrections. To that end, we first discuss the total fractional radiative correction up to and including NLO $_{\alpha}$  accuracy, i.e.,  $\delta_{2\gamma} = \delta_{2\gamma}^{(0)} + \delta_{2\gamma}^{(1)}$  (i.e.,

excluding NNLO $_{\alpha}$ ). Table I displays the LO $_{\alpha}$  and NLO $_{\alpha}$  corrections as well as their sum  $\delta_{2\gamma}$ , for both lepton and antilepton scatterings off the proton (i.e.,  $e^{\pm}p$  and  $\mu^{\pm}p$ ). As observed in the table, we make a comparison of the relative magnitudes of the two chiral-order corrections, viz., NLO $_{\alpha}$  to LO $_{\alpha}$  ratio (i.e.,  $\delta_{2\gamma}^{(1)}:\delta_{2\gamma}^{(0)}$ ). The results for muon scattering indicate ratios which change with momentum transfer  $|Q^2|$  and incident lepton beam momentum  $p = |\vec{p}|$ , from about 2:3 for the largest  $|Q^2|$  and  $p$  values to about 1:110 for the smallest  $|Q^2|$  and  $p$  values. In comparison, for electron scattering the comparable ratios are about 1:5 and 1:25 for the largest and smallest  $|Q^2|$ ,  $p$  values, respectively. Evidently, there are drastic changes in the NLO $_{\alpha}$  to LO $_{\alpha}$  ratio in going from the lowest to the largest possible

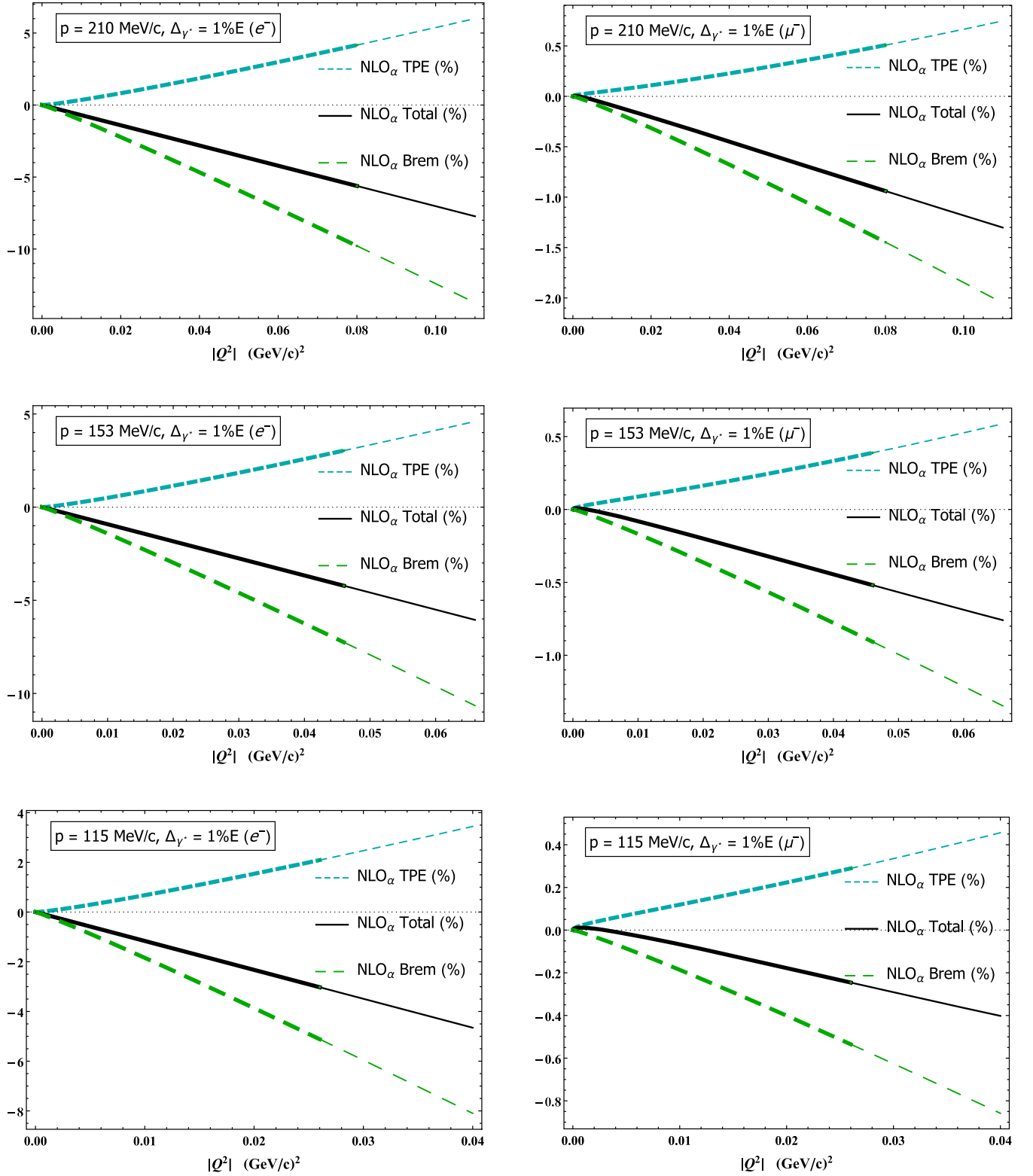


FIG. 12. The fractional  $\text{NLO}_\alpha$  virtual corrections (in percentage) due to the two-photon contributions  $\bar{\delta}_{\gamma\gamma}^{(1)}$  (short-dashed curves), the soft photon bremsstrahlung corrections  $\bar{\delta}_{\gamma\gamma^*}^{(1)}$  (dashed curves), and their sum  $\bar{\delta}_{2\gamma}^{(1)}$  (solid curves). The left (right) panel displays the results for  $e$ - $p$  ( $\mu$ - $p$ ) elastic cross section vs the squared four-momentum transfer  $|Q^2|$ , for the MUSE beam momenta of  $|\vec{p}| = p = 115, 153, 210$  MeV/ $c$ . Each plot covers the full kinematical scattering range,  $0 < |Q^2| < |Q_{\text{max}}^2|$ , when  $\theta \in [0, \pi]$ . The thickened portion of each curve corresponds to the MUSE kinematic cut, where  $\theta \in [20^\circ, 100^\circ]$ . The lab frame detector acceptance  $\Delta_{\gamma^*}$  is taken as 1% of the incident lepton energy  $E$ .

TABLE I. The fractional radiative corrections with respect to the LO elastic Born cross section,  $\delta_{2\gamma}^{(0)}$  at  $\text{LO}_\alpha$ ,  $\delta_{2\gamma}^{(1)}$  at  $\text{NLO}_\alpha$  and their sum  $\delta_{2\gamma} = \delta_{2\gamma}^{(0)} + \delta_{2\gamma}^{(1)}$ , evaluated in  $\text{HB}\chi\text{PT}$  for  $\ell^\pm p$  elastic scattering. The incident lepton beam momenta,  $|\vec{p}| = p = 0.115, 0.153, 0.210$  GeV/c, at some specific  $|Q^2|$  values within the allowed MUSE kinematic range are used. The above numerical figures correspond to the lab frame detector acceptance  $\Delta_{\gamma^*} = 1\%$  of the incident lepton energy  $E$ .

$p =  \vec{p} $ GeV/c	$ Q^2 $ (GeV/c) <sup>2</sup>	LO: $\delta_{2\gamma}^{(0)}$		NLO: $\delta_{2\gamma}^{(1)}$		LO+NLO: $\delta_{2\gamma}$		LO+NLO: $\delta_{2\gamma}$	
		$e^\pm p$	$\mu^\pm p$	$e^\pm p$	$\mu^\pm p$	$e^- p$	$\mu^- p$	$e^+ p$	$\mu^+ p$
0.115	0.005	-0.1485	0.0222	$\pm 0.0058$	$\pm 0.0002$	-0.1543	0.0220	-0.1427	0.0224
	0.015	-0.1671	0.0197	$\pm 0.0174$	$\pm 0.0012$	-0.1846	0.0185	-0.1497	0.0209
	0.025	-0.1760	0.0171	$\pm 0.0291$	$\pm 0.0023$	-0.2050	0.0147	-0.1469	0.0194
0.153	0.01	-0.1598	0.0211	$\pm 0.0092$	$\pm 0.0008$	-0.1689	0.0203	-0.1506	0.0219
	0.025	-0.1752	0.0171	$\pm 0.0230$	$\pm 0.0026$	-0.1981	0.0145	-0.1523	0.0197
	0.04	-0.1831	0.0137	$\pm 0.0367$	$\pm 0.0045$	-0.2199	0.0092	-0.1465	0.0181
0.210	0.02	-0.1709	0.0185	$\pm 0.0140$	$\pm 0.0020$	-0.1850	0.0165	-0.1569	0.0206
	0.04	-0.1829	0.0137	$\pm 0.0281$	$\pm 0.0045$	-0.2105	0.0092	-0.1543	0.0182
	0.06	-0.1892	0.0099	$\pm 0.0421$	$\pm 0.0069$	-0.2313	0.0030	-0.1470	0.0169

kinematical limits in the case of the muon scattering at MUSE. Furthermore, we note that the TPE and the soft bremsstrahlung corrections at  $\text{NLO}_\alpha$  depend on the *lepton* ( $\ell^\pm$ ) *charge*. Hence, not only do the  $\text{NLO}_\alpha$  corrections  $\delta_{2\gamma}^{(1)}$  corresponding to the  $\ell^\pm p$  scattering processes change sign, the total corrections,  $\delta_{2\gamma} = \delta_{2\gamma}^{(0)} + \delta_{2\gamma}^{(1)}$ , are somewhat smaller (larger) for  $\mu^- p$  ( $e^- p$ ) scattering than the  $\mu^+ p$  ( $e^+ p$ ) scattering.

In our treatment of the radiative corrections presented hitherto, we only considered the dominant  $\mathcal{O}(\alpha)$  or leading QED contributions. The higher-order QED corrections (of negative sign) proportional to  $\alpha^n$  where  $n = 2, 3, \dots$  will tend to cause deviations from the leading QED predictions, especially at momentum transfers much larger than the typical kinematic scale; e.g., in our case of lepton scattering, such enhancements are typically expected for  $|Q^2| \gg m_l^2$ . In practice, to evaluate higher-order QED effects involves a very intricate task of calculating multiple photon-loop diagrams that is evidently beyond the scope of this work. It is, however, well known that the double-logarithmic Sudakov terms are responsible for the largest enhancements, especially in the soft and collinear kinematical regions for near-massless particles (such as the electron) in the soft photon limit. Schwinger [74,75], based on work by Bloch and Nordsieck [76] (see also Refs. [57,77–83]), showed that one could by and large compensate for such large enhanced negative contributions to *all orders* in  $\alpha$  by the exponentiation of their contribution to the elastic cross section. Symbolically, this means that if  $\delta_{n\gamma}(Q^2) < 0$  denotes the  $n$ th-order photon-loop and soft photon bremsstrahlung corrections (not including VP contributions), then the replacement,

$$1 + \delta_{n\gamma}(Q^2) \rightarrow \exp\{\delta_{n\gamma}(Q^2)\},$$

leads to an essential suppression of such “artificial” enhancements resulting from the truncation of perturbative expansions. Theoretically, a tacit assumption in this regard is that the emission and reabsorption of an infinite number of soft photons are statistical independent and that these do not alter the elastic kinematics. Furthermore, as seen in our  $\text{LO}_\alpha$  results, there is significant contribution from the VP corrections which are comparable in magnitude but opposite in sign to the photon-loop (vertex) contributions. Consequently, following Ref. [61], commensurate with the exponentiation of the radiative corrections arising from the photon-loop terms, we find it consistent to include the resummation of the one-particle irreducible VP diagrams to all orders. This is useful to preserve essential cancellations that can manifest themselves among the higher-order radiative corrections. To this end, the  $\ell$ - $p$  elastic differential cross section reads

$$\left. \frac{d\sigma_{el}(Q^2)}{d\Omega_l'} \right|_{\text{lab}} \approx \left[ \frac{d\sigma_{el}(Q^2)}{d\Omega_l'} \right]_0 \{1 + \delta_\chi^{(2)}(Q^2) + \delta_{\text{resum}}^{el}(Q^2)\}, \quad (100)$$

where  $\delta_\chi^{(2)}$  includes the  $\text{NNLO}_\chi$  chiral corrections (cf. Sec. II), while the *modified* fractional QED corrections, taking into account the partial resummation of all the potentially large double-logarithm terms, is given by

$$\delta_{\text{resum}}^{el}(Q^2) = \frac{\exp\{\delta_{2\gamma}(Q^2) - \delta_{\text{vac}}(Q^2)\}}{[1 - \delta_{\text{vac}}(Q^2)/2]^2} - 1; \quad (101)$$

$$\delta_{2\gamma}(Q^2) = \delta_{2\gamma}^{(0)}(Q^2) + \delta_{2\gamma}^{(1)}(Q^2) + \delta_{2\gamma}^{(2)}(Q^2),$$

with  $\delta_{2\gamma}^{(2)}$  (the explicit expression is not displayed) representing the additional  $\text{NNLO}_\alpha$  error terms. The VP contribution is assigned as  $\delta_{\text{vac}} \rightarrow \delta_{\text{vac}}^{(0)}$ , the  $\text{LO}_\alpha$  VP correction [cf. Eq. (51)], in the absence of the  $\text{NLO}_\alpha$  [i.e.,  $\mathcal{O}(\alpha Q/M)$ ]

VP term.<sup>7</sup> While estimating the theoretical error due to NNLO<sub>α</sub> corrections, the VP contributions must be modified as

$$\delta_{\text{vac}}(Q^2) = \delta_{\text{vac}}^{(0)}(Q^2) \left[ 1 + \mathcal{R}_Q \left\{ 1 + \frac{1}{2} (1 + \kappa_p)^2 \times \left( \frac{Q^2 + 4(m_l^2 - E^2)}{Q^2 + 4E^2} \right) \right\} \right]. \quad (102)$$

In Fig. 13, we plot the total fractional radiative corrections  $\delta_{2\gamma}$ , up to and including NLO<sub>α</sub> in HB $\chi$ PT, and compare with the LO<sub>α</sub> corrections  $\delta_{2\gamma}^{(0)}$ , Eq. (69), and the corresponding partially resummed QED results  $\delta_{\text{resum}}^{el}$ , Eq. (101), for low-energy  $\ell$ -p scatterings. In the case of electron scattering with large negative bremsstrahlung contributions, the total radiative corrections  $\delta_{2\gamma}$  stay negative, and the magnitude of  $\delta_{2\gamma}$  monotonically increases with increasing squared four-momentum transfer  $|Q^2|$ . The total corrections vary in the range of (22–27)% in the MUSE kinematic range. On the other hand, for muon scattering, the total radiative corrections reach no larger than 1.5% in the same region. However, as distinct from the electron scattering case, the  $\delta_{2\gamma}^{(0)}$  corrections for the muon undergo a sign change at these low energies. As seen in the figure,  $\delta_{2\gamma}^{(0)}$  is positive for very small momentum transfers, say,  $|Q^2| \lesssim 0.04$  (GeV/c)<sup>2</sup>, due to the dominance of the VP contributions in that region. However, for larger  $|Q^2|$  values,  $\delta_{2\gamma}^{(0)}$  turns negative as the VP corrections are eventually superseded by the dominant soft bremsstrahlung contributions. Nevertheless, for the lowest MUSE muon beam momentum,  $p = |\vec{p}| \gtrsim 115$  MeV/c, even the total correction  $\delta_{2\gamma}$  remains positive due to VP dominance. It is also quite evident that there is no significant lepton beam momentum dependence on the individual LO<sub>α</sub> and NLO<sub>α</sub> components of the radiative corrections in the MUSE kinematical range,  $115 < p < 210$  MeV/c.

<sup>7</sup>It is worth noting that Schwinger’s method of exponentiating radiative corrections is strictly applicable only for the “IR-enhanced” double-log terms, e.g., ones proportional to  $\ln(m_e^2/|Q^2|)$  or  $\ln(\Delta_\gamma^2/|Q^2|)$ , where the so-called *Sudakov regions* are clearly defined with the only relevant scale as  $|Q^2| \rightarrow \infty$ . However, it is not immediately apparent how to generalize such ultrarelativistic results to low energies, especially with other relevant scales, such as  $m_\mu^2, M^2 \gtrsim Q^2$ , etc., and constitutes a topic certainly beyond the scope of the present discussion. Consequently, in a simplified approach, we naively approximate the large double-log resummation by exponentiating our NLO<sub>α</sub> result (also including the NNLO<sub>α</sub> errors)  $\delta_{2\gamma}$ , save the VP contributions  $\delta_{\text{vac}}$ , which do not contain IR-enhanced terms.

Figure 13 also displays the  $\delta_{\text{resum}}^{el}$  results where the potentially large double-logarithms have been effectively iterated to all orders in  $\alpha$ . The exponentiated radiative effects leads to the well-known *Sudakov suppression*, as is clearly evident in the electron scattering results. This  $Q^2$  suppression effect is almost numerically comparable to the  $\mathcal{O}(\alpha)$  NLO<sub>α</sub> corrections. In contrast, for muon scattering, there is no discernible NLO<sub>α</sub> suppression. Such contrasting results can be easily anticipated in regard to the MUSE kinematics, since the same  $|Q^2|$  range that may be identified with typical low-momentum transfer dynamics for  $\mu$ -p scattering becomes a region of high-momentum transfer in relativistic  $e$ -p scattering. For example, in Ref. [68], the same reason was attributed to the validity of the high-energy *peaking approximation* for electron scattering at MUSE, when it fails for muon scattering. We therefore anticipate such characteristic suppression to manifest itself in the radiatively corrected future MUSE data for electron-proton scattering.

The theoretical uncertainties involved in our calculations are categorized as the pure chiral hadronic corrections and the radiative corrections. The following sources of uncertainties are identified in our treatment of the effective Born cross section. First, the proton’s rms charge radius  $r_p$  [cf. Eq. (26)] is an essential input to our chirally corrected result at  $\nu = 2$  order. An uncertainty due to the numerical differences in the different proton’s rms radius measurements is required. These differences in the extracted charge radius from high-precision electronic and muonic measurements result in an appreciable error in the value of the chiral correction  $\delta_\chi^{(\text{rms})}$ , namely,  $\Delta_{\text{rms}} \sim 6.4\%$  (i.e., with respect to our central result) [cf. Fig. 2]. However, given the ongoing contentious radius puzzle scenario [10–14], it seems not too unreasonable to estimate an error of such magnitude.<sup>8</sup> Second, the hadronic corrections beyond NNLO<sub>χ</sub> constitute an important corrections to the LO

<sup>8</sup>For instance, using the measured rms radius from the recent PRad Collaboration [21],  $r_p^{(ep)} = 0.831 \pm 0.007(\text{stat}) \pm 0.012(\text{syst})$  fm, and from the erstwhile CREMA Collaboration [12],  $r_p^{(\mu H)} = 0.84087(39)$  fm, we could obtain an effective error estimate due to the input rms radius contributions in the chiral corrections  $\delta_\chi^{(\text{rms})}$  as  $\Delta_{\text{rms}} = \sqrt{\Delta_{\text{PRad}}^2 + \Delta_{\text{CREMA}}^2 + \Delta_{\text{diff}}^2 + \Delta_{\text{NNLO}}^2} \sim 6.4\%$ , where  $\Delta_{\text{NNLO}} \sim 1\%$ , and  $\Delta_{\text{PRad}} = \frac{2r_p^{(ep)}(\delta r_p^{(ep)})_{\text{exp}}}{(r_p^{(ep)})^2 - \frac{3\kappa_p}{2M^2}} \sim 5.5\%$ ,  $\Delta_{\text{CREMA}} = \frac{2r_p^{(\mu H)}(\delta r_p^{(\mu H)})_{\text{exp}}}{(r_p^{(\mu H)})^2 - \frac{3\kappa_p}{2M^2}} \sim 0.1\%$ ,  $\Delta_{\text{diff}} = \frac{2r_p^{(\mu H)}(r_p^{(ep)} - r_p^{(\mu H)})}{(r_p^{(\mu H)})^2 - \frac{3\kappa_p}{2M^2}} \sim 3.1\%$ , where  $(\delta r_p^{(\mu H)})_{\text{exp}}$  stands for respective experimental uncertainties. Note that the above-quoted percentage errors are not relative to the LO Born contributions but are with respect to the central values of  $\delta_\chi^{(\text{rms})}$ .



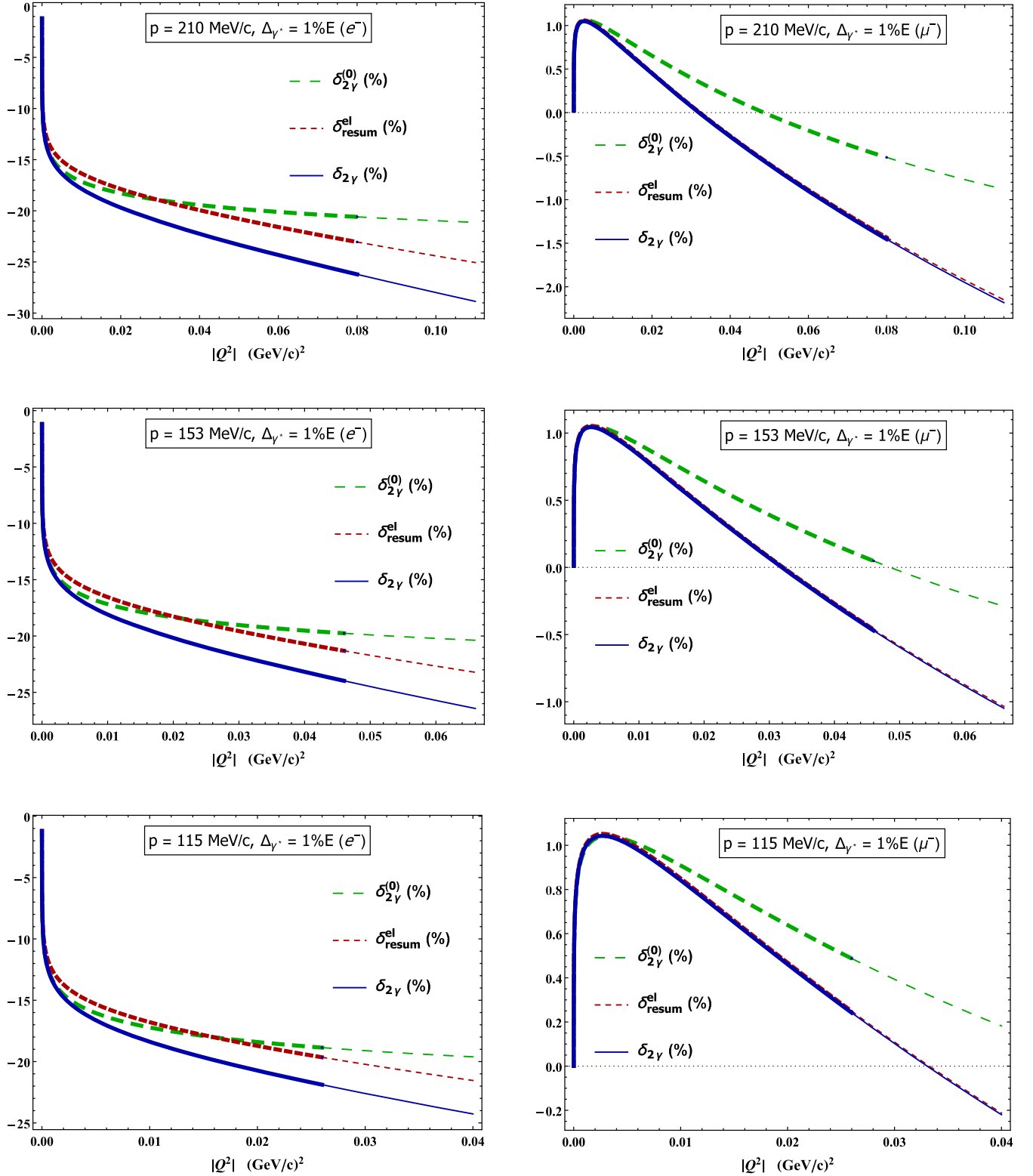


FIG. 13. The total fractional radiative corrections (in percentage) at LO<sub>α</sub>,  $\delta_{2\gamma}^{(0)}$ , and up to and including NLO<sub>α</sub>,  $\delta_{2\gamma} = \delta_{2\gamma}^{(0)} + \delta_{2\gamma}^{(1)}$ , in HB $\chi$ PT for  $e$ - $p$  (left panel) and  $\mu$ - $p$  (right panel) elastic cross sections as a function of  $|Q^2|$  for the MUSE beam momenta,  $|\vec{p}| = p = 115, 153, 210$  MeV/c. Each plot covers the full kinematically allowed scattering range  $0 < |Q^2| < |Q_{\max}^2|$  when  $\theta \in [0, \pi]$ . The thickened portion of each curve corresponds to the MUSE kinematic cut, where  $\theta \in [20^\circ, 100^\circ]$ . The lab frame detector acceptance  $\Delta_{\gamma^*}$  is taken to be 1% of the incident lepton energy  $E$ . The corresponding total fractional resummed results,  $\delta_{\text{resum}}^{\text{el}}$ , Eq. (101), are also displayed for comparison.

Born cross section, Eq. (23). As mentioned, the  $N^3LO_\gamma$  [i.e.,  $\mathcal{O}(Q^3/M^3) \sim 0.008$ ] corrections due to the exclusion of  $\nu = 3$  chiral-order hadronic interactions constitute an uncontrolled error, the estimation of which really lies beyond the present scope of this work. Nevertheless, commensurate with our discussions of our EFT power counting (cf. Sec. I), an error of  $\Delta_{NNLO} \sim 1\%$  on each of the two types of chiral corrections, viz., rms and recoil contributions [cf. Eq. (25)], can naively be attributed for the low-energy MUSE kinematics (cf. Fig. 2). Third, other sources of hadronic uncertainties arise from nonperturbative effects due to various resonances and excited nucleon states (see, e.g., Refs. [51,52,55,56]. Furthermore, nonperturbative techniques, such as dispersively improved  $\chi$ PT [33,37–39] are needed for rigorous estimation of the inherent systematics which are not captured in the perturbative framework such as ours. However, such contributions also constitute uncontrolled uncertainties that we cannot readily assess.

The uncertainties in our treatment of the radiative corrections can be summarized as follows:

1. The only free parameter in this work is the soft-photon detector acceptance factor  $\Delta_{\gamma^*}$ . The sensitivity of our result on the parametric dependence on this cutoff parameter is illustrated in Fig. 14. This figure depicts our analytical results corresponding to the partially resummed  $NLO_\alpha$  radiative corrections  $\delta_{\text{resum}}^{el}$ , as  $\Delta_{\gamma^*}$  is varied in the reasonable range (0.5–2)% of the incident lepton beam energy  $E$ , with  $\Delta_{\gamma^*} = 1\%$  being our benchmark value of the acceptance. As expected, for electron scattering, the radiative corrections decrease in magnitude with larger values of the acceptance. However, for muon scattering, the behavior is somewhat atypical due the change of sign of  $\delta_{2\gamma}^{(0)}$  versus  $|Q^2|$ .
2. Our  $HB\chi$ PT calculations indicate much larger than expected  $NLO_\alpha$  to  $LO_\alpha$  relative corrections in the case of muon scattering close to the upper limit of the MUSE kinematic range. As mentioned, for muon scattering,  $\delta_{2\gamma}$  goes through a zero at some small  $Q^2$  value. Especially, when  $\delta_{2\gamma}^{(0)} \approx 0$ , the  $NNLO_\alpha$  contributions are needed for a more robust evaluation of radiative corrections. We, however, provide a partial assessment of the  $NNLO_\alpha$  effects that reveals a

maximal uncertainty of 3% and 0.1%, respectively, to effect the LO elastic Born cross section for electron and muon scatterings at MUSE energies (cf. Fig. 15).

3. One source of uncontrolled systematics afflicting our evaluations is attributed to the inherent differences in the TPE evaluations with and without invoking SPA. As already mentioned, an exact evaluation of our IR-divergent one-loop diagrams with an insertion of a heavy baryon propagator is rather intricate and has not been pursued earlier. We already referred to Ref. [42], in which an attempt was made in order to include the hard two-photon effects in the TPE contributions. We are, however, unable to currently assess the uncertainty due to the missing hard-photon contribution based solely on this work. We simply refer to an ongoing effort [73] to analytically evaluate a family of such TPE direct and crossed box diagrams at  $NLO_\alpha$ , wherein the large cancellations among them in the  $k \rightarrow 0$  limit, as noted in Ref. [58], are not explicitly manifest without SPA. A detailed investigation of the TPE diagrams without SPA shall be presented in a future publication.

Figure 15 displays our  $HB\chi$ PT results for the total corrections (chiral plus radiative) to the  $\ell$ -p elastic differential cross section, Eq. (101), where all tractable sources of systematic uncertainties are consolidated. Our central results for the total fractional corrections,  $\delta_\chi^{(2)} + \delta_{\text{resum}}^{el}$ , as denoted by the solid red curves, correspond to the radiative corrections up to and including  $NLO_\alpha$  partially resummed to all orders in QED. Likewise, our partially resummed results including the  $NNLO_\alpha$  terms, that contribute to the theoretical uncertainty, are denoted by the dashed blue curves. For electron scattering, the largest conceivable source of theoretical uncertainty evidently stems from the parametric dependence on the detector acceptance  $\Delta_{\gamma^*}$  (yellow bands), which overwhelms the proton's  $\delta_\chi^{(2)}$  uncertainty (cyan bands). In contrast, for muon scattering, the uncertainty in both  $\delta_{\text{resum}}^{el}$  and  $\delta_\chi^{(2)}$  is rather moderate with the latter slightly larger than the former. Only for electron scattering do we find a moderate difference (about 3% of the LO Born cross section) between our complete  $NLO_\alpha$  and partially included  $NNLO_\alpha$  results.

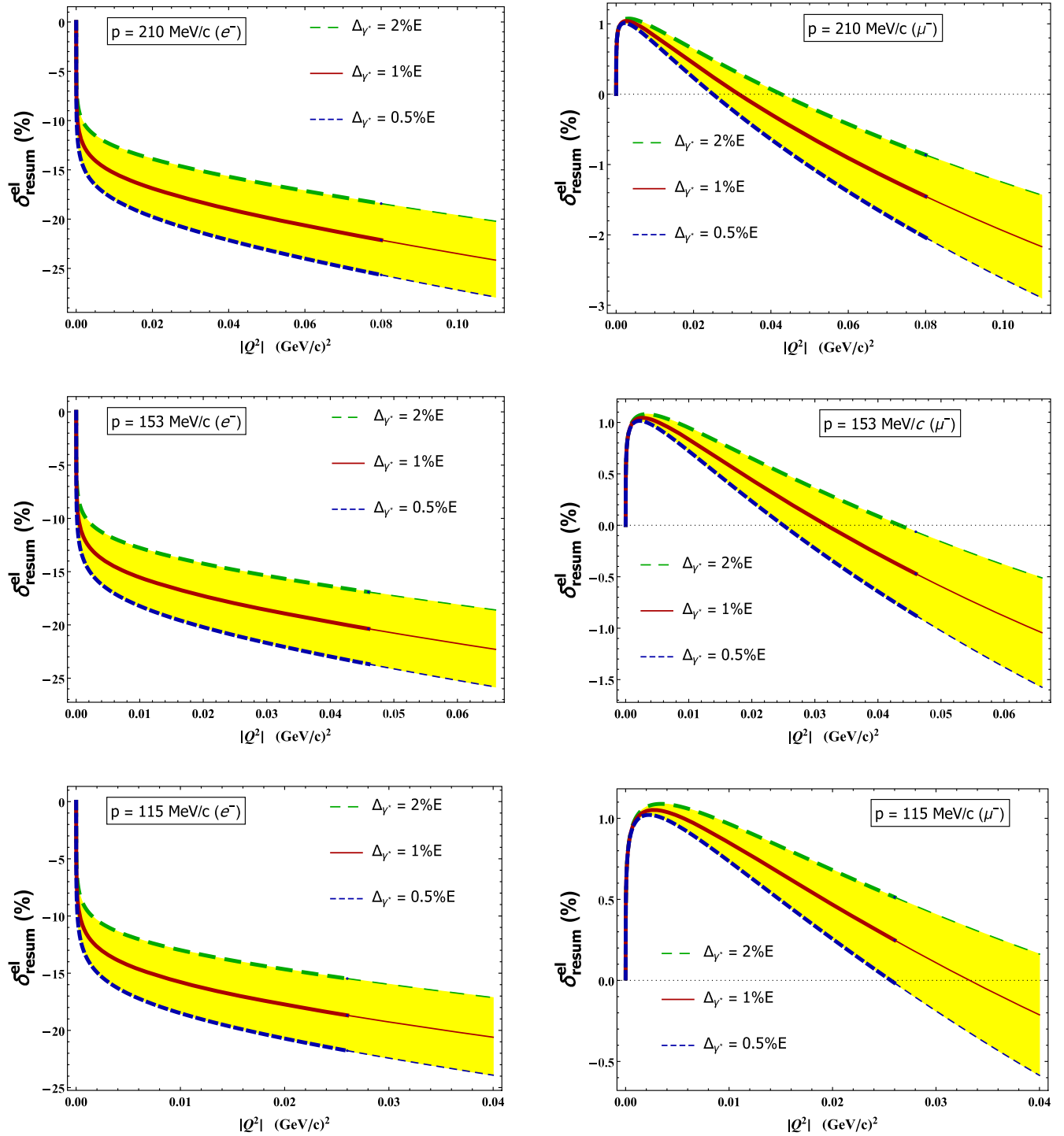


FIG. 14. Variation of the partially resummed fractional radiative correction up to and including  $\text{NLO}_\alpha$ ,  $\delta_{\text{resum}}^{\text{el}}$ , in  $\text{HB}\chi\text{PT}$  to  $e$ - $p$  (left panel) and  $\mu$ - $p$  (right panel) elastic cross sections as a function of  $|Q^2|$  for the MUSE beam momenta,  $|\vec{p}| = p = 115, 153, 210$  MeV/ $c$ . Each plot covers the full kinematic range  $0 < |Q^2| < |Q_{\text{max}}^2|$  when  $\theta \in [0, \pi]$ . The thickened portion of each curve corresponds to the MUSE kinematic cut, where  $\theta \in [20^\circ, 100^\circ]$ . The (yellow) bands correspond to the variation of the results with the lab frame detector acceptance in the range,  $0.5\% < \Delta_{\gamma^*} < 2\%$ , of the incident lepton energy  $E$ .

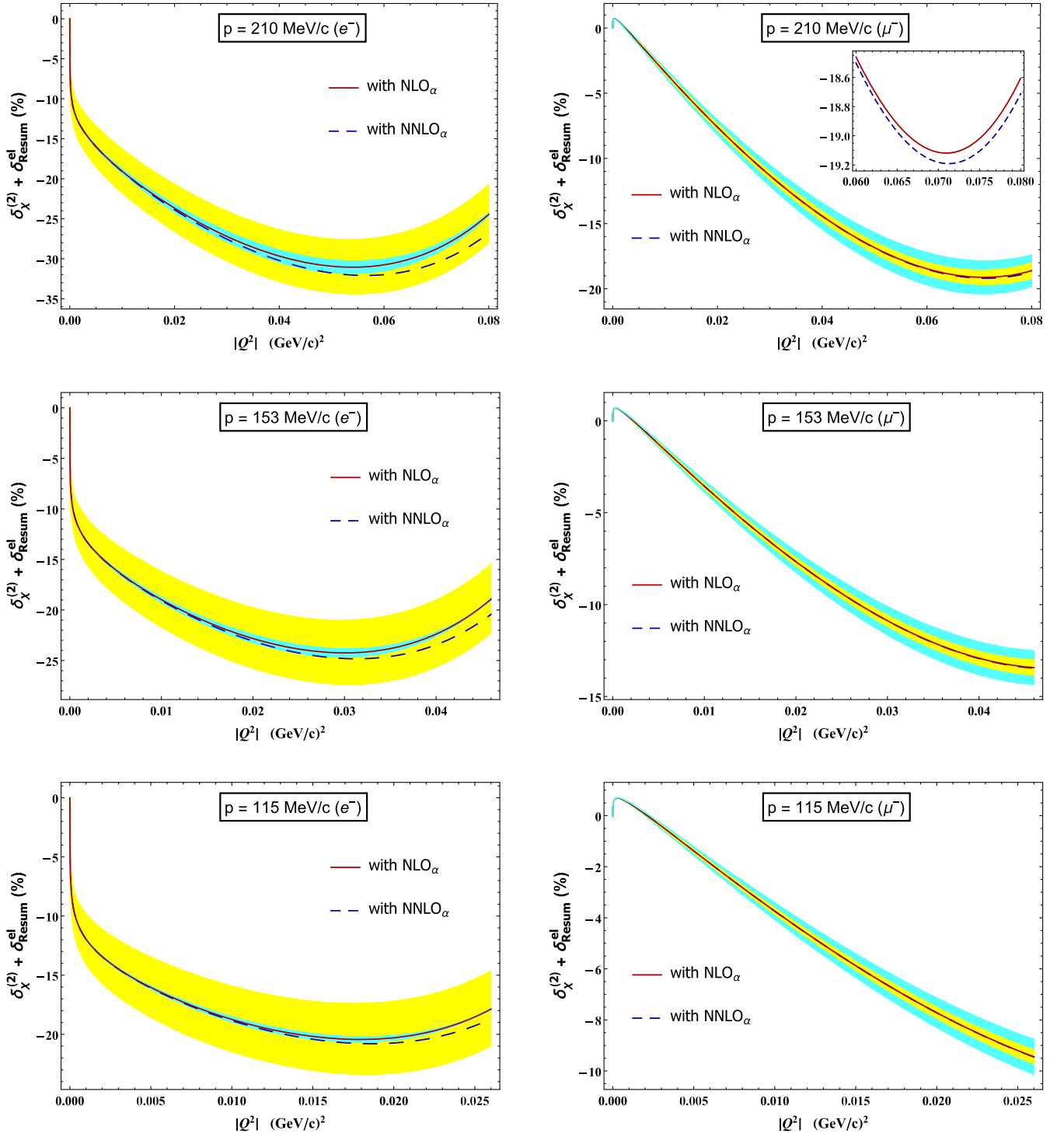


FIG. 15. The total fractional corrections considered in this work, i.e.,  $\delta_\chi^{(2)} + \delta_{\text{resum}}^{\text{el}}$ , (in percentage) for  $e$ - $p$  (left panel) and  $\mu$ - $p$  (right panel) elastic scattering cross sections as a function of  $|Q^2|$ . Each plot covers only the MUSE kinematic range of  $|Q^2|$  values where the scattering angle lies within the range,  $\theta \in [20^\circ, 100^\circ]$ , at specific incoming lepton momenta,  $|\vec{p}| = p = 115, 153, 210$  MeV/ $c$ . The solid (dashed) red (blue) curves correspond to the partially resummed radiative corrections up to and including NLO $_\alpha$  (including NNLO $_\alpha$ ), with the lab frame detector acceptance  $\Delta_{\gamma^*}$  being 1% of the incident lepton energy  $E$ . The yellow bands correspond to the error in the radiative corrections due to the variation,  $0.5\% < \Delta_{\gamma^*} < 2\%$ , while the bands in cyan correspond to the error in the pure hadronic chiral corrections  $\delta_\chi^{(2)}$ .

## VI. CONCLUSIONS

Within the framework of HB $\chi$ PT, we have evaluated up-to-and-including-NNLO $_{\chi}$  hadronic chiral corrections as well as the NLO $_{\alpha}$  radiative corrections to elastic lepton-proton scattering cross section. The hadronic chiral corrections include the pion loop effects and LECs parametrizing the proton structure. We found that in the MUSE kinematic range the NNLO $_{\chi}$  fractional corrections with respect to the leading-order Born cross section are about 10% and 20% for electron and muon scattering processes, respectively. We further estimated that the next-higher-order hadronic corrections (N<sup>3</sup>LO $_{\chi}$ ) do not contribute a larger uncertainty than the current experimental discrepancies pertaining to the rms radius. Regarding the radiative corrections, we included all possible virtual photon loops as well as soft photon bremsstrahlung corrections. We demonstrated that the IR divergences systematically cancel at each radiative chiral-order, i.e., at LO $_{\alpha}$  and NLO $_{\alpha}$ .

Only in our analytical calculations of the one-loop TPE box diagrams, do we invoke SPA following our evaluations in the previous work outlined in Ref. [58]. With methodological difficulties associated with the exact evaluation of the box diagrams in DR, the SPA methodology offers a standard analytical procedure in assessing the contribution from the elastic intermediate proton state, as advocated in Refs. [1,45].<sup>9</sup> Unfortunately, the contribution of the kinematically hard two-photon-loops integration regions is left out in the process. It is, however, a well-accepted fact that the contribution from the hard part of the TPE loops becomes significant only at large- $|Q^2|$  values and lepton beam energies as well as in the proximal region of backscattering. On the other hand, given the very low-energy dynamics of our calculations, it is conceivable that the hard part (those essentially stemming from the inelastic dynamics of partons) would not effect the TPE contributions in any significant way (see, e.g., Ref. [84] for recent discussions). Nevertheless, the issue of including the two-hard-photon exchange should be considered in a future investigation in order to reduce the systematic errors in the TPE evaluation. In order to minimize possible model dependence, our approach utilizes the existing analytically derived  $\chi$ PT form factors [51,52,54], consistent with our power counting scheme. By directly relying on the input proton's rms radius, we tacitly bypassed the introduction of model form factors,  $F_{1,2}^p$  at the photon-proton vertices, unlike in the work of, e.g., Ref. [42], in which the finite part of the TPE amplitudes was evaluated numerically in a relativistic framework. What is still not clear is how large

the two-hard-photon contributions are relative to the SPA they employed in order to isolate the IR-singularity following Ref. [1]. For this reason, and since we cannot assess the influence the form factors on their results, we are at this point unable to estimate the possible systematic uncertainties incurred due of the use of SPA in our evaluation.

In our estimate of the bremsstrahlung contributions due to the undetected soft photons with energies below the detector threshold  $\Delta_{\gamma^*}$ , we use the soft photon momentum limit  $k \rightarrow 0$  in our calculations, a methodology widely used to extract the IR divergences as introduced in Ref. [57]. However, the introduction of the artificial dependence on the free parameter  $\Delta_{\gamma^*}$  is certainly a demerit of the current methodology that needs to be improved in future, e.g., by the inclusion of the hard or detectable part of the elastic radiative tail for a realistic estimation of the radiative corrections. All our analytical results presented in this paper depend on  $\Delta_{\gamma^*} \sim 1\%$ , which theoretically complies with the expected lowest bremsstrahlung photon energy detectable in present-day experiments. We simply note here that in the case of the MUSE setup with a single arm beam line arrangement, only high-energy photons at forward angles can be detected. Thus, from a more practical viewpoint, a modification of our current analysis incorporating the anticipated MUSE features must be employed for a more pertinent future data analysis.

Notably, in all our evaluations in this work, we have explicitly included the masses of the leptons and also the often neglected Pauli form factor contributions to the lepton-photon vertex corrections. Our calculations revealed that both the TPE and the proton bremsstrahlung process start to contribute to the radiative corrections only at NLO $_{\alpha}$  in HB $\chi$ PT. Our work suggests that in the MUSE kinematic range, the total radiative corrections up to and including NLO $_{\alpha}$  for electron scattering can be as large as 25%, while for muon scattering, they are no more than 2% (cf. Fig. 14). Furthermore, we observe that for the muon scattering, the LO $_{\alpha}$  radiative correction  $\delta_{2\gamma}^{(0)}$  goes through zero in the MUSE kinematic range; i.e., in this energy range, the NLO $_{\alpha}$  contributions dominate. This naturally indicates the importance of the NNLO $_{\alpha}$  corrections in order to correctly assess the insofar neglected proton's structure-dependent chiral-radiative effects. Although such NNLO $_{\alpha}$  corrections have been partially included in this work for the sake of estimating the theoretical error, a complete NNLO $_{\alpha}$  evaluation is relegated to a possible future project. We finally remark that in the work of Ref. [68], a HB $\chi$ PT estimation of the elastic radiative tail distribution was considered at NLO $_{\alpha}$  accuracy, where IR divergences were not explicitly addressed. Thus, a renewed low-energy HB $\chi$ PT approach is needed in order to explore the prospects of a systematic inclusion of the radiative tail effects in a complete radiative “unfolding” analysis in close analogy to the erstwhile work of Ref. [61].

<sup>9</sup>To contrast our nonrelativistic chiral expansion in inverse powers of the proton mass  $M$ , the analysis of the TPE amplitudes, e.g., in Ref [45], were evaluated relativistically, meaning that they preserve terms to all orders in  $1/M$ .

## ACKNOWLEDGMENTS

We are thankful to Dipankar Chakrabarti, Poonam Choudhary, Daniel Phillips, Maciej Rybczyński, and Steffen Strauch for useful discussions at various stages of this work. P. T. acknowledges the kind hospitality of the Department of Physics, IIT Kanpur, where part of the work was done, and V. S. acknowledges the financial support through the Narodowe Centrum Nauki (NCN) via the OPUS Project No. 2019/33/B/ST2/00613.

## APPENDIX A: S-FRAME

In this Appendix, we discuss the  $\bar{\Gamma}$  between the lab frame and the boosted  $S$ -frame [1,59–62]. The  $S$ -frame is defined as the center-of-mass system of the recoil proton and the soft bremsstrahlung photon, such that

$$\vec{p}'_p + \vec{k} = \vec{Q} \xrightarrow{S\text{-frame}} \vec{Q}_S = \vec{0}. \quad (\text{A1})$$

Here,  $\vec{p}'_p$  and  $\vec{k}$  are the respective lab frame three-momenta of the recoil proton and the emitted soft photon, and  $\vec{Q} = \vec{p} - \vec{p}' = \vec{p}'_p - \vec{p}_p$  is the three-momentum transferred in the  $\ell$ - $p$  elastic scattering process in the lab frame, i.e., the target proton three-momentum  $\vec{p}_p = \vec{0}$ . The maximum energy of the soft (undetected) photon fixes the upper limit of the bremsstrahlung energy integration and is conventionally taken as detector acceptance  $\Delta_{\gamma^*}$  in the lab frame. This in essence corresponds to the maximal deviation of the outgoing lepton energy  $E'^{el}$  from its theoretical elastic limit  $E'$  while practically preserving elastic conditions, i.e.,  $E' - E'^{el} \leq \Delta_{\gamma^*}$ . In the ensuing treatment using the soft photon limit, namely,  $k = (E_{\gamma^*}, \vec{k}) \rightarrow 0$ , we shall use  $E'^{el} \approx E'$ .<sup>10</sup> In a boosted frame, the maximum photon energy limit becomes a frame-dependent quantity, which we denote as  $\Delta_S \neq \Delta_{\gamma^*}$  in the  $S$ -frame. The phase-space integration for the lab frame differential cross section for the soft bremsstrahlung process,  $\ell p \rightarrow \ell p \gamma_{\text{soft}}^*$ , namely,

$$[\tilde{d}\sigma_{\text{br}}^{(\text{LO}_\alpha, \text{NLO}_\alpha)}]_{\gamma\gamma^*} = \frac{(2\pi)\delta_k^{\text{lab}}}{8ME'_p E} \frac{d^3\vec{p}'}{(2\pi)^3 2E'} \frac{d^3\vec{k}}{(2\pi)^3 2E_{\gamma^*}} \times \frac{1}{4} \sum_{\text{spins}} |\widetilde{\mathcal{M}}_{\gamma\gamma^*}^{(\text{LO}_\alpha, \text{NLO}_\alpha)}|^2, \quad (\text{A2})$$

with the  $\text{LO}_\alpha$  and  $\text{NLO}_\alpha$  squared bremsstrahlung amplitudes  $\widetilde{\mathcal{M}}_{\gamma\gamma^*}^{(\text{LO}_\alpha, \text{NLO}_\alpha)}$  in the respective soft photon limits [cf. Eqs. (62)

<sup>10</sup>In general, with real photon emissions,  $E'^{el} \leq E'$ . The equality only holds for the “strictly elastic” (nonradiative) kinematics, which is evidently unrealistic in a given laboratory experiment. In this work, since we are concerned with the “physical” elastic process that is naturally accompanied by soft photon bremsstrahlung,  $E'^{el} \approx E'$  is implicitly understood.

and (88) in the main text], is complicated by the dependence on the photon emission angles present in the energy conserving  $\delta$ -function, namely,

$$\delta_k^{\text{lab}} \equiv \delta\left(E + M - E' - \sqrt{(\vec{Q} - \vec{k})^2 + M^2} - E_{\gamma^*}\right),$$

appearing in the above expression. Consequently, the emitted photon radiation spectrum in the lab frame becomes anisotropic, being defined over a ellipsoidal integration volume, which is difficult to evaluate analytically. However, by boosting to the  $S$ -frame, the integration simplifies into a standard spherical one (see, e.g., Ref. [59]), with the above  $\delta$ -function becoming free of the photon angles in the soft photon limit. This effectively transforms the  $S$ -frame kinematics into one akin to a “reversed” elastic scenario in the soft photon limit, denoted by the constraint,

$$\delta^S \equiv \delta(E^S + E_p^S - E'^S - E_p'^S),$$

where all  $S$ -frame quantities are denoted by the superscript “ $S$ ”. In terms of the lab frame quantities, the following relationships can then be justified,

$$\begin{aligned} \text{(i)} \quad E_p'^S &\approx M, & \text{(ii)} \quad E^S &\approx E' = \frac{E}{\eta}, \\ \text{(iii)} \quad E'^S &\approx E, & \text{(iv)} \quad E_p^S &\approx E'_p, \\ \text{(v)} \quad \cos\theta_S &\approx \cos\theta, & \text{(vi)} \quad \Delta_S &\approx \eta\Delta_{\gamma^*}, \end{aligned} \quad (\text{A3})$$

where  $\eta = 1 + 2E \sin^2(\theta/2)/M$  is the lab frame proton recoil factor. In other words, the energy transformations between the two frames are easily effected by simply interchanging the energies between the initial and final states of the elastic process.

In view of pedagogical interests, we derive these relations between the two frames using the limit of soft photons. We make use of the four-momentum conservation relation for the bremsstrahlung process, namely,  $p + P - p' = P' + k$ :

(i) First, we consider the invariant  $(P' + k)^2$  in the  $S$ -frame:

$$(P'^S + k^S)^2 = M^2 + 2E_p'^S E_{\gamma^*}^S + 2(E_{\gamma^*}^S)^2 \xrightarrow{\gamma_{\text{soft}}} M^2.$$

Since  $\vec{p}'_p^S + \vec{k}^S = \vec{0}$ , we must have

$$(P'^S + k^S)^2 = (E_p'^S + E_{\gamma^*}^S)^2 \xrightarrow{\gamma_{\text{soft}}} (E_p'^S)^2,$$

which implies  $E_p'^S \approx M$ .

(ii) Second, we consider the invariant  $p \cdot (P' + k)$ . In the  $S$ -frame, we have

$$p^S \cdot (P'^S + k^S) = E^S (E_p'^S + E_{\gamma^*}^S) \xrightarrow{\gamma_{\text{soft}}} M E^S,$$

while in the lab frame, we have

$$\begin{aligned} p \cdot (P' + k) &= p \cdot (P + Q) \\ &= ME + \frac{Q^2}{2} = ME'. \end{aligned}$$

This implies  $E^S \approx E'$ .

(iii) Third, we consider the invariant  $p' \cdot (P' + k)$ :

$$\begin{aligned} p' \cdot (P' + k) &= p'^S \cdot (P'^S + k^S) \\ \hookrightarrow p' \cdot (P + Q) &= E'^S (E_p'^S + E_{\gamma^*}^S) \\ &\stackrel{\gamma_{\text{soft}}}{\rightsquigarrow} ME' - \frac{Q^2}{2} \approx ME'^S. \end{aligned}$$

Since,  $E = E' - Q^2/(2M)$ , the above relation implies  $E'^S \approx E$ .

(iv) Fourth, we consider the energy conservation in the  $S$ -frame,

$$\begin{aligned} E^S + E_p^S - E'^S &= E_p'^S + E_{\gamma^*}^S, \\ E_p^S &= E_p'^S + E_{\gamma^*}^S + E'^S - E^S \\ &\stackrel{\gamma_{\text{soft}}}{\rightsquigarrow} M + E - E' \approx E_p', \end{aligned}$$

where we have used the relations derived for  $E^S$ ,  $E'^S$ , and  $E_p^S$ . Thus  $E_p^S \approx E_p'$ .

(v) Fifth, we use the invariant expression for the squared four-momentum transfer  $Q^2 = Q_S^2$  in each frame,

$$\begin{aligned} Q^2 &= 2m_l^2 - 2EE'(1 - \beta\beta' \cos \theta), \\ Q_S^2 &= 2m_l^2 - 2E^S E'^S (1 - \beta_S \beta'_S \cos \theta_S) \\ &\stackrel{\gamma_{\text{soft}}}{\rightsquigarrow} 2m_l^2 - 2E'E(1 - \beta'\beta \cos \theta_S), \end{aligned}$$

where the incoming and outgoing lepton velocities in the lab frame and  $S$ -frame are ( $\beta = |\vec{p}|/E$ ,  $\beta' = |\vec{p}'|/E'$ ) and ( $\beta_S = |\vec{p}^S|/E^S$ ,  $\beta'_S = |\vec{p}'^S|/E'^S$ ), respectively, and  $\theta$ ,  $\theta_S$  are the corresponding scattering angles. Using the relations derived for  $E^S$ ,  $E'^S$ , it follows that  $\cos \theta_S \approx \cos \theta$ .

(vi) Finally, squaring the aforementioned four-momentum conservation relation and then expressing the left- and right-hand sides in terms of the lab frame and  $S$ -frame quantities, respectively, yields

$$\begin{aligned} 2m_l^2 - 2p \cdot p' + 2M(E - E'^{el}) &= 2P'^S \cdot k^S \\ &= 2M\Delta_S \sqrt{1 + \left(\frac{\Delta_S}{M}\right)^2} + 2\Delta_S^2, \end{aligned}$$

where  $E' - E'^{el} \leq \Delta_S$ , with  $\Delta_S$  being the maximal limit of the emitted soft photon energy in the  $S$ -

frame, i.e.,  $E_{\gamma^*}^S = |\vec{k}^S| \lesssim \Delta_S \ll M$ . Next, to obtain an estimate for  $\Delta_S$  in the soft photon limit, we further neglect the lepton mass,  $m_l \ll M$ , such that the above relation becomes

$$\begin{aligned} M(E - E'^{el}) - EE'^{el}(1 - \cos \theta) \\ = M\Delta_S \left[ 1 + \mathcal{O}\left(\frac{\Delta_S}{M}\right) \right]. \end{aligned}$$

Furthermore, in the elastic limit, i.e., with  $\Delta_S \rightarrow 0$  and  $E'^{el} \rightarrow E'$ , the above equation reduces to

$$M(E - E') - EE'(1 - \cos \theta) = 0.$$

Then, subtracting the latter relation from the former yields our desired expression for  $\Delta_S$ :

$$\begin{aligned} \Delta_S &= (E' - E'^{el}) \left[ 1 + \frac{2E}{M} \sin^2\left(\frac{\theta}{2}\right) \right] \\ &+ \mathcal{O}\left(\frac{\Delta_S}{M}\right) \approx \eta\Delta_{\gamma^*}. \end{aligned}$$

Thus, the upper limit of the soft photon bremsstrahlung integrals (see Appendix B) in the  $S$ -frame is taken as  $\Delta_S \leq \eta\Delta_{\gamma^*}$ .

## APPENDIX B: SOFT BREMSSTRAHLUNG INTEGRALS

As detailed in this paper, the one-loop virtual radiative corrections possess IR divergences at the amplitude level. These integrals are conveniently evaluated by boosting to the  $S$ -frame following, e.g., Refs. [1,59–62], and some details of these calculations will be outlined in this Appendix. For the bremsstrahlung corrections, similar IR divergences have to be extracted at the cross section level, which involves integration over the soft photon radiative tail below the detector threshold, i.e.,  $E_{\gamma^*} < \Delta_{\gamma^*}$ . The IR divergences so extracted in each case were demonstrated to cancel order by order. Below, we demonstrate the process of extracting the IR divergences using DR from the phase-phase integration of Eq. (A2). Notably, the assumption that the soft photon emission (i.e.,  $k \rightarrow 0$ ) does not effectively alter the elastic kinematics, implies that the four-momentum transfer for the bremsstrahlung process,  $q = (Q - k)$ , is approximately equal to the four-momentum transfer  $Q$  for the elastic process. This simplification allows the photon phase-space integration to be performed analytically in closed form. Using the  $\text{LO}_\alpha$  and  $\text{NLO}_\alpha$  squared bremsstrahlung amplitudes [cf. Eqs. (62) and (88) in the main text] results in the following type of integrals:

$$\text{@LO}_\alpha \ \& \ \text{NLO}_\alpha: \int \frac{d^3\vec{k}}{k} \frac{1}{(p \cdot k)^2} \delta_k^{\text{lab}}, \quad (\text{B1})$$

$$\text{@LO}_\alpha \ \& \ \text{NLO}_\alpha: \int \frac{d^3\vec{k}}{k} \frac{1}{(p' \cdot k)^2} \delta_k^{\text{lab}}, \quad (\text{B2})$$

$$\text{@LO}_\alpha \ \& \ \text{NLO}_\alpha: \int \frac{d^3\vec{k}}{k} \frac{p' \cdot p}{(p \cdot k)(p' \cdot k)} \delta_k^{\text{lab}}, \quad (\text{B3})$$

$$\text{@NLO}_\alpha: \int \frac{d^3\vec{k}}{k} \frac{l}{(v \cdot k)(p \cdot k)} \delta_k^{\text{lab}}, \quad (\text{B4})$$

$$\text{@NLO}_\alpha: \int \frac{d^3\vec{k}}{k} \frac{l}{(v \cdot k)(p' \cdot k)} \delta_k^{\text{lab}}. \quad (\text{B5})$$

Especially, the first three types of integrals appearing in both the  $\text{LO}_\alpha$  and  $\text{NLO}_\alpha$  contributions to the bremsstrahlung process were known from earlier works, e.g., in Refs. [61,85]. The presence of the *bremsstrahlung*  $\delta$ -function constraint  $\delta_k^{\text{lab}}$  (see Appendix A) in the above integrals complicates their evaluation in the lab frame. However, this apparent hurdle is overcome by employing Tsai's technique [59] of boosting to the  $S$ -frame in the soft photon limit. The corresponding *elastic*  $\delta$ -function  $\delta^S$  (see Appendix A) becomes  $|\vec{k}| = E_{\gamma^*}$  independent and can therefore be readily taken outside the integrals. The resulting integrals in the  $S$ -frame are evaluated by analytically continuing to  $d-1$  spatial dimensions, where  $d-1 = 3 - 2\epsilon_{\text{IR}}$  with  $\epsilon_{\text{IR}} < 0$ . Thus, in terms of laboratory frame variables, the following  $S$ -frame integrals are required to be evaluated via dimensional regularization,

$$\begin{aligned} L_{\text{ii}}^{(S)} &= \frac{m_l^2}{2} \int \frac{d^3\vec{k}^S}{k^S} \frac{1}{(p^S \cdot k^S)^2} \xrightarrow{\text{DR}} \frac{m_l^2}{2} \int \frac{d^{d-1}k^S}{k^S} \frac{1}{(p^S \cdot k^S)^2} \\ &= \frac{m_l^2}{2} (2\pi\mu)^{2\epsilon_{\text{IR}}} \int_0^{\eta_{\Delta\gamma^*}} (k^S)^{d-3} dk^S \oint d^{d-2}\Omega_k^S \frac{1}{(p^S \cdot k^S)^2} \\ &= \pi \left[ \frac{1}{|\epsilon_{\text{IR}}|} + \gamma_E - \ln\left(\frac{4\pi\mu^2}{-Q^2}\right) \right] + 2\pi\tilde{L}_{\text{ii}}^{(S)}, \end{aligned} \quad (\text{B6})$$

where  $\mu$  is the subtraction scale, and similarly,

$$L_{\text{ff}}^{(S)} \xrightarrow{\text{DR}} \frac{m_l^2}{2} \int \frac{d^{d-1}k^S}{k^S} \frac{1}{(p'^S \cdot k^S)^2} = \pi \left[ \frac{1}{|\epsilon_{\text{IR}}|} + \gamma_E - \ln\left(\frac{4\pi\mu^2}{-Q^2}\right) \right] + 2\pi\tilde{L}_{\text{ff}}^{(S)}, \quad (\text{B7})$$

$$L_{\text{if}}^{(S)} \xrightarrow{\text{DR}} \int \frac{d^{d-1}k^S}{k^S} \frac{(p'^S \cdot p^S)}{(p^S \cdot k^S)(p'^S \cdot k^S)} = \pi \left[ \frac{1}{|\epsilon_{\text{IR}}|} + \gamma_E - \ln\left(\frac{4\pi\mu^2}{-Q^2}\right) \right] \frac{\nu^2 + 1}{\nu} \ln\left[\frac{\nu + 1}{\nu - 1}\right] + 2\pi\tilde{L}_{\text{if}}^{(S)}, \quad (\text{B8})$$

$$L_{\text{i}}^{(S)} \xrightarrow{\text{DR}} \frac{1}{2} \int \frac{d^{d-1}k^S}{k^S} \frac{1}{(v \cdot k^S)(p^S \cdot k^S)} = \frac{\pi}{\beta' E'} \left[ \frac{1}{|\epsilon_{\text{IR}}|} + \gamma_E - \ln\left(\frac{4\pi\mu^2}{-Q^2}\right) \right] \ln\sqrt{\frac{1 + \beta'}{1 - \beta'}} + 2\pi\tilde{L}_{\text{i}}^{(S)}, \quad (\text{B9})$$

$$L_{\text{f}}^{(S)} \xrightarrow{\text{DR}} \frac{1}{2} \int \frac{d^{d-1}k^S}{k^S} \frac{1}{(v \cdot k^S)(p'^S \cdot k^S)} = \frac{\pi}{\beta E} \left[ \frac{1}{|\epsilon_{\text{IR}}|} + \gamma_E - \ln\left(\frac{4\pi\mu^2}{-Q^2}\right) \right] \ln\sqrt{\frac{1 + \beta}{1 - \beta}} + 2\pi\tilde{L}_{\text{f}}^{(S)}. \quad (\text{B10})$$

Here,  $k^S = |\vec{k}^S| = E_{\gamma^*}^S$  is the soft photon three-momentum or energy;  $\beta = p/E$  and  $\beta' = p'/E' \approx \beta'^{\text{el}} = p'^{\text{el}}/E'^{\text{el}}$  are the incoming and elastically scattered outgoing lepton velocities; and as found ubiquitous in the main text,  $\nu = \sqrt{1 - 4m_l^2/Q^2}$  is an invariant kinematical variable associated with the radiative corrections to the lepton scattering. Note that we additionally encounter an integral stemming from Eq. (88) (main text), formally contributing to the bremsstrahlung cross section at  $\text{NLO}_\alpha$  but kinematically suppressed to  $\text{NNLO}_\alpha$  being proportional to  $\mathcal{R}_Q$ , namely,

$$2\mathcal{R}_Q \int \frac{d^3\vec{k}^S}{(k^S)^3} \xrightarrow{\text{DR}} 2\mathcal{R}_Q \int \frac{d^{d-1}k^S}{(k^S)^3} \rightarrow 0,$$

which is scaleless and vanishes trivially on using DR. Next, after isolating the finite parts,  $\tilde{L}_{\text{ii}}^{(S)}$ ,  $\tilde{L}_{\text{ff}}^{(S)}$ , and  $\tilde{L}_{\text{if}}^{(S)}$ , from their respective IR-divergent parts, we revert back to the lab frame. In this case, the corresponding lab frame integrals are readily obtained by substituting the energy transformation relations (see Appendix A), namely,



$$L_{\text{ii}} = \pi \left[ \frac{1}{|\epsilon_{\text{IR}}|} + \gamma_E - \ln \left( \frac{4\pi\mu^2}{-Q^2} \right) \right] + 2\pi\tilde{L}_{\text{ii}}; \quad \tilde{L}_{\text{ii}} = \frac{1}{2} \ln \left( \frac{4\eta^2\Delta_{\gamma^*}^2}{-Q^2} \right) - \frac{1}{4\beta} \ln \sqrt{\frac{1+\beta}{1-\beta}}, \quad (\text{B11})$$

$$L_{\text{ff}} = \pi \left[ \frac{1}{|\epsilon_{\text{IR}}|} + \gamma_E - \ln \left( \frac{4\pi\mu^2}{-Q^2} \right) \right] + 2\pi\tilde{L}_{\text{ff}}; \quad \tilde{L}_{\text{ff}} = \frac{1}{2} \ln \left( \frac{4\eta^2\Delta_{\gamma^*}^2}{-Q^2} \right) - \frac{1}{4\beta'} \ln \sqrt{\frac{1+\beta'}{1-\beta'}}, \quad (\text{B12})$$

$$L_{\text{if}} = \pi \left[ \frac{1}{|\epsilon_{\text{IR}}|} + \gamma_E - \ln \left( \frac{4\pi\mu^2}{-Q^2} \right) \right] \frac{\nu^2 + 1}{\nu} \ln \left[ \frac{\nu + 1}{\nu - 1} \right] + 2\pi\tilde{L}_{\text{if}};$$

$$\tilde{L}_{\text{if}} = \frac{\nu^2 + 1}{2\nu} \left[ \ln \left( \frac{4\eta^2\Delta_{\gamma^*}^2}{-Q^2} \right) \ln \left[ \frac{\nu + 1}{\nu - 1} \right] + \ln^2 \sqrt{\frac{1+\beta'}{1-\beta'}} - \ln^2 \sqrt{\frac{1+\beta}{1-\beta}} - \text{Sp} \left( 1 - \frac{\lambda_\nu E' - E}{(1-\beta')E'\xi_\nu} \right) \right. \\ \left. - \text{Sp} \left( 1 - \frac{\lambda_\nu E' - E}{(1+\beta)E\lambda_\nu\xi_\nu} \right) + \text{Sp} \left( 1 - \frac{\lambda_\nu E' - E}{(1-\beta)E\lambda_\nu\xi_\nu} \right) + \text{Sp} \left( 1 - \frac{\lambda_\nu E' - E}{(1+\beta)E\lambda_\nu\xi_\nu} \right) \right], \quad (\text{B13})$$

$$L_{\text{i}} = \frac{\pi}{\beta E} \left[ \frac{1}{|\epsilon_{\text{IR}}|} + \gamma_E - \ln \left( \frac{4\pi\mu^2}{-Q^2} \right) \right] \ln \sqrt{\frac{1+\beta}{1-\beta}} + 2\pi\tilde{L}_{\text{i}};$$

$$\tilde{L}_{\text{i}} = \frac{1}{2\beta E} \left[ \ln \left( \frac{4\eta^2\Delta_{\gamma^*}^2}{-Q^2} \right) \ln \sqrt{\frac{1+\beta}{1-\beta}} + \frac{1}{2} \text{Sp} \left( \frac{2\beta}{\beta+1} \right) - \frac{1}{2} \text{Sp} \left( \frac{2\beta}{\beta-1} \right) \right], \quad (\text{B14})$$

$$L_{\text{f}} = \frac{\pi}{\beta' E'} \left[ \frac{1}{|\epsilon_{\text{IR}}|} + \gamma_E - \ln \left( \frac{4\pi\mu^2}{-Q^2} \right) \right] \ln \sqrt{\frac{1+\beta'}{1-\beta'}} + 2\pi\tilde{L}_{\text{f}};$$

$$\tilde{L}_{\text{f}} = \frac{1}{2\beta' E'} \left[ \ln \left( \frac{4\eta^2\Delta_{\gamma^*}^2}{-Q^2} \right) \ln \sqrt{\frac{1+\beta'}{1-\beta'}} + \frac{1}{2} \text{Sp} \left( \frac{2\beta'}{\beta'+1} \right) - \frac{1}{2} \text{Sp} \left( \frac{2\beta'}{\beta'-1} \right) \right], \quad (\text{B15})$$

where  $\xi_\nu = \frac{2\nu}{(\nu+1)(\nu-1)}$  and  $\lambda_\nu = \frac{3\nu-1}{\nu-1}$ .

Finally, we present the expression for the nonfactorizable finite part [i.e., not proportional to the LO Born contribution, Eq. (23) in the main text] of the bremsstrahlung differential cross sections at NLO $_\alpha$  [cf. Eq. (91) in the main text] involving an exact analytical evaluation (viz., without considering the soft photon limit) by boosting to the  $S$ -frame:

$$\left[ \frac{d\sigma_{\text{br}}(Q^2)}{d\Omega_l'} \right]_{\gamma\gamma^*}^{l_{p(1);v}} \Big|_{S\text{-frame}} = -\frac{4\alpha^3}{\pi^2 Q^2 M} \left( \frac{\eta\beta}{\beta'} \right) \int_0^{\eta\Delta_{\gamma^*}} \frac{k^S dk^S}{Q^2 - 2k^S(E' - E)} \left[ 4\pi(E + E') + m_l^2(E + E')(L_{\text{iv}}^{(S)} - L_{\text{fv}}^{(S)}) \right. \\ \left. - E' L_{\text{iv}}^{(S)} - E L_{\text{iv}}^{(S)} + k^S \left( \frac{1}{2} Q^2 - m_l^2 \right) (L_{\text{iv}}^{(S)} + L_{\text{iv}}^{(S)}) \right], \\ = -\frac{8\alpha^3 \eta \Delta_{\gamma^*}}{\pi Q^4 M} \left( \frac{\eta\beta}{\beta'} \right) \left[ \eta \Delta_{\gamma^*} (E + E') - \left\{ 2m_l^2 (E - E') - \eta \Delta_{\gamma^*} \left( \frac{1}{2} Q^2 - m_l^2 \right) \right\} \right. \\ \times \left\{ \frac{1}{E\beta} \ln \sqrt{\frac{1+\beta}{1-\beta}} - \frac{1}{E'\beta'} \ln \sqrt{\frac{1+\beta'}{1-\beta'}} \right\} - \eta \Delta_{\gamma^*} \frac{E^2}{E'\beta'} \left\{ \left( 1 - \frac{\beta}{\beta'} \right) \ln \sqrt{\frac{1+\beta'}{1-\beta'}} - \beta \right\} \right. \\ \left. - \eta \Delta_{\gamma^*} \frac{E'^2}{E\beta} \left\{ \left( 1 - \frac{\beta'}{\beta} \right) \ln \sqrt{\frac{1+\beta}{1-\beta}} - \beta' \right\} + o \left( \frac{\{Q, \eta \Delta_{\gamma^*}\}}{M} \right) \right]. \quad (\text{B16})$$

Here, the evaluated integral is expressed in terms of lab frame quantities for convenience. Noting that  $E - E' = -Q^2/2M$ , the symbol “o” represents other possible  $1/M$ -order terms which arise due to the soft bremsstrahlung integration over the  $\Delta^{(1/M)}$ s [cf. Eqs. (90)] and contribute to the NNLO $_\alpha$  theoretical error. Since these terms are eventually dropped from our central analytical results intended at NLO $_\alpha$  accuracy, for brevity, we refrain from displaying such lengthy

expressions. They are, nonetheless, evaluated numerically while estimating the error. Finally, in the above expression,  $L_{iv}^{(S)}$ ,  $\mathbb{L}_{iv}^{(S)}$ ,  $L_{fv}^{(S)}$ , and  $\mathbb{L}_{fv}^{(S)}$  are the finite two-dimensional angular integrals:

$$L_{iv}^{(S)} = \oint\!\!\!\oint d\Omega_k^S \frac{1}{p^S \cdot k^S} = \frac{4\pi}{E' \beta' k^S} \ln \sqrt{\frac{1+\beta'}{1-\beta'}}, \quad (\text{B17})$$

$$\mathbb{L}_{iv}^{(S)} = \oint\!\!\!\oint d\Omega_k^S \frac{p'^S \cdot k^S}{p^S \cdot k^S} = \frac{4\pi E}{E' \beta'} \left[ \left(1 - \frac{\beta}{\beta'}\right) \ln \sqrt{\frac{1+\beta'}{1-\beta'} - \beta} \right], \quad (\text{B18})$$

$$L_{fv}^{(S)} = \oint\!\!\!\oint d\Omega_k^S \frac{1}{p'^S \cdot k^S} = \frac{4\pi}{E \beta k^S} \ln \sqrt{\frac{1+\beta}{1-\beta}}, \quad (\text{B19})$$

$$\mathbb{L}_{fv}^{(S)} = \oint\!\!\!\oint d\Omega_k^S \frac{p^S \cdot k^S}{p'^S \cdot k^S} = \frac{4\pi E'}{E \beta} \left[ \left(1 - \frac{\beta'}{\beta}\right) \ln \sqrt{\frac{1+\beta}{1-\beta} - \beta'} \right]. \quad (\text{B20})$$

On reverting back to the laboratory frame from the  $S$ -frame, we again use the same set of kinematical transformations (see Appendix A) to obtain the contribution to the fractional NLO $_{\alpha}$  bremsstrahlung corrections  $\delta_{\gamma\gamma^*}^{(1)}$  [cf. Eq. (94) in the main text] to the LO elastic (Born) differential cross section:

$$\begin{aligned} \delta_{\gamma\gamma^*}^{lp(1);v}(Q^2) &= \left[ \frac{d\sigma_{br}(Q^2)}{d\Omega'_l} \right]_{\gamma\gamma^*}^{lp(1);v} / \left[ \frac{d\sigma_{el}(Q^2)}{d\Omega'_l} \right]_0 \\ &= -\frac{\alpha}{\pi M \eta} \left( \frac{8\Delta_{\gamma^*}}{\eta Q^2 + 4E^2} \right) \left[ \Delta_{\gamma^*}(E + E') - \left\{ 2\eta m_l^2(E - E') + \Delta_{\gamma^*} \left( \frac{1}{2} Q^2 - m_l^2 \right) \right\} \right. \\ &\quad \times \left\{ \frac{1}{E\beta} \ln \sqrt{\frac{1+\beta}{1-\beta}} - \frac{1}{E'\beta'} \ln \sqrt{\frac{1+\beta'}{1-\beta'}} \right\} - \Delta_{\gamma^*} \frac{E^2}{E'\beta'} \left\{ \left(1 - \frac{\beta}{\beta'}\right) \ln \sqrt{\frac{1+\beta'}{1-\beta'} - \beta} \right\} \\ &\quad \left. - \Delta_{\gamma^*} \frac{E'^2}{E\beta} \left\{ \left(1 - \frac{\beta'}{\beta}\right) \ln \sqrt{\frac{1+\beta}{1-\beta} - \beta'} \right\} \right] + o\left(\alpha \frac{Q^2}{M^2}\right). \quad (\text{B21}) \end{aligned}$$

- 
- [1] L. C. Maximon and J. A. Tjon, *Phys. Rev. C* **62**, 054320 (2000).  
[2] M. K. Jones *et al.*, *Phys. Rev. Lett.* **84**, 1398 (2000).  
[3] C. F. Perdrisat, V. Punjabi, and M. Vanderhaeghen, *Prog. Part. Nucl. Phys.* **59**, 694 (2007).  
[4] A. J. R. Puckett *et al.*, *Phys. Rev. Lett.* **104**, 242301 (2010).  
[5] V. Punjabi, C. F. Perdrisat, M. K. Jones, E. J. Brash, and C. E. Carlson, *Eur. Phys. J. A* **51**, 79 (2015).  
[6] J. Arrington, *Phys. Rev. C* **68**, 034325 (2003).  
[7] P. A. M. Guichon and M. Vanderhaeghen, *Phys. Rev. Lett.* **91**, 142303 (2003).  
[8] P. G. Blunden, W. Melnitchouk, and J. A. Tjon, *Phys. Rev. Lett.* **91**, 142304 (2003).  
[9] J. Arrington, P. G. Blunden, and W. Melnitchouk, *Prog. Part. Nucl. Phys.* **66**, 782 (2011).  
[10] R. Pohl *et al.* (CREMA Collaboration), *Nature (London)* **466**, 213 (2010).  
[11] R. Pohl, R. Gilman, G. A. Miller, and K. Pachucki, *Annu. Rev. Nucl. Part. Sci.* **63**, 175 (2013).  
[12] A. Antognini *et al.*, *Science* **339**, 417 (2013).  
[13] J. C. Bernauer and R. Pohl, *Sci. Am.* **310**, 18 (2014).  
[14] C. E. Carlson, *Prog. Part. Nucl. Phys.* **82**, 59 (2015).  
[15] M. Mihovilovic *et al.*, *Phys. Lett. B* **771**, 194 (2017).  
[16] A. Beyer *et al.*, *Science* **358**, 79 (2017).  
[17] H. Fleurbaey, S. Galtier, S. Thomas, M. Bonnaud, L. Julien, F. Biraben, F. Nez, M. Abgrall, and J. Guéna, *Phys. Rev. Lett.* **120**, 183001 (2018).  
[18] B. Adams *et al.*, arXiv:1808.00848.  
[19] M. Mihovilovic and H. Merkel (A1-Collaboration), *EPJ Web Conf.* **218**, 04001 (2019).

- [20] N. Bezginov, T. Valdez, M. Horbatsch, A. Marsman, A. C. Vutha, and E. A. Hessels, *Science* **365**, 1007 (2019).
- [21] W. Xiong *et al.* (PRad Collaboration), *Nature (London)* **575**, 147 (2019).
- [22] A. Grinin, A. Matveev, Dylan C. Yost, L. Maisenbacher, V. Wirthl, R. Pohl, T. W. Hänsch, and T. Udem, *Science* **370**, 1061 (2020).
- [23] A. De Rujula, *Phys. Lett. B* **693**, 555 (2010).
- [24] A. De Rujula, *Phys. Lett. B* **697**, 26 (2011).
- [25] B.-Y. Wu and C.-W. Kao, [arXiv:1108.2968](https://arxiv.org/abs/1108.2968).
- [26] D. T. Smith and I. Yavin, *Phys. Rev. D* **83**, 101702 (2011).
- [27] V. Barger, C-W. Chiang, W-Y. Keung, and D. Marfatia, *Phys. Rev. Lett.* **106**, 153001 (2011).
- [28] V. Barger, C-W. Chiang, W-Y. Keung, and D. Marfatia, *Phys. Rev. Lett.* **108**, 081802 (2012).
- [29] C. E. Carlson and B. C. Rislow, *Phys. Rev. D* **86**, 035013 (2012).
- [30] L-B. Wang and W-T. Ni, *Mod. Phys. Lett. A* **28**, 1350094 (2013).
- [31] S. G. Karshenboim, D. McKeen, and M. Pospelov, *Phys. Rev. D* **90**, 073004 (2014).
- [32] C. Paset and A. Pineda, *Nucl. Phys.* **B887**, 69 (2014).
- [33] I. T. Lorenz, U.-G. Meißner, H. W. Hammer, and Y-B. Dong, *Phys. Rev. D* **91**, 014023 (2015).
- [34] J. C. Bernauer and M. O. Distler, [arXiv:1606.02159](https://arxiv.org/abs/1606.02159).
- [35] J. C. Bernauer, *EPJ Web Conf.* **234**, 01001 (2020).
- [36] H. W. Hammer and U. G. Meißner, *Sci. Bull.* **65**, 257 (2020); Y. H. Lin, H. W. Hammer, and U. G. Meißner, *Phys. Lett. B* **816**, 136254 (2021).
- [37] M. Horbatsch, E. A. Hessels, and A. Pineda, *Phys. Rev. C* **95**, 035203 (2017).
- [38] J. M. Alarcón, D. W. Higinbotham, C. Weiss, and Z. Ye, *Phys. Rev. C* **99**, 044303 (2019).
- [39] G. Lee, J. R. Arrington, and R. J. Hill, *Phys. Rev. D* **92**, 013013 (2015).
- [40] J. Arrington, *J. Phys. Chem. Ref. Data* **44**, 031203 (2015).
- [41] I. Sick, *Atoms* **6**, 2 (2018).
- [42] O. Tomalak and M. Vanderhaeghen, *Phys. Rev. D* **90**, 013006 (2014).
- [43] O. Tomalak and M. Vanderhaeghen, *Phys. Rev. D* **93**, 013023 (2016).
- [44] O. Tomalak and M. Vanderhaeghen, *Eur. Phys. J. C* **76**, 125 (2016).
- [45] O. Koshchii and A. Afanasev, *Phys. Rev. D* **96**, 016005 (2017).
- [46] O. Tomalak and M. Vanderhaeghen, *Eur. Phys. J. C* **78**, 514 (2018).
- [47] R. Gilman *et al.* (MUSE Collaboration), *AIP Conf. Proc.* **1563**, 167 (2013).
- [48] R. Gilman *et al.* (MUSE Collaboration), [arXiv:1709.09753](https://arxiv.org/abs/1709.09753).
- [49] S. Strauch, University of South Carolina (private communication).
- [50] S. Scherer, *Adv. Nucl. Phys.* **27**, 277 (2003).
- [51] V. Bernard, N. Kaiser, J. Kambor, and U.-G. Meißner, *Nucl. Phys.* **B388**, 315 (1992).
- [52] V. Bernard, N. Kaiser, and U.-G. Meißner, *Int. J. Mod. Phys. E* **04**, 193 (1995).
- [53] N. Fettes, U.-G. Meißner, and S. Steininger, *Nucl. Phys.* **A640**, 199 (1998); Corrections to misprints can be found in N. Fettes, Ph.D. thesis, Bonn University, 2000 (unpublished).
- [54] V. Bernard, H. W. Fearing, T. R. Hemmert, and U.-G. Meißner, *Nucl. Phys.* **A635**, 121 (1998); **642**, 563(E) (1998).
- [55] T. R. Hemmert, B. Holstein, and J. Kambor, *Phys. Lett. B* **395**, 89 (1997).
- [56] T. R. Hemmert, B. Holstein, and J. Kambor, *J. Phys. G* **24**, 1831 (1998).
- [57] D. R. Yennie, S. C. Frautschi, and H. Suura, *Ann. Phys. (N.Y.)* **13**, 379 (1961).
- [58] P. Talukdar, V. C. Shastry, U. Raha, and F. Myhrer, *Phys. Rev. D* **101**, 013008 (2020).
- [59] Y. S. Tsai, *Phys. Rev.* **122**, 1898 (1961).
- [60] L. W. Mo and Y.-S. Tsai, *Rev. Mod. Phys.* **41**, 205 (1969).
- [61] M. Vanderhaeghen, J. M. Friedrich, D. Lhuillier, D. Marchand, L. Van Hooft, and J. Van de Wiele, *Phys. Rev. C* **62**, 025501 (2000).
- [62] R. D. Bucoveanu and H. Spiesberger, *Eur. Phys. J. A* **55**, 57 (2019).
- [63] R. Gastmans and R. Meuldermans, *Nucl. Phys.* **B63**, 277 (1973).
- [64] W. Marciano and A. Sirlin, *Nucl. Phys.* **B88**, 86 (1975).
- [65] N. N. Bogoliubov and D. V. Shirkov, *Introduction to the Theory of Quantized Fields* (Wiley-Interscience, New York, 1959).
- [66] A. I. Akhiezer and V. B. Berestetskii, *Quantum Electrodynamics* (Interscience Publishers, New York, 1965).
- [67] J. B. Zuber and C. Itzykson, *Quantum Field Theory* (International Series in Pure and Applied Physics, McGraw-Hill, New York, 1985).
- [68] P. Talukdar, F. Myhrer, G. Meher, and U. Raha, *Eur. Phys. J. A* **54**, 195 (2018).
- [69] R. P. Feynman, *Phys. Rev.* **76**, 769 (1949).
- [70] R. N. Euwema and J. A. Wheeler, *Phys. Rev.* **103**, 803 (1956).
- [71] Y. S. Tsai, *Phys. Rev.* **120**, 269 (1960).
- [72] F. Low, *Phys. Rev.* **110**, 974 (1958).
- [73] P. Choudhary *et al.* (to be published).
- [74] J. Schwinger, *Phys. Rev.* **76**, 790 (1949).
- [75] J. Schwinger, *Phys. Rev.* **75**, 898 (1949); **21**, 383(E) (1949).
- [76] F. Bloch and A. Nordsieck, *Phys. Rev.* **52**, 54 (1937).
- [77] J. M. Jauch and F. Rohrlich, *Helv. Phys. Acta* **27**, 613 (1954).
- [78] E. L. Lomon, *Nucl. Phys.* **1**, 101 (1956).
- [79] E. L. Lomon, *Phys. Rev.* **113**, 726 (1959).
- [80] R. Perrin and E. L. Lomon, *Ann. Phys. (N.Y.)* **33**, 328 (1965).
- [81] K. E. Eriksson, *Nuovo Cimento* **19**, 1010 (1961); **19**, 1029 (E) (1961); **21**, 383(E) (1961); **30**, 1434 (1963).
- [82] S. Okubo, *Nuovo Cimento* **18**, 70 (1960).
- [83] E. R. Caianiello and S. Okubo, *Nuovo Cimento* **17**, 355 (1960).
- [84] J. Bernauer, V. D. Burkert, E. Cline, A. Schmidt, and Y. Sharabian (CLASS Collaboration) *Eur. Phys. J. A* **57**, 144 (2021).
- [85] C. dezCalan, H. Navelet, and J. Picard, *Nucl. Phys.* **B348**, 47 (1991).